Design and investigation of the emission dynamics of a mode-locked SBS-laser oscillator

Dissertation

zur Erlangung des akademischen Grades

"doctor rerum naturalium"

(Dr. rer. nat.)

in der Wissenschaftsdisziplin

"Experimentalphysik"

eingereicht an der

Mathematisch-Naturwissenschaftlichen Fakultät

der Universität Potsdam

von

Philip Kappe

Potsdam, Oktober 2006

Contents

Chapter 1

Introduction

With the first experimental realization of the laser in 1960 by Maiman [1] a unique source of light was born. At that time it was impossible to predict the impact it would have on science, industry and on our everyday life and as the variety of available features of laser sources increases it continues to conquer new fields of application. Its coherence is used for high precision measurements and wavelength tunable lasers as well as ultra short pulse sources offer new possibilities in the field of spectroscopy. Owing to their compactness, their low cost and easy control, semiconductor lasers have made their way into our everyday life where they serve as sensors and transmitters of information remaining almost unnoticed. High brilliance lasers are used to investigate and exploit nonlinear optical effects that were unaccessible before and the power densities available through temporal and spatial focussing of light provide new opportunities for fundamental research in particle physics and atomic fusion, to name just a few examples.

One of the earliest and by far the most important high power laser application in terms of economic turnover is materials processing. In this field, worldwide turnover amounts to 4.8 Billion Euro and has grown with an average annual rate of 12 % over the last decade [2]. This can to a considerable extent be attributed to the dramatic progress in the development of commercially available laser systems in terms of reliability, flexibility, power, compactness and affordability and the ever improving understanding and control of laser – matter interaction processes. The laser substitutes conventional processing procedures and allows for new production techniques. For continuous wave applications such as cutting, welding and surface hardening laser – matter interactions are already well understood and described by numerical simulations with good agreement with the experiments. For the more complex case of laser ablation and drilling where pulsed lasers are applied the understanding is not as far progressed due to the various possible temporal and spatial energy distributions and the multiple materials phases and phase transitions to be considered. However, it is known that there are several effects such as shielding by plasma, vapor and particles, melt ejection, shock waves and residual heat that lead to an interaction between temporally adjacent pulses [3, 4, 5, 6, 7, 8, 9, 10].

In order to study these effects in detail a universal laser tool is needed which provides a most flexible temporal energy distribution of its output. The focus of this work is the design, investigation and control of the output dynamics of a laser which provides the desired flexibility in its temporal energy distribution necessary to carry out systematic experimental investigations of pulse adjacency effects in laser – materials interactions. The laser that was chosen to answer these demands is an SBS-laser oscillator. This type of laser uses a nonlinear mirror on the basis of the stimulated Brillouin scattering (SBS). The nonlinear SBS-mirror generates a passive Q-switch and leads to bursts of pulses with ns-durations and temporal distances in the μs-range. The resulting pulse parameters can be easily tuned by altering the starting conditions for the passive Q-switch. Another advantage of SBS-mirrors is their phase conjugating reflection with potentially high fidelity. By use of a phase conjugating mirror (PCM) in a laser oscillator, phase distortions due to aberrations in thermal lensing or inhomogeneties in the laser rod can be compensated when the light passes the rod for the second time after the phase conjugating reflection. This effect allows for the realization of excellent beam qualities even at high output powers which is essential for materials processing in order to allow for a well defined spatial energy deposition.

The SBS-reflection already has a phase coupling effect on the longitudinal resonator modes which leads to an irregular modulation of the Q-switch pulses on a ps-timescale. This mode coupling can be controlled by additional active mode-locking and leads to a splitting up of each individual ns-pulse into a series of pulses with ps-durations underneath the envelope of the passive Q-switch. The principles of the stimulated Brillouin scattering and its application for nonlinear mirrors in laser oscillators as well as the theory of mode-locking will be treated in Chapter 2. The laser oscillator setup as well as experimental results relating to the SBS-laser's output dynamics will be the subject matter of Chapter 3.

In order to gain a fundamental understanding and a well defined control of the output dynamics numerical simulations of the laser dynamics were carried out. Therefore, two novel numerical models will be introduced in Chapter 4 which are supposed to display the dynamics of the output of the laser. In the first model the laser rate equations are applied for all longitudinal resonator modes individually while all modes share the stored inversion in the homogeneously broadened Nd:YAG. The numerical solution of these equations yield the evolution of the longitudinal modes throughout an SBS-Q-switch pulse. Consequentially, the intensity dynamics on the ps-timescale can be calculated from the spectrum of these modes. The second model describes all dynamics in the time domain. The propagation of a pulse in the resonator is considered and all changes that the pulse experiences during each round trip are recorded. The SBS-Q-switch will be taken into account by a phenomenological description which is identical for both models. Results from numerical simulations based on the two models are also presented in Chapter 4 and used to discuss the influences of different parameters such as modulation depth, modulation frequency detuning, SBS-Stokes-shift, SBS-Q-switch parameters and the starting conditions on the intensity distribution and the longitudinal mode dynamics.

Chapter 2

Theoretical basis

2.1 SBS-laser oscillator

First experimental investigations on the scattering of light at random thermal sound waves were carried out by Brillouin in the early 1920ies and therefore this process is called Brillouin scattering. The first part of this section deals with Stimulated Brillouin scattering (SBS) which is given if the reflecting sound wave is induced by the light wave itself. This feedback mechanism leads to a nonlinear reflectivity of the SBS that depends on the energy of the incident light. Also, a reflection based on SBS typically has phase conjugating properties which means that by reflection the wavefront will be inverted with regard to the propagation direction. The phase conjugating properties will be discussed in the second part of this section. They can be exploited for the compensation of phase distortions in high power master-oscillator power-amplifier (MOPA) systems and laser oscillators. If a mirror on the basis of the SBS is applied as a resonator mirror of a laser oscillator its nonlinear reflectivity leads to a passive Q-switching of the resonator and the laser yields bursts of pulses with ns-duration. The implementation of an SBS-mirror in a laser oscillator is the subject matter of the third part of this section.

2.1.1 Stimulated Brillouin scattering (SBS)

Stimulated Brillouin scattering is the coherent scattering of light at a self induced acoustic wave and can be demonstrated in gases, liquids, solids and also plasmas. Sound waves are periodic modulations of density and light experiences them as a refractive index grating. Incident light is scattered at the successive wavefronts and for coherent waves a macroscopic reflection occurs if the portions of light scattered from the various acoustic wavefronts interfere constructively. The condition for constructive interference is given by Bragg's law:

$$N \cdot n \cdot \lambda_{op} = \frac{2 \cdot \lambda_{ac}}{\cos \Theta}. \tag{2.1}$$

With N being an integer (the order of refraction), n the mean refractive index of the material, $\lambda_{op, ac}$ the wavelengths of the light and the acoustic wave respectively and Θ is the angle of incidence of the light with regard to the normal of the scattering wavefront. While the process starts with the scattering at thermal random acoustic waves [11, 12] these waves are amplified and maintained via electrostriction [11, 13] by the beatmode resulting from the superposition of the electrical fields of the incident and the reflected light. Due to the movement of the acoustic wave, the reflected light experiences a Doppler-shift. If the movement of the acoustic wave occurs in the same direction as the incident light, the scattered light shifts to lower frequencies — it is Stokes-shifted. In a particle picture the energy as well as the momentum of the incident photon have to be maintained. Thus, the energy that the scattered photon loses due to the Stokes-shift is emitted as a Stokes-phonon that contributes to the scattering sound wave. The angular frequencies and wave vectors of the incident pump photon ω_p, k_p the reflected Stokes-photon ω_s, k_s and the phonon ω_B, k_B are therefore related by:

$$\omega_B = |\omega_p - \omega_s| \tag{2.2}$$

$$\vec{k}_B = \vec{k}_p - \vec{k}_s. \tag{2.3}$$

SBS is a third order nonlinear effect, the coupling between the electrical field $\vec{E}$ of the incident and scattered light can be described by a nonlinear polarization P_{NL} of the material:

$$\vec{P}_{NL} = \frac{\vec{E}}{4\pi} \cdot \left[\left(\frac{\partial \varepsilon}{\partial \rho} \right)_T \cdot \bar{\rho} + \left(\frac{\partial \varepsilon}{\partial T} \right)_\rho \cdot \bar{T} \right]. \tag{2.4}$$

Two fundamental effects contribute to the generation of the nonlinear polarization of the material namely the dependence of the dielectric constant ε of the material on the density ρ and on the temperature T. $\bar{\rho}$ and $\bar{T}$ in (2.4) refer to the modulation of the density and the temperature respectively. In most cases and particularly for materials with low absorption the dependence of the dielectric constant on the temperature may be neglected, which yields with the introduction of the electrostrictive coupling coefficient $\gamma_e = \rho_0 \cdot \left(\frac{\partial \varepsilon}{\partial \rho} \right)_T$ and the average density of the material ρ_0 [14, 16]:

$$\vec{P}_{NL} = \frac{\vec{E} \cdot \gamma_e \cdot \bar{\rho}}{4\pi \cdot \rho_0}. \tag{2.5}$$

The SBS is a distributed reflection and therefore we have to describe the propagation of the electric field as well as the acoustic wave in the Brillouin medium. The propagation of the electric field is described by the Maxwell equations which can be combined to yield the wave equation for non-absorbing media:

$$\Delta \vec{E} - \frac{n^2}{c^2} \frac{\partial^2 \vec{E}}{\partial t^2} = \frac{4\pi}{c^2} \frac{\partial^2 \vec{P}_{NL}}{\partial t^2}. \tag{2.6}$$

The effective electrical field $\vec{E}$ is the superposition of the incident Pump field $\vec{E}_p$ and the reflected Stokes-field $\vec{E}_s$. In the following we will confine ourselves to the case of directly back reflected light while the incident light beam propagates along the positive z-axes. In a plane wave approximation the electrical field can than be written as:

$$\vec{E} = \vec{E}_p(\vec{r},t) + \vec{E}_s(\vec{r},t) \tag{2.7}$$

$$\vec{E}_p = \left(\frac{1}{2}E_p(\vec{r},t) \cdot \exp[i(k_p z - \omega_p t)] + c.c.\right)\vec{e}_p \tag{2.8}$$

$$\vec{E}_s = \left(\frac{1}{2}E_s(\vec{r},t) \cdot \exp[i(-k_s z - \omega_s t)] + c.c.\right)\vec{e}_s. \tag{2.9}$$

Introducing (2.7)–(2.9) into (2.6) and neglecting the second order derivatives according to the slowly varying envelope approximation (SVEA) we obtain for the propagation of the electric fields the SBS field equations:

$$\left(\frac{\partial}{\partial z} + \frac{n}{c}\frac{\partial}{\partial t} + \nabla_T^2\right)E_p(\vec{r},t) = i\frac{\omega_p \cdot \gamma_e}{4c \cdot n \cdot \rho_0}\bar{\rho}(\vec{r},t) \cdot \vec{E}_s(\vec{r},t) \tag{2.10}$$

$$\left(\frac{\partial}{\partial z} + \frac{n}{c}\frac{\partial}{\partial t} + \nabla_T^2\right)E_s(\vec{r},t) = -i\frac{\omega_p \cdot \gamma_e}{4c \cdot n \cdot \rho_0}\bar{\rho}^*(\vec{r},t) \cdot \vec{E}_p(\vec{r},t). \tag{2.11}$$

Here ∇_T^2 denotes the transverse component of the Laplace operator. Similar to the electrical fields we follow the formulation

$$\bar{\rho} = \left(\frac{1}{2}\hat{\rho} \cdot \exp[i(k_B z - \omega_B t)]\right) + c.c. \tag{2.12}$$

for the density modulation $\bar{\rho}$ with $\hat{\rho}$ being the maximal amplitude of the density modulation. The propagation of the sound wave is also described by a wave equation that is derived from the equation of continuity, the Navier-Stokes- and the energy transport equation [14]. Neglecting again the contribution of the absorbtion to the nonlinear polarization we obtain:

$$-\frac{\partial^2\bar{\rho}}{\partial t^2} + \frac{v_B^2}{\gamma}\Delta\bar{\rho} + \frac{1}{\tau_B \cdot k_B^2}\frac{\partial\Delta\bar{\rho}}{\partial t} = \frac{\gamma_e}{8\pi}\Delta E^2. \tag{2.13}$$

Here v_B denotes the velocity of the sound wave and $\gamma = C_p/C_v$ the adiabatic exponent — the ratio of the specific heats at constant pressure and volume. The third term on the left hand side describes the damping of the acoustic wave which is governed by the phonon lifetime τ_B while the right hand side of Equation 2.13 represents the electrostrictive driving force of the sound wave. The sound wave Equation 2.13 can be considerably simplified if

- the period of the sound wave $T_B = 2\pi/\omega_B$ is short compared to the phonon lifetime τ_B, the inverse Bandwidth $1/\Delta\nu_p$ of the pump light and to the pump pulse duration Δt_p,

- the damping of the sound wave is so strong that the phonon propagation can be neglected compared to their generation,

- the SVEA can be applied to the sound wave as well, meaning that changes in E_p, E_s and $\bar{\rho}$ are slow compared to the Brillouin-frequency ω_B [17].

With these restrictions in mind (2.13) turns into

$$\left(\frac{\partial}{\partial t} + \frac{1}{\tau_B}\right)\bar{\rho} = i\frac{\omega_p^2 \cdot \gamma_e^2 \cdot n}{8\pi \cdot c^2 \cdot \omega_B}\vec{E}_p \cdot \vec{E}_s^*. \tag{2.14}$$

The set of differential equations (2.10), (2.11) and (2.14) can be utilized to display the SBS-reflection with temporal and spatial resolution. In [18] the temporal SBS-reflectivity for an input pulse was calculated with spatial resolution along the axes of propagation. In [19] and [20] the transversal field distribution is additionally considered by a transversal mode decomposition for the transient case and in [21] for steady state conditions.

Influence of pump spectrum on SBS

For a continuous wave pump beam and without consideration of the transverse field distribution first order differential equations are obtained that display the steady state reflectivity along the z-axes and where the electrical fields can be substituted by the intensities $I_{p,s} = |E_{p,s}|^2$ [11, 22, 23]:

$$\frac{dI_{p,s}}{dz} = C \cdot g_B \cdot I_p \cdot I_s \qquad \text{with} \qquad g_B = \frac{\omega_p^2 \cdot \gamma_e^2 \cdot n}{8\pi \cdot c^2 \cdot \omega_B}. \tag{2.15}$$

Here g_B is called the Brillouin-gain coefficient and the factor C comprises a reduction of the SBS-reflectivity depending on the spectral properties of the pump beam [24]. The reason for this reduction is the generation of a second sound wave that is counter propagating with regard to the original one and scatters energy from the Stokes-field back into the pump field [24, 25]. For a single frequency input beam $E_p(\omega_p)$ its beat-mode with the reflected light $E_s^*(\omega_p - \omega_B)$ efficiently generates a coherent sound-wave Q_A that moves in the direction of the pump light. In this case C equals unity. And for a multi-mode input beam with an arbitrary longitudinal mode spacing each individual mode $E_p^j(\omega^j)$ will contribute to the maintenance of the sound wave by the beat mode with its respective Stokes-shifted mode $E_s^{j*}(\omega^j - \omega_B)$. In general the beat modes of pump- and Stokes-fields with different mode number j will not be resonant with the Brillouin-frequency ω_B and will therefore not efficiently generate any sound waves.

Again the SBS-reflectivity is not affected as long as the coherence length exceeds the interaction length [26]. If, however, the longitudinal mode spacing $\Delta\nu$ is resonant with the Brillouin-frequency ν_B:

$$\nu_B = \frac{\omega_B}{2\pi} = N \cdot \Delta\nu \qquad \text{with } N \text{ being an integer;} \qquad (2.16)$$

then all terms $E_p^j \cdot E_s^{j-N*}$ will contribute to the generation of Q_A and the terms $E_p^j \cdot E_s^{j+N*}$ will generate sound waves Q_B counter propagating with respect to Q_A. The generation of the counter propagating soundwaves by the pump- and Stokes-modes is schematically depicted in Figure 2.1.
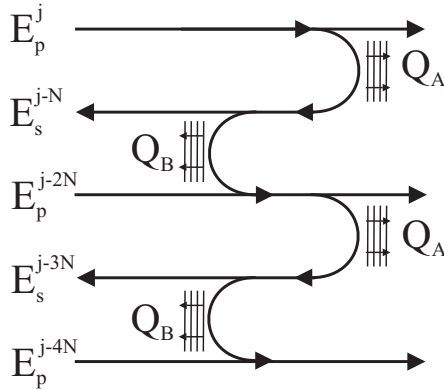
Figure 2.1: Schematic of the generation of the counter propagating soundwaves Q_A and Q_B by the pump- and the Stokes-modes

If the phases of the input modes E_p^j are random all contributions $E_p^j \cdot E_s^{j+N*}$ to Q_B will average to zero while the contributions to Q_A are synchronized by the scattering at Q_A itself. So for random phases there is still no decline in SBS-reflectivity compared to the single mode pump. Contrarily, for pump powers near the SBS-threshold a beneficial effect with regard to SBS-reflectivity has been reported for multi-mode pumping that was attributed to the high peak powers which lead to self focussing [27]. So only a mode-locked input beam with a spectral mode spacing that is resonant with the Brillouin-frequency ω_B leads to a substantial generation of a counter propagating sound wave Q_B which scatters energy from the Stokes-wave back into the pump beam. These higher Stokes-orders also increase the bandwidth. The factor C can be given by

$$C = \frac{|Q_A|^2 - |Q_B|^2}{|Q_A|^2 + |Q_B|^2} \qquad (2.17)$$

and approaches zero with increasing bandwidth for a mode-locked input beam [24].

SBS-threshold

Due to the mutual coupling between the pump- and Stokes-field and the sound wave, the resulting SBS-reflectivity is strongly dependent on the input parameters such as input power, focussing conditions and transient behavior [28, 29, 30]. Low energy input beams will transmit the SBS-medium without noticeable changes because too little energy is provided for the build-up of the sound wave. But then, the overall energy reflection can reach values in excess of 90 % for input beams with large energy densities [15, 16, 31]. However, the SBS-threshold is not a real threshold like the laser threshold, but rather a gradual transition from transmission to reflection with increasing input energy. Accordingly, an arbitrary threshold is defined for energy reflection values of 1 % [12, 23].

For pulsed pump beams the threshold energy is a function of the pulse duration Δt_P and the phonon lifetime τ_B, and of course the reflectivity is a function of time. The leading edge of the pulse will transmit the SBS-mirror more or less unattenuated but triggers the generation of the sound wave so that the body of the pulse will experience an almost total reflection. Munch et al. demonstrated experimentally that for focussed beams the threshold strongly depends on the effective interaction length which is given by the shorter of i) the physical cell length, ii) three times the coherence length or iii) 5 times the Rayleigh range [32]. It was proposed in [32, 33] and could be shown by numerical simulations in [18] that the spatial distribution of the SBS-reflection can change significantly in the course of the pulse. For focussed beams the generation of the sound wave initially starts in the vicinity of the focal plane. With an increasing Stokes-field the sound wave will also effectively be generated in front of the focal plane so that the maximum of the sound wave amplitude and hence the location where the reflection prevailingly occurs gradually moves from the focal position to the front of the SBS-medium.

The transient spatial distribution of the SBS-reflection can be exploited for pulse compression [34, 35, 36, 37]: The early parts of the pump pulse will be reflected at the far side of the SBS-medium while the later parts will be reflected in the front. Consequently, in the Stokes-beam these parts will overlap. The dimension of an SBS-pulse-compressor has to match the pulse duration of the pump pulses. Therefore, tapered waveguides are particularly suitable for this purpose [38].

There are several concepts to reduce the SBS-threshold: For pulses in quick succession the threshold is reduced by virtue of a residual sound wave [28, 29]. The threshold can also be reduced by enhancing the interaction length [16, 31], by feeding back the transmitted light [39, 40] or by enhancing the Stokes-field noise [41]. Another method of injecting the Stokes-field into the SBS-mirror is by use of a second SBS-cell with a strong focus while the beam is comparatively wide in the first cell [42, 43]. The Stokes-field is initiated in the second cell and injected into the first where other competing nonlinear effects will be prevented by the low intensity.

2.1.2 SBS-phase conjugation

It was demonstrated for the first time by Zel'dovich [44] in 1972 that a reflection based on stimulated Brillouin scattering can have phase conjugating properties. Reviews of optical phase conjugation are given in [45, 46, 47]. Phase conjugation means that the wavefront is inverted with respect to the propagation direction by the reflection, whereas for a conventional reflection at a plane mirror the orientation of the wavefront is maintained. As a consequence a beam which is reflected at a phase conjugating mirror (PCM) is always reflected back to its origin independent of the angle of incidence (see also Fig. 2.2). Furthermore, the phase conjugate beam has the same transverse amplitude distribution as the original beam. In other words, the phase conjugate beam is a reproduction of the incident beam. Therefore, phase conjugation is also termed "time reversal" [48] or "wavefront reversal" [49].

conventional mirror **phase conjugating mirror**
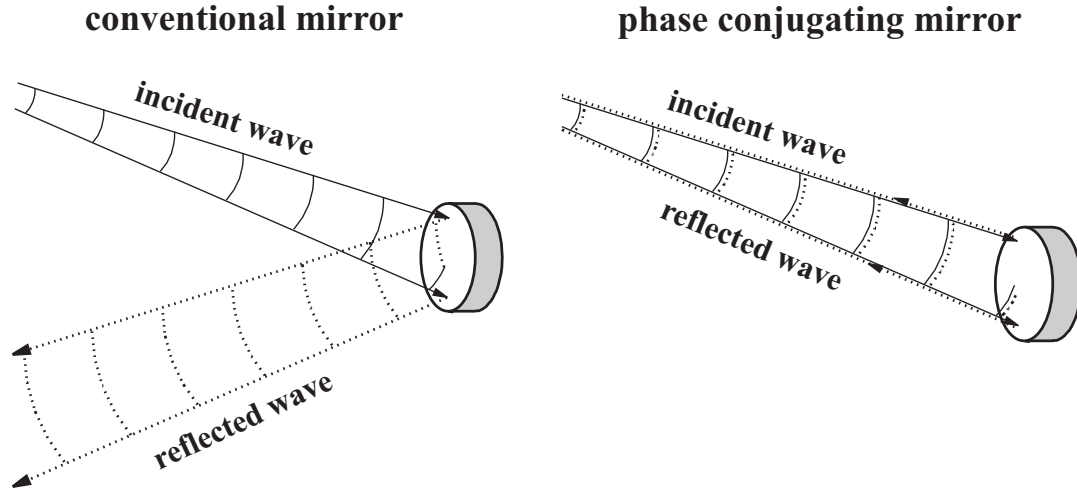
Figure 2.2: Beam propagation and wavefronts for reflection at a conventional mirror (left) and phase conjugating mirror (right)

If the incident beam is given by

$$E(x, y, z, \omega) = E(x, y, z) \cdot e^{-i\omega t} = A_0(x, y, z) \cdot e^{i[kz + \phi(x,y,z)]} \cdot e^{-i\omega t} \tag{2.18}$$

with the complex field amplitude $E(x, y, z)$, the real amplitude $A_0(x, y, z)$ and the phase distortion $\phi(x, y, z)$ describing the deviation form the plane wave, then the conjugate of this beam is written as

$$E'(x, y, z, \omega) = r \cdot E^*(x, y, z) \cdot e^{-i\omega t} = r \cdot A_0(x, y, z) \cdot e^{-i[kz + \phi(x,y,z)]} \cdot e^{-i\omega t} \tag{2.19}$$

where r is the amplitude reflection of the phase conjugate mirror [47].

A phase conjugating reflection can for instance be achieved for spherical wave fronts if the radius of curvature of a conventional mirror matches the radius of curvature of the wave fronts. The simplest case of phase conjugation is the reflection of a plane wave at a plane mirror with proper alignment. For incident beams with arbitrary wavefronts the curvature has to adapt to the incident light. This can be achieved with adaptive optics, but is more conveniently implemented by use of nonlinear processes such as four-wave-mixing (FWM) [45, 50, 51] or stimulated scattering [45] which can also be considered a collinear FWM process [47, 52]. For technical applications nonlinear scattering processes such as SBS, stimulated Raman scattering (SRS) and stimulated Rayleigh-wing scattering (SRWS) have the pronounced advantage that only one strong input beam is necessary to generate its conjugate.

The phase conjugating properties of the SBS can be attributed to the fact that the reflecting sound wave is build up by the beat mode in the electrical field resulting from the superposition of the incident and the reflected wave. The overlap of incident and reflected field becomes maximal for a phase conjugating reflection [48] and therefore the acoustic wave — among all sound waves that constitute the thermal acoustic noise — which leads to a phase conjugating reflection will experience the strongest amplification upon the scattering of a strong incident pump beam.

However, for a real PCM the reproduction of the wavefronts and the spatial intensity distribution is not compellingly ideal. There are several influences that lead to an imperfect phase conjugation. SBS-mirrors for instance exhibit a transversal profile in the effective amplitude reflection that leads to a different intensity distribution of the reflected beam. This can also entail a deviation in the propagation behavior since the intensity distribution and the divergence of the beam are coupled by the diffraction limit. The quality of the SBS-phase conjugation is characterized by the fidelity F:

$$F = \frac{|\int E_s \cdot E_p^* dx dy|^2}{\int |E_s|^2 dx dy \cdot \int |E_p|^2 dx dy}. \tag{2.20}$$

For an ideal reproduction of the incident wave the fidelity becomes unity.

A very important application of phase conjugation is the compensation of phase distortions [53]. The mechanism is schematically illustrated in Figure 2.3. If a plane wave passes through an aberrator — a medium with an inhomogeneous spatial distribution of the index of refraction — the wavefront becomes distorted (Fig. 2.3 top). This situation can be described by Equation 2.18 with the phase distortion $\phi(x, y, z)$ caused by the passing of the aberrator. If the beam is reflected at a conventional mirror the propagation direction is reversed but the wavefront is maintained with respect to the propagation direction:

$$E(x, y, z, \omega) = A_0(x, y, z) \cdot e^{i[-kz + \phi(x,y,z)]} \cdot e^{-i\omega t}. \tag{2.21}$$

If the beam now passes the aberrator for a second time it experiences the same phase shift as for the first pass:
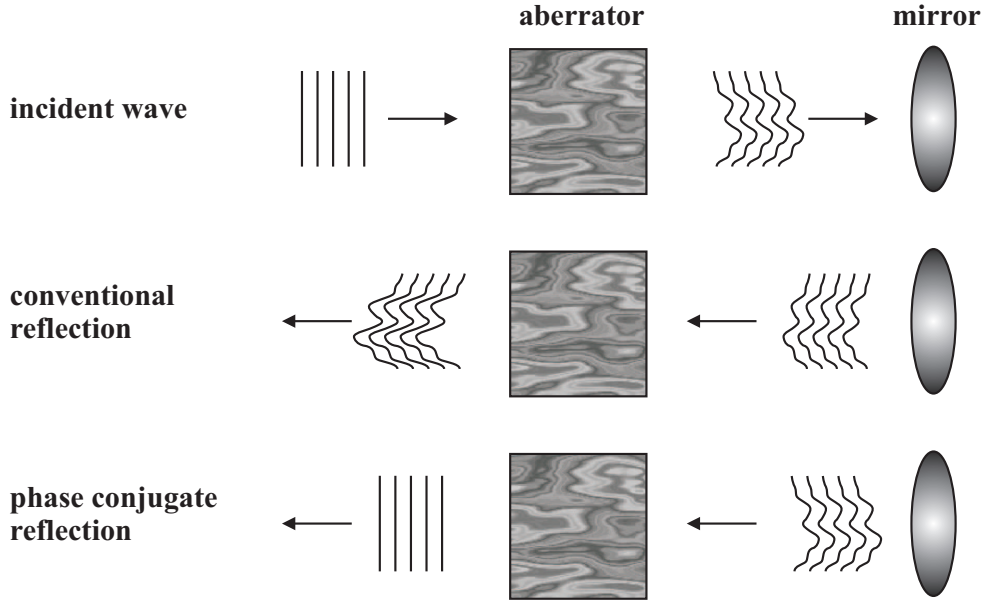
Figure 2.3: Compensation of phase distortions by second pass through aberrator after phase conjugating reflection, comparison with conventional double pass

$$
\begin{aligned}
E(x,y,z,\omega) &= r \cdot A_0(x,y,z) \cdot e^{i[-kz+\phi(x,y,z)]} \cdot e^{-i\omega t} \cdot e^{\phi(x,y,z)} \\
&= r \cdot A_0(x,y,z) \cdot e^{i[-kz+2\phi(x,y,z)]} \cdot e^{-i\omega t}
\end{aligned}
\tag{2.22}
$$

and as a result the magnitude of the phase distortion is doubled (Fig. 2.3 middle). For a phase conjugating reflection the sign of the phase term changes so that the phase distortions of the first and second pass through the aberrator cancel each other out (Fig. 2.3 bottom):

$$
\begin{aligned}
E'(x,y,z,\omega) &= r \cdot A_0(x,y,z) \cdot e^{-i[kz+\phi(x,y,z)]} \cdot e^{-i\omega t} \cdot e^{\phi(x,y,z)} \\
&= r \cdot A_0(x,y,z) \cdot e^{-ikz} \cdot e^{-i\omega t}.
\end{aligned}
\tag{2.23}
$$

One source of aberrations in solid state lasers are the aberrations of the thermal lenses [54, 55]. There are several effects that entail these aberrations — inhomogeneous pump light distribution in the laser active material, temperature dependent heat conduction, nonlinearities in the temperature dependence of the refractive index — and they are often the reason for power scaling limits and beam quality degradation at high powers. Therefore the application of phase conjugate mirrors in laser oscillators as well as master oscillator power amplifier (MOPA) systems ameliorates the power

scalability of these systems and prevents beam quality degradation at high powers. In MOPA-systems PCMs are applied to realize a double pass [56] or multiple passes [57, 58] through the amplifiers. Besides the compensation of phase distortions multiple passes in MOPA-systems lead to a considerable improvement of the energy extraction efficiency. In [58] 362 W average infrared output power at a repetion rate of 1 kHz with a beam quality of 1.2 times diffraction limited is reported from 6 passes through a single slab amplifier using an SBS-PCM. In addition to the virtue of the compensation of phase distortions, by use of PCMs no adjustment of the mirror and no additional control of the beam radius for the second pass is necessary. The phase conjugating reflection will always guarantee for a reproduction of the beam propagation of the first pass. The application of SBS-PCMs in laser oscillators is the subject matter of the following section.

2.1.3   Application of SBS-mirrors in a laser resonator

The simplest layout of a resonator with a phase conjugating mirror consists of a PCM and a conventional reflector. Similar to the MOPA-system a phase conjugating mirror applied as part of a laser resonator can be used to compensate the phase distortions of successive passes through the laser active material. But there are still other aspects that are connected with the application of a phase conjugating mirror and an SBS-mirror in particular in a laser resonator.

The reflection at an ideal PCM leads to a reproduction of the transversal field distribution and the wavefront curvatures of the incident beam independent of the angle of incidence. Thus, a PCM is always properly aligned and the only requirement for eigensolutions of a resonator with a PCM is that the wavefront of the respective field matches the radius of curvature of the conventional reflector. Accordingly, a resonator with a PCM has an infinite number of eigensolutions and there is no restriction with regard to the beam radius at the conventional mirror [59, 60]. For the laser resonator with a PCM this means that it is always stable independent of the magnitude of the thermal lens.

The nonlinearity of the SBS-reflection has several implications: Unless saturation of the Brillouin-gain is achieved, an SBS-mirror exhibits a spatial and in particular a transversal distribution of the reflectivity entailing a discrimination of higher order modes. Another implication of the nonlinearity is that the SBS-reflectivity is a function of time and will therefore lead to a Q-switching of the laser resonator. In order to understand this Q-switching behavior we will have a look at the setup of a typical SBS-laser and follow the processes that occur from the beginning of the pump process to the emission of the pulse:

Passive Q-switching of the linear SBS-laser

Since the SBS-mirror is virtually transparent for low incident powers a simple resonator consisting of an SBS-mirror and a conventional one will in general not be self-starting.

However, in the first report on an SBS-laser implementation, Q-switched laser operation with such a configuration was already successfully demonstrated [61] and this was even before the discovery of the phase conjugating properties of SBS-mirrors [44]. Typically, the SBS-mirror is embedded in a conventional resonator — the start resonator. The simplest case of a self starting SBS-laser resonator consequently consists of two coupled resonators (see schematic in Fig. 2.4). The conventional start resonator is given by the output coupler OC and the start resonator mirror R_{start}. The nonlinear SBS-mirror and the OC form the SBS-resonator.
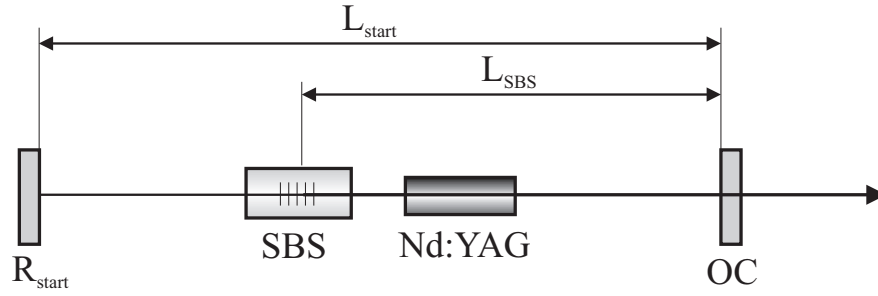
Figure 2.4: Schematic of the linear SBS-laser oscillator

When the pumping sets in the inversion is gradually build up in the laser active material. Laser oscillation will arise as soon as the resonator losses will be compensated by the gain of the laser active material:

$$G \cdot V \cdot \sqrt{R_1 \cdot R_2} = 1 \qquad \text{with} \qquad G = e^{\Delta n \cdot \sigma \cdot l}. \tag{2.24}$$

Here G denotes the gain factor, $R_{1,2}$ the reflectivities of the resonator mirrors, V the linear resonator loss, Δn the inversion density, l the length and σ the stimulated emission cross section of the laser active material. Since at this time the SBS-mirror is transparent and the quality of the SBS-resonator will be zero the oscillation will arise in the start resonator.

With increasing intensity during the leading edge of the first spike in the start resonator the SBS-reflectivity increases quickly and the oscillation switches from start- to SBS-resonator. In most implementations of SBS-lasers the quality Q of the start resonator is low. Since the SBS-mirror can reach very high overall reflectivity values the switch from start resonator to SBS-resonator is also connected with a switch in the quality of the resonator that the light experiences. Due to the high quality the stored inversion can now be quickly depleted and the oscillation ceases again — a Q-switch pulse has been emitted. The duration of a Q-switch pulse is in the order of magnitude of tens of ns, the pulse build up takes around 100 ns to 1 μs while the pump duration until the lasing threshold is reached for the start resonator ranges around 10–100 μs. Therefore, the initial inversion Δn_i at the time of the onset of the Q-switch pulse is

in a first order approximation identical to the one fulfilling Equation 2.24 for the start resonator:

$$\Delta n_i = \frac{-\ln(V_{start} \cdot \sqrt{R_{start} \cdot R_{OC}})}{\sigma \cdot l}. \tag{2.25}$$

The stored inversion at the time of the Q-switch increases with decreasing R_{start} since it takes a higher inversion to reach the lasing threshold for low quality resonators. It is demonstrated in [62] that key parameters such as optimal output coupling reflectivity R_{op} and pulse energy E_{op} and duration t_{op} for the optimal case can be expressed as a function of a single dimensionless variable $z = 2g_o l/\mathcal{L}$ with $g_o = \Delta n \sigma$ being the small signal gain coefficient and $\mathcal{L} = \ln V^2$:

$$R_{op} = \exp\left[-\mathcal{L}\left(\frac{z - 1 - \ln z}{\ln z}\right)\right] \tag{2.26}$$

$$E_{op} = \frac{A \cdot h \cdot \nu \cdot \mathcal{L}}{2\sigma}(z - 1 - \ln z) \tag{2.27}$$

$$t_{op} = \frac{T}{\mathcal{L}}\left(\frac{\ln z}{z[1 - a \cdot (1 - \ln a)]}\right). \tag{2.28}$$

Here A is the effective cross section of the beam in the laser active material, $h \cdot \nu$ the photon energy, T the resonator round trip time and $a = (z-1)/(z \ln z)$. Equations 2.26–2.28 are plotted in Figure 2.5 and it can be seen that the pulse energy for optimal output coupling reflectivity increases with increasing stored inversion and therefore with decreasing start resonator mirror reflectivity R_{start}, while the pulse duration decreases.

After the emission of the first Q-switch pulse the inversion is depleted and the SBS-resonator gets below the lasing threshold. Now inversion can be accumulated in the laser material again until the laser threshold is reached in the start resonator and the next Q-switch pulse arises from a spike in the start resonator. Hence, several Q-switch pulses can be emitted in quick succession within a single pump pulse. Thereby bursts of pulses are emitted by the laser. The temporal distance between the pulses and thus the number of pulses in a burst is determined by the pump parameters on the one hand and the quality of the start resonator on the other hand. For a high loss factor it takes a longer pumping period until lasing threshold is reached since the gain that satisfies condition (2.24) is higher. Thus the time between the pulses will be longer and, for a given pump pulse duration and intensity, the number of pulses will be smaller for high start resonator losses. A higher gain results in shorter pulses of higher energy. To summarize, a low quality of the start resonator leads to a small number of short pulses with high energy, while a high quality results in an emission of a large number of longer low energy pulses in quick succession.
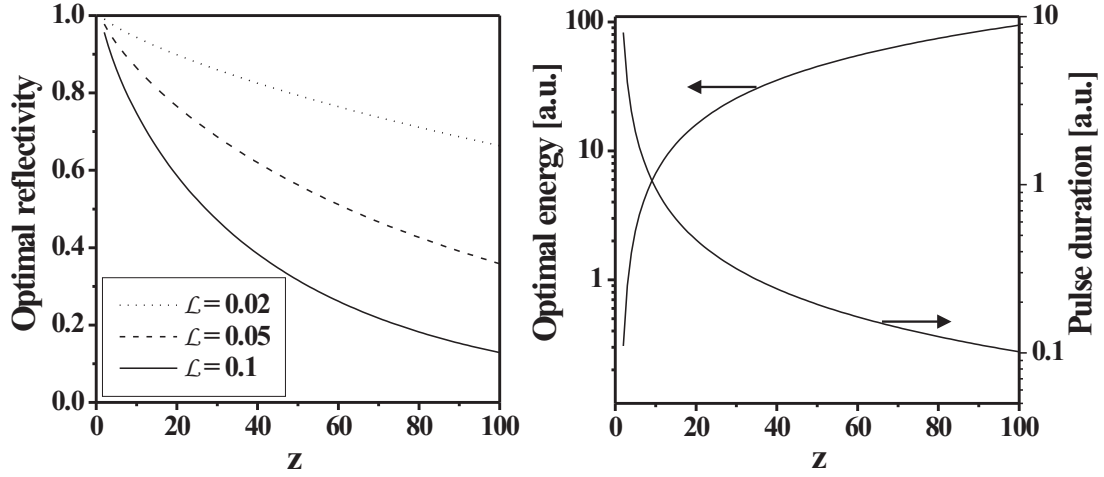
Figure 2.5: Calculated optimal output coupling reflectivity for different resonator losses (left) and pulse energy and duration for optimal reflectivity (right) as a function of $z = 2\Delta n\sigma l/\mathcal{L}$

Alternative SBS-oscillator concepts

In the literature several different concepts can be found to adjust the start resonator losses in order to control the Q-switch properties. Summaries can be found in [63, 64]. The most wide spread method is the aforementioned tuning of the start resonator mirror reflectivity R_{start}. Examples can be found in [65, 66] while in [67] neutral-density filters are utilized to serve the purpose of loss tuning. Furthermore the start resonator can be setup unstably [63] or the start resonator mirror can be misaligned [68]. Also an aberrator or an aberating laser crystal would lead to an enhancement of the start resonator losses while the SBS-resonator would not be affected owing the the compensation of phase distortions by virtue of the phase conjugating SBS-reflection [69].

Apart from these minor variations with regard to the resonator loss control, some alternative layouts of oscillators employing SBS-mirrors can be found that exhibit fundamentally different properties. One alternative to the linear SBS-oscillator is the so called sidearm SBS-laser as introduced in [70]. Its setup is schematically depicted in Figure 2.6. In this concept the start resonator and the SBS-resonator are coupled by a polarizer and a quarter wave plate while the coupling strength is governed by the rotation of the quarter wave plate. In contrast to the linear SBS-laser the start resonator is never switched off, but the SBS-reflectivity merely evokes an additional feedback. Q-switching is still obtained for strong coupling since the overall quality of the coupled cavities is enhanced by the feedback from the SBS-arm. The advantage of this concept is that there is no need for lenses in the start resonator which allows for an easier alignment. In the linear SBS-laser these are usually necessary to generate a focus inside the SBS-cell in order to obtain sufficiently high power densities to overcome the SBS-threshold. Also aberrations of the elements of the SBS-mirror will not affect
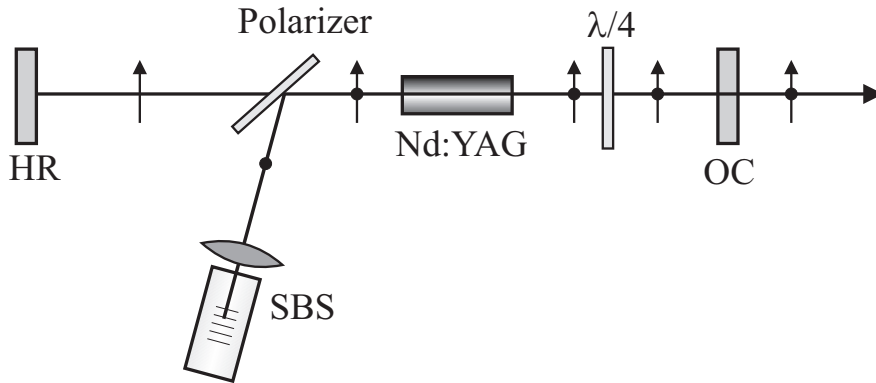
Figure 2.6: Schematic of the sidearm SBS-laser as introduced in [70]

the beam quality during the process of the pulse build up in the start resonator when
the SBS-mirror is still transparent and no compensation of phase distortions by phase
conjugation is available. The drawbacks of this concept compared to the linear SBS-
laser are that the amplitude in the switch in quality is limited and that no threshold
reduction by Brillouin enhanced four-wave-mixing can be exploited. This issue will be
discussed in detail below. Other implementations of sidearm SBS-lasers can be found
in [71] for an Excimer laser and in [72] for a Nd:YAG laser.

Quite similar properties are obtained if the SBS-mirror is placed outside the start
resonator in a linear setup [73, 74], but Q-switching is only obtained for very low start
resonator mirror reflectivities. All these aforementioned SBS-laser concepts have in
common that the reiterated reflection at the SBS-mirror round trip by round trip will
inevitably lead to a multiple frequency output signal due to the shift in frequency that
is connected with the SBS-reflection. The contrary result — a single frequency output
signal — can be achieved with ring resonators. Two similar layouts for SBS-lasers with
ring resonators are illustrated in Figure 2.7 [75, 76].

Just like in the linear SBS-laser and identical for both layouts the oscillation starts
in a conventional resonator. The Q-switch is initiated by the saturable absorber but
supported by the increased feedback of the SBS-mirror after the threshold is reached.
In fact both concepts are something in between an oscillator and a MOPA-system since
after the reflection at the SBS-mirror the light is doing only approximately two round
trips in the ring resonator for configuration (a) and exactly one single pass through the
laser active material for the variant (b). But then, the enhanced feedback from the
SBS-mirror leads to a quick depletion of the stored inversion resulting in a considerable
reduction of the pulse durations. Therefore, the SBS-mirror can be considered a part
of the oscillator.

To obtain single frequency operation spatial hole burning in the laser active material
has to be prevented. Spatial hole burning is the inhomogeneous gain depletion that
results from standing waves in a resonator due to counter propagating fields. Thus,
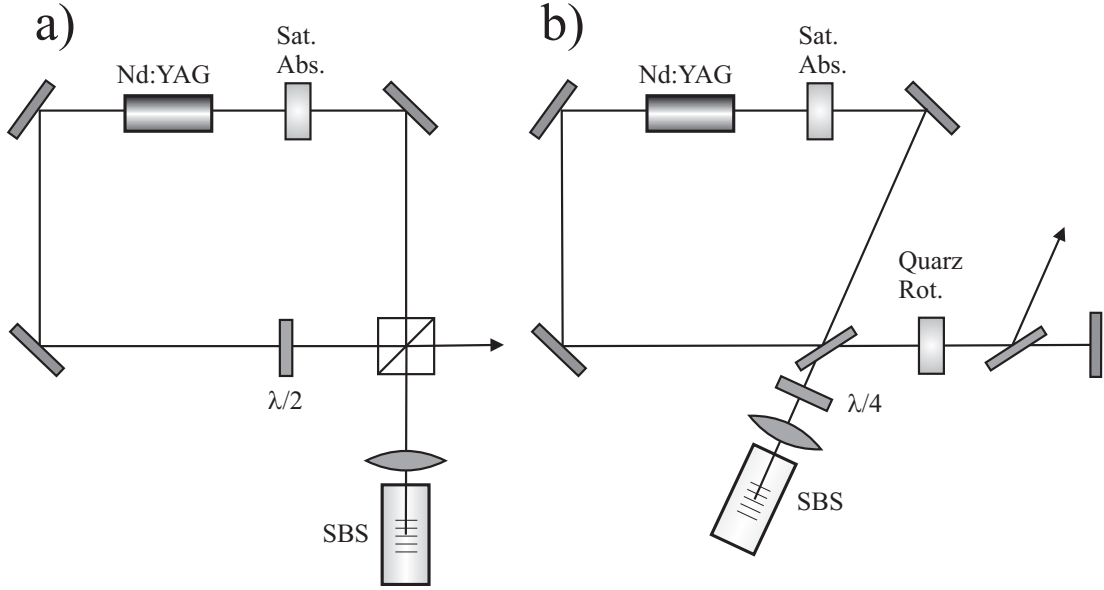
Figure 2.7: Two layouts for SBS-ring oscillators as reported in [75] (a) and [76] (b)

to establish circumstances in a ring resonator that allow for single mode operation one propagation direction has to be suppressed. In configuration (b) this is done by supporting the clockwise propagation via the feedback of the conventional reflector.

Resonator length tuning of the linear SBS-laser

As mentioned before the reflection at the SBS-mirror inevitably leads to a shift in frequency. It can be exploited for the generation of bandwidth and to lock the phases of the laser modes. This subject matter will, however, be detailed in Section 2.2.4. Here we want to have a look at the restrictions regarding the resonator setup that are connected with the frequency shift. As can be seen from Equation 2.2 the Stokes-shift amounts to the frequency of the acoustic wave — the Brillouin-frequency — which is a constant of the material. So light revolving in the SBS-resonator is shifted by the amount of the Brillouin-frequency to lower frequencies for each round trip. A high quality resonator, however, will only accommodate a set of discrete frequencies ν_j or modes that constitute eigensolutions of the resonator and obey

$$\nu_j = \frac{j \cdot c}{2L} \qquad \text{and are spaced by} \qquad \Delta\nu = \frac{c}{2L}. \tag{2.29}$$

Here j is the integer longitudinal mode number and L the optical resonator length. All frequencies that do not fulfill (2.29) suffer strong losses and will quickly decay in the resonator. Thus, if the SBS-reflected light is supposed to be accommodated in the

resonator, the Brillouin-frequency ν_B has to be an integer multiple of the longitudinal mode spacing $\Delta\nu$:

$$\nu_B = N \cdot \Delta\nu. \tag{2.30}$$

Combining (2.29) and (2.30) results in a condition demanding the SBS-resonator length L_{SBS} to be an integer multiple of the fundamental Brillouin-length L_B:

$$L_{SBS} = N \cdot \frac{c}{2\nu_B} = N \cdot L_B. \tag{2.31}$$

Contrasting these considerations it could be demonstrated experimentally, that the efficient energy extraction is in general not significantly affected by a misfit of L_{SBS} [77] which can be attributed to the bandwidth of the SBS.

The regular SBS-process is initiated from spontaneous scattering at the thermal acoustic noise. The superposition of the backward scattered light which is shifted by the amount of the Brillouin-frequency and the incident light leads to a beat mode corresponding to the Brillouin-frequency that builds up the sound wave. This leads to high SBS-thresholds especially for materials with low SBS-gain coefficients such as gases. As discussed in Section 2.1.1 the threshold can be reduced considerably if by any means the initiation of the sound wave is supported. This can for example be achieved by an enhancement of the acoustic noise or by seeding of frequencies spaced by the Brillouin-frequency. In a linear SBS-laser oscillator the initiation of the sound wave can be efficiently induced by Brillouin-enhanced four-wave-mixing (BEFWM) [78, 79] of the longitudinal start resonator modes if their mode spacing is also resonant with the Brillouin-frequency. In other words, condition (2.31) has to be met by the start resonator as well [80]:

$$L_{start} = M \cdot \frac{c}{2\nu_B} = M \cdot L_B. \tag{2.32}$$

In this case pairs of longitudinal modes $E_f^j(\omega) \cdot E_b^{j-M}(\omega - \omega_B)$ which are spaced by the Brillouin-frequency will build up an initial sound wave that will constitute the seed for the SBS-process. Here the indexes f and b denote the forward and backward traveling waves in the SBS cell from the perspective of the laser active material and again j is the longitudinal mode number.

One more aspect has to be mentioned when the length tuning of the linear SBS-laser is discussed. It has been reported in several experimental investigations that the SBS is suppressed for a configuration where the start resonator length L_{start} is exactly two times the SBS-resonator length L_{SBS} [77, 80]. Nevertheless, setups with L_{start} being approximately two times L_{SBS} can be realized if the SBS-cell is moved from the very center of the start resonator by just a few millimeters. In this case the threshold reduction by BEFWM can still be exploited since the linewidth of the

Brillouin-frequency is big enough to allow for this deviation and the suppression of the SBS is not observed [80, 81]. The reason for the suppression of the SBS, when the SBS-cell is situated in the very center of the start resonator, however, is still obscured.

2.2 Mode-locking

The pulses resulting from a Q-switch as discussed in Section 2.1.3 or similar techniques such as cavity dumping typically have durations in the ns-range. For Q-switching the cavity feedback is turned off during the pump process in order to accumulate a high gain in the laser active material. When the cavity feedback is turned on it takes several resonator round trips for a Q-switch pulse to build up, to deplete the stored energy and to be coupled out of the high quality resonator. In the case of cavity dumping a high photon density is accumulated in a resonator of very high quality and upon switching down the resonator feedback the accumulated photons are suddenly emitted which takes at least a full round trip. Therefore, durations of pulses that originate from these mechanisms are of the same order of magnitude if not longer than the resonator round trip time T, and the repetition rate f at which the pulses occur depends solely on the repetition rate of the switch. In contrast for mode-locking the pulse dynamics are short compared to the resonator round trip time T and the repetition rate f is identical or an integer multiple of the resonator round trip time T.

There are two complementary approaches to describe and to understand mode-locking. In the time-domain approach mode-locking can be understood as a spatial shaping of the instantaneous photon density inside the resonator (see Fig. 2.8). By propagation inside the resonator and by linear output coupling the spatial distribution of the photon density is transformed into a repetitive output signal with dynamics that are short compared to the resonator round trip time T. In the simplest case this would be a single pulse that circulates in the resonator and each time it passes the output coupling mirror a certain portion of the pulse is coupled out. For continuous wave mode-locking these output coupling losses as well as all other losses would be compensated by the gain of the laser active material.
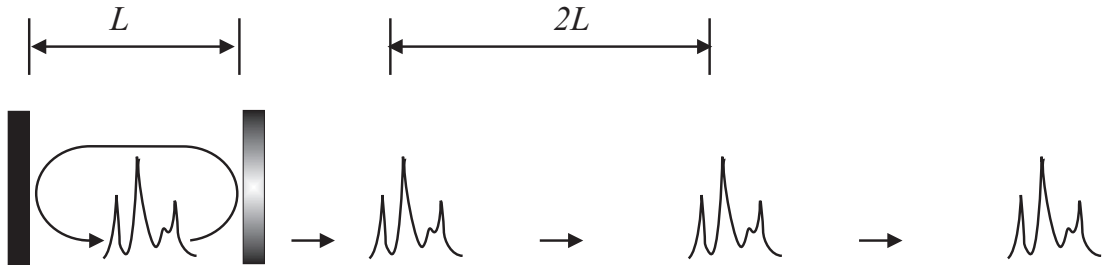
Figure 2.8: Time domain explanation for mode-locking phenomena: Spatially structured photon density in a resonator

In the frequency domain approach we can interpret the dynamics which are short compared to the round trip time as interferences of longitudinal laser modes. The specific temporal shape of the resulting repetitive signal is determined by the relative phase relations and the amplitudes of the occurring modes. In case of random phases random fluctuations of the intensity are obtained. The repetition rate of the occurrence of these fluctuations is governed by the length of the resonator. This can be explained by the fact that the spectral spacing $\Delta\nu = c/2L$ of the longitudinal modes is determined by the length L of the resonator. Therefore, after each period of $1/\Delta\nu$ the set of longitudinal modes that are spectrally spaced by $\Delta\nu$ will have the same relative phase relations again.

In the simplest case the phases of all modes are identical at a certain time (and space along the optical axis). This corresponds to the occurrence of a single pulse revolving in the resonator. A phasor representation of an example of the superposition of three longitudinal modes at different times is depicted in Figure 2.9. The amplitude of each longitudinal mode is represented by the length and the phase by the orientation of the phasor while the phase is normalized to the phase of the center mode. We start with all modes having identical phases (Fig. 2.9 left). In this case the summation of the fields which is illustrated in the bottom line of Figure 2.9 is maximal. If we commence in time the phases of the three modes drift apart until the fields cancel each other out after $t = T/3$ (Fig. 2.9 middle). At $t = T$ the orientations of the phasors of the three modes are again identical resulting in the second maximum of the resulting field amplitude (Fig. 2.9 right).
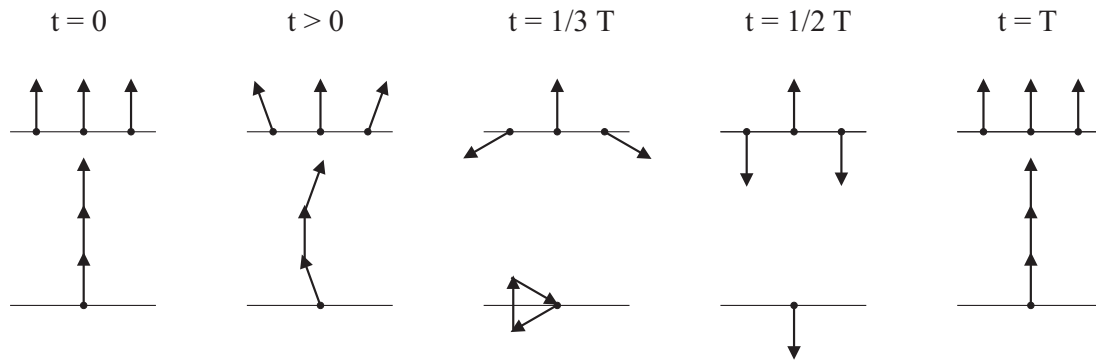
Figure 2.9: Phasor representation of three locked modes and their summation

On the basis of these two complementary pictures — the time domain description and the frequency domain description — the mode-locking dynamics of the SBS-laser will be modeled and numerically simulated in Chapter 4.

There are again two fundamental approaches how mode-locking can be experimentally implemented. Active mode-locking is achieved if an active modulation of the phase, the gain or the loss in the resonator is applied and the modulation frequency is tuned to the round trip time. For passive mode-locking nonlinear effects such as saturable

absorption or second harmonic generation (SHG) are exploited to amplify statistical fluctuations in the photon density. These two concepts to generate mode-locking will be recapitulated in the following two sections. In Section 2.2.3 the possibility of combining mode-locking with Q-switching will be discussed. As mentioned above nonlinear optical effects can be exploited for passive mode-locking. The nonlinear SBS-reflection leads to a shift in frequency of the reflected light, but the phases of the reflected and the incident light remain coupled. Therefore, applied in a resonator an SBS-mirror has the potential to generate phase coupled bandwidth which results in emission dynamics on a ps-timescale. Mode-locking effects offered by the SBS as well as examples of SBS-mode-locking in the literature will be presented in the last section of this chapter.

2.2.1 Active mode-locking

The most straightforward way to obtain mode-locking and consequently emission dynamics on a timescale shorter than the round trip time is to modulate the loss or the gain in the resonator. Both cases are referred to as amplitude modulation. Another possibility is to modulate the optical path length of the resonator which is equivalent to a phase modulation of the light contained in the resonator. Loss modulation as well as phase modulation can for example be achieved by an acousto optic modulator. Gain modulation also referred to as synchronous pumping can conveniently be applied for mode-locking of diode pumped lasers or semiconductor lasers itself by simply modulating the injection current.

Amplitude modulation

Let us assume a sinusoidal modulation of the cavity loss while the frequency of modulation f_m equals the inverse round trip time T^{-1} and start with a homogeneous distribution of the photon density inside the resonator. In the frequency domain picture the homogeneous distribution of the photon density corresponds to the operation of the laser at a single longitudinal cavity mode. After the first round trip the photon density will have a sinusoidal modulation which is equivalent to the superposition of modes that are spectrally spaced by the modulation frequency f_m. So the loss modulation is equivalent to a generation of side modes at either side of the original mode in the spectrum. And since the modulation frequency is chosen to match the longitudinal mode spacing the newly generated modes fall on the adjacent longitudinal cavity modes and can thus be accommodated in the resonator as well.

Since the round trip time matches the modulation period, upon the second pass the peak of the modulated photon density distribution passes the modulator exactly at the time of minimum or zero loss. Hence, the peak passes unattenuated while the edges experience a further attenuation with the result that the evolving pulse experiences a further narrowing. For the spectrum this means that more energy is shifted from the original modes to the side modes and that additional side modes in the spectral distance of $2f_m$ from the original mode are generated.

So with each resonator round trip and with each pass through the modulator the pulse is shortened and the spectrum is widened. The pulse width would approach zero if it was not for the limited bandwidth Δf_g of the gain medium. While the action of the modulator leads to a steady increase in laser bandwidth and a uniform spectral distribution of the energy the spectral distribution of the gain response leads to a discrimination of modes far away from the maximum of this distribution and a preference of the modes closest to it. These two contrary effects lead to a steady state in terms of pulse duration, pulse energy and laser linewidth where the effects of loss modulation and linear resonator losses are exactly balanced by the gain medium.

A very thorough analytical scrutiny of this equilibrium in continuous wave active mode-locking of lasers with a homogeneously broadened gain linewidth was undertaken by Kuizenga and Siegman [82, 83, 84]. They pursued the propagation of a temporally and spectrally Gaussian pulse through a phase modulated or loss modulated resonator and registered all interactions with the gain medium and the modulator, allowing no net change for the complete round trip.

Under the condition that the modulation frequency f_m is small compared to the gain linewidth Δf_g and assuming a spectrally Gaussian gain profile with the unsaturated round trip gain factor G_0 they obtained expressions for the steady state duration τ_{p0} and bandwidth Δf_{p0} of the pulse — both defined by the half intensity points (FWHM) — for the case of amplitude modulation (AM):

$$\tau_{p0}(\mathrm{AM}) = \frac{\sqrt{\sqrt{2}\ln 2}}{\pi} \cdot \left(\frac{G_0}{m_E}\right)^{\frac{1}{4}} \cdot \left(\frac{1}{f_m \cdot \Delta f_g}\right)^{\frac{1}{2}} \tag{2.33}$$

$$\Delta f_{p0}(\mathrm{AM}) = \sqrt{\sqrt{2}\ln 2} \cdot \left(\frac{m_E}{G_0}\right)^{\frac{1}{4}} \cdot (f_m \cdot \Delta f_g)^{\frac{1}{2}}. \tag{2.34}$$

So the pulse can be shortened by enhancing the depth of modulation m_E which is defined by the transmission function $\tilde{t}_{AM}(t)$ of the modulator for the electric field amplitude E:

$$\tilde{t}_{AM}(t) = \exp[-m_E \cdot (1 - \cos\omega_m t)] \quad \text{with} \quad \omega_m = 2\pi \cdot f_m \tag{2.35}$$

$$\approx 1 - m_E + m_E \cdot \cos\omega_m t \quad \text{for} \quad m_E \ll 1. \tag{2.36}$$

The obtained pulse duration is proportional to $m_E^{1/4}$. m_E is linearly proportional to the RF power of acousto optic modulators. Therefore the pulse duration is proportional to the RF power to the power of -1/4. A more efficient pulse shortening in contrast is obtained by increasing the modulation frequency f_m since $\tau_p(AM) \propto f_m^{-1/2}$.

Now the pulse width – bandwidth product can be given for ideal amplitude modulation:

$$\tau_p(\text{AM}) \cdot \Delta f_p(\text{AM}) = \frac{2 \ln 2}{\pi} = 0.440. \tag{2.37}$$

This value for the pulse width – bandwidth product is the smallest possible for Gaussian pulses and corresponds to the case with no chirp generation in the resonator. A chirped pulse exhibits a continuous shift in oscillation frequency throughout the pulse. Thus, the color of the front edge of a chirped pulse is different from the back edge. By ideal sinusoidal amplitude modulation no such chirp is obtained. Pulses that have a pulse width-bandwidth product close to the ideal case are called transform limited pulses.

As indicated above these results apply to lasers with homogeneously broadened gain linewidths only. Lasers with a prevailingly inhomogeneous gain distribution such as gas lasers in the visible or near IR typically run on a large number of longitudinal resonator modes already in order to deplete the complete gain linewidth. In this case the modulators task is just to synchronize all the laser lines, or in other words, to lock their phases rather than to generate bandwidth. Hence, for inhomogeneously broadened lasers the demand on modulation depth is low and the pulse width is predominantly determined by the gain linewidth Δf_g [84]:

$$\tau_p(\text{inhomogeneous}) \approx \frac{0.5}{\Delta f_g} \approx \frac{0.5}{N_0 \cdot f_m}. \tag{2.38}$$

Here N_0 is the number of oscillating modes and f_m is the modulation frequency which is equivalent to the repetition rate.

The fact that the amplitude modulation leads to the generation of bandwidth becomes apparent if the transmission function (2.36) is applied to an electric field $E(t) = E_0 \cdot e^{i\omega t}$ and by use of the relation $\cos \alpha = \frac{1}{2}(e^{i\alpha} + e^{-i\alpha})$:

$$E'(t) = E(t) \cdot \tilde{t}_{AM}(t) \tag{2.39}$$

$$\approx (1 - m_E) \cdot E_0 \cdot e^{i \cdot \omega t} + \frac{m_E \cdot E_0}{2} \cdot \left[e^{i(\omega + \omega_m)t} + e^{i(\omega - \omega_m)t} \right]. \tag{2.40}$$

While the input frequency ω is diminished by a fraction corresponding to the modulation depth m_E, new sidebands are generated at a distance corresponding to the modulation frequency ω_m at either side of the input frequency.

Phase modulation

Just like the modulation of the resonator loss a modulation of the phase of the light contained in the resonator can lead to the generation of short pulses [85]. However the

underlying mechanism is not as obvious as for the AM case. For the case of phase modulation the transmission of the modulator can be expressed similar to the transmission of the AM-modulator in Equation 2.35 by the complex transmission function $\tilde{t}_{FM}(t)$ for the electric field amplitude E:

$$\tilde{t}_{FM}(t) = \exp[i \cdot m_E \cdot \cos \omega_m t] \tag{2.41}$$

$$\approx 1 + i \cdot m_E \cdot \cos \omega_m t \tag{2.42}$$

$$= 1 + i \cdot \frac{m_E}{2} \cdot \left[e^{i\omega_m t} + e^{-i\omega_m t} \right]. \tag{2.43}$$

In fact the modulation of the phase is equivalent to modulating the optical path length of the resonator, or literally, to a back and forth movement of a cavity mirror with a period corresponding to the resonator round trip time. Light which is reflected at the moving mirror experiences a Doppler-shift in frequency, while the sign and the amount of the shift depends on the phase of the mirror movement. If the shift in frequency does not correspond to a multiple of the longitudinal mode spacing the frequency shifted light experiences severe losses. The periodic shift in frequency leads to the formation of a pulse that passes the modulator i.e. hits the mirror at one of its extremal positions where the frequency shift is zero and hence the effective resonator loss becomes minimal. It is therefore equivalent to the short pulse passing the amplitude modulator at minimum loss and similarly for cw-operation an equilibrium is reached when the bandwidth increasing effect of the phase modulator is compensated by the limitations of the gain linewidth.

Contrary to the loss modulation two time slots for the pass of the pulse are possible — at either turning point of the mirror — and in fact for the phase modulated operation the pulse can switch between both positions. Less often pulses occur at both instances simultaneously.

Another consequence of the periodic phase or frequency modulation is that the resulting pulse exhibits a chirp meaning that the frequency shifts in the course of the pulse. An example for a chirped pulse is depicted in Figure 2.10.

Similarly to the amplitude modulation the steady state solutions for the pulse width τ_p and bandwidth Δf_p for the case of phase modulation (FM) can be derived [82, 83]:

$$\tau_p(\text{FM}) = \frac{\sqrt{2\sqrt{2}\ln 2}}{\pi} \cdot \left(\frac{g_0}{m} \right)^{\frac{1}{4}} \cdot \left(\frac{1}{f_m \cdot \Delta f_g} \right)^{\frac{1}{2}} \tag{2.44}$$

$$\Delta f_p(\text{FM}) = \sqrt{\sqrt{2}\ln 2} \cdot \left(\frac{m}{g_0} \right)^{\frac{1}{4}} \cdot (f_m \cdot \Delta f_g)^{\frac{1}{2}}. \tag{2.45}$$

Comparing these results with (2.33) and (2.34) we see that only the expression for the pulse width differs by a factor of $\sqrt{2}$. Accordingly the pulse width – bandwidth
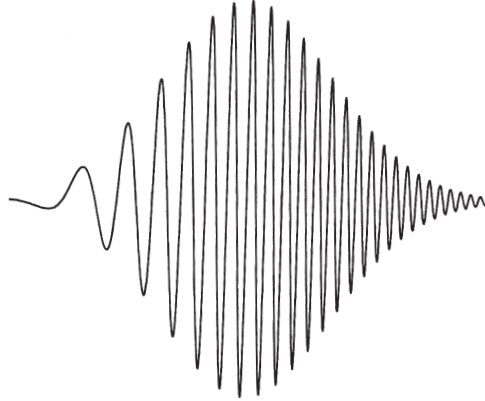
Figure 2.10: Example of the field distribution of a pulse with a strong chirp

product is larger by the same factor:

$$\tau_p(AM) \cdot \Delta f_p(AM) = \frac{2\sqrt{2}\ln 2}{\pi} = 0.626. \tag{2.46}$$

The main distinguishing fact between AM mode-locking and FM mode-locking is that phase modulation leads to chirped pulses which have a larger pulse width − bandwidth product. These pulses are not ideally compressed, but for ideal phase modulation the frequency chirp is linear and the pulses can easily be further compressed by optical devices that have a group velocity dispersion that is complementary to the linear chirp of the pulse. By these means FM mode-locking can still issue transform-limited pulses.

2.2.2 Passive mode-locking

In most cases passive mode-locking is achieved by the use of saturable absorbers. In order to explain how their nonlinear absorbtion leads to the generation of short pulses let us assume an arbitrary photon density distribution revolving in a resonator and showing statistical fluctuations. If we now introduce a nonlinear saturable absorber peaks in the intensity distribution will experience lower attenuation compared to the mean intensity because of the saturation of the absorber. Since the recovery time and the saturation fluence of the gain medium are typically larger by orders of magnitude compared to those of the absorber the amplification can in a first order approximation be considered as linear. Therefore, upon each pass through the amplifier and absorber the low intensity parts will be attenuated compared to the peaks until only the highest peak of the intensity distribution that experiences the lowest losses prevails.

In general there are two kinds of absorbers that are distinguishable by their saturation behavior: fast saturable absorbers and slow saturable absorbers. Fast saturable

absorbers are characterized by a recovery time T_1 that is short compared to the pulse width τ_p. In this case the absorber is saturated by the instantaneous intensity of the pulse [86]. The instantaneous transmission depends only on the incident intensity. The peak of a pulse for instance will experience lower losses than the edges. As a result the edges are cut off and the pulse is shortened. The transmitted intensity distribution $I_2(t)$ for an arbitrary incident intensity distribution $I_1(t)$ can then be calculated by [87]

$$\ln \frac{I_2(t)}{I_1(t)} + \frac{I_2(t) - I_1(t)}{I_{sat}} = \ln T_0. \tag{2.47}$$

Here the saturation intensity I_{sat} and the small signal transmission or unsaturated transmission T_0 are the characteristic constants of the absorber.

Slow saturable absorbers in contrast have a recovery time T_1 that is long compared to the pulse width τ_p. Accordingly, the saturation is a process that integrates the intensity over the time and is therefore achieved by the incident energy rather than by the instantaneous intensity [88]. For the case of slow saturable absorbers the transmission $I_2(t)$ of an arbitrary incident intensity distribution $I_1(t)$ can implicitly be calculated using

$$\frac{I_2(t)}{I_1(t)} = \frac{T_0 \cdot \exp[U_1(t)/U_{sat}]}{1 + T_0[\exp[U_1(t)/U_{sat}] - 1]} \tag{2.48}$$

with $U_{sat} = I_{sat} \cdot T_1$ and $U_1(t) = \int_{-\infty}^{t} I_1(t)dt$. As a consequence of this energy integration the leading edge provides the energy for the saturation of the absorber and experiences a significant attenuation while the trailing edge passes the absorber unchanged. As a result an asymmetry is forced upon the pulses generated by slow saturable absorbers which typically exhibit steep slopes at the front edges and rather gentle trailing edges.

One pronounced advantage of passive over active mode-locking is that the modulation frequency and thus the repetition rate inherently equals the round trip time of the resonator. In contrast to active mode-locking there is no need of a length tuning of the resonator. Contrarily, the cavity length can be chosen according to the desired repetition rate and pulse energy if a suitable absorber is available. Probably the most important advantage is that passive mode-locking can result in considerably shorter pulse durations than active mode-locking. The reason for this circumstance is that the temporal loss function of the absorber adapts to the incident temporal pulse shape. So the pulse is shortened by a fixed ratio for each pass through the absorber independent of the pulse width already achieved. For active loss modulation the temporal loss function is fixed and hence the pulse shortening effect will decrease the shorter the pulses get.

The major drawback of passive mode-locking is that its control is rather challenging and that the parameter space in which the saturable absorber produces satisfying results is very limited. If, for instance, the intensity in the cavity is too high the saturation of the absorber is reached very early and therefore the modulation depth becomes

negligible. If the intensity is too low or the saturation fluence too high, no saturation and therefore no mode-locking will be achieved. One particular problem in this context is the occurrence of so called Q-switching instabilities: Besides the mode-locking effect of a saturable absorber it also introduces a tendency for Q-switching that can surface as a jitter in pulse energy and repetition rate, as simultaneous Q-switching and mode-locking (QML-regime) or for short cavities also as a pure Q-switch.

It affords a thorough choice and balance of the involved characteristics of the gain medium, the saturable absorber and the resonator cavity to obtain pure cw-mode-locking from a saturable absorber. Such characteristics are the relaxation times and saturation energies for both gain medium and saturable absorber, pump rate, initial transmission, linear cavity losses and cavity length. Since for most applications cw-mode-locking is desired, the limits which separate the mode-locking regime from the QML-regime are very well explored theoretically by a perturbation analysis of the rate equations [89]. The essential conclusion which was experimentally validated [90] is that perturbations are damped and therefore stable cw-mode-locking can be expected, if

$$E_p > (E_{sat,L} \cdot E_{sat,A} \cdot \Delta R)^{1/2} = (F_{sat,L} \cdot A_{eff,L} \cdot F_{sat,A} \cdot A_{eff,A} \cdot \Delta R)^{1/2}. \quad (2.49)$$

Here E_p is the intra cavity pulse energy, $E_{sat,L}$ and $E_{sat,A}$ are the saturation energies of the laser gain material and the absorber and ΔR is the maximum change in reflectivity of a semiconductor saturable absorber mirror (SESAM) and in general represents the modulation depth. $F_{sat,L}$ and $F_{sat,A}$ are the saturation fluences and $A_{eff,L}$ and $A_{eff,A}$ the effective mode cross sections at the gain medium and the absorber respectively.

Power scaling of short pulsed cw-mode-locked lasers is still a problem [91]. One of these problems arises from the demands on the gain medium, that has on the one hand to provide sufficient bandwidth to allow for short pulses and on the other hand to have good thermal properties as well as a large emission cross section to allow for high average powers. Good thermal properties of the laser material are important to sustain good beam quality. It is vital to have excellent beam quality since higher transverse spatial frequencies in the field distribution would be disturbing for the mode-locking considering the nonlinear absorbtion.

A further issue of power scaling are the saturable absorbers that have to withstand the high peak and average powers. A saturable absorber can consist of either a gas, a liquid such as a dye solution or a solid state material. For high average power solid state lasers Cr-doped YAG, as well as SESAMs are very popular since they offer high damage thresholds. Recently, carbon nanotubes have been tried as saturable absorbers for mode-locking and have exhibited promising characteristics in terms of damage threshold and cost efficiency [92]. With an Yb:YAG thin-disk laser oscillator and applying a SESAM, 16 W of average power at pulse durations of 0.7 ps were demonstrated [93]. 27 W of average output power with pulse durations of 19 ps and 0.5 μJ pulse energy were demonstrated for an oscillator with three Nd:YAG rods and again using a SESAM for mode-locking [94]. Today, for average powers and pulse energies of short pulsed lasers in excess of those mentioned, master oscillator power amplifier concepts are implemented.

Alternative techniques for passive mode-locking to the use of saturable absorption are nonlinear mirror (NLM) mode-locking [95] and Kerr lens mode-locking. The NLM used for mode-locking replaces the output coupler and consists of a frequency doubling nonlinear crystal and a dichroic mirror that partially reflects the fundamental wave but totally reflects the second harmonic beam. The fundamental wave that passes the nonlinear crystal is partially transformed into the second harmonic. The second harmonic is totally reflected at the dichroic mirror and if it experiences a proper phase shift with respect to the fundamental wave it is almost completely retransformed into the fundamental wave upon the second pass of the crystal. Since the second harmonic generation is a second order nonlinear effect and is thus strongly intensity dependent we obtain an intensity dependent overall reflection of the nonlinear mirror that leads to passive mode-locking.

Kerr media exhibit an intensity dependent index of refraction that leads to a lensing effect for high intensity pulses. If a Kerr medium and an aperture are introduced into a resonator, high intensity pulses experience lower losses at the aperture thanks to the stronger focussing compared to low intensity pulses.

An additional section will be devoted to the discussion of the mode-locking effects of nonlinear mirrors based on stimulated Brillouin scattering (see Section 2.2.4).

2.2.3 Transient mode-locking

As already indicated in the previous section it is likely to obtain mode-locking and Q-switching at the same time if saturable absorbers are used for mode-locking. Since in most cases actually cw-mode-locking (cw-ML) is desired simultaneous mode-locking and Q-switching (QML) is in this context also referred to as Q-switching instabilities. QML yields bursts of ultra-short mode-locked pulses underneath the envelope of a Q-switch pulse and the individual pulses are spaced according to the round trip time T. Compared to a simple Q-switch QML leads to considerably higher peak powers and in contrast to the cw-mode-locking QML can still issue mode-lock pulse energies in the mJ-range. It is thus a very elegant way to combine high pulse energies with ps-pulse durations from a laser oscillator. To obtain comparable pulse energies from a cw-mode-locked system typically several amplification stages have to be used to amplify the limited pulse energy of cw-ML oscillators to the desired energy range.

The first report on simultaneous mode-locking and Q-switching was published in 1965 by Mocker and Collins [96]. They used cryptocyanine as a saturable absorber to mode-lock and Q-switch a ruby laser. More recent implementations of QML in solid state lasers predominantly apply solid state materials as saturable absorbers. In most publications just one absorber is used to generate the mode-locking and the Q-switching as well. The most popular materials today in particular for YAG-lasers are doped YAGs such as Cr^{4+}:YAG [97, 98, 99, 100, 101] and V^{3+}:YAG [102, 103] because of their high damage thresholds and good thermal properties. Furthermore, they can be conveniently bonded to YAG laser crystals [100]. Another favored materials class for saturable absorbers are semiconductors due to their large bandwidth and their wide

tuning range [104].

Examples of QML operation by nonlinear mirror mode-locking yielding peak pulse powers of up to 341 kW were demonstrated by Datta et al. [105, 106]. An example where Q-switching is achieved by saturable absorption while mode-locking is done by the nonlinear mirror technique is given in [107].

Common to all these examples of QML operation are pulse trains with single pulse durations of 100 to a few 100 ps and single pulse energies in the μJ-range. Therefore, the peak pulse power does not exceed the kW-regime. Higher pulse energies are gained from active Q-switching. In [108] Jones and Palmer present a laser which is actively mode-locked by an AOM and Q-switched by a Pockels cell. This laser issues 60 ps pulses with up to 10 mJ of single pulse energy. Another yet unsatisfying feature of the QML-operation generated by a single saturable absorber is its lack of reliability that may surface in the various systems either as time and energy jitter or an incomplete modulation depth. More stable operation is obtained if either mode-mocking or Q-switching or both are implemented or at least supported by an active switching [109].

One challenge which typically arises for QML is to reach steady state pulse durations τ_{p0} as given by Equation 2.33. The reason why they will in general not be reached is that the build up of the mode-lock pulses from noise can only start as soon as the Q-switch opens and the build up time of the Q-switch pulse is usually to short to allow for enough passes through the modulator to reach steady state conditions [111]. In the early phase of the pulse build up, when the bandwidth of the pulse is small enough so that it is not affected by the gain linewidth, the pulse duration τ_p can be determined by using

$$\tau_p(\text{QML}) = \sqrt{\frac{\ln 2}{2} \cdot \frac{1}{\pi} \cdot \frac{1}{f_m \sqrt{m \cdot M}}} \tag{2.50}$$

where M is the number of round trips that occur during the build up of the Q-switch pulse. Since this time is typically by far longer than the duration of the Q-switch pulse itself, the mode-locked pulse duration does not change significantly in the course of the Q-switch pulse. As the pulse width of the mode-locked pulses approaches steady state conditions the influence of the limited gain linewidth has to be considered. The pulsewidth is then given by

$$\tau_p(\text{QML}) = \frac{\tau_{p0}}{[\tanh(M/M_0)]^{1/2}} \quad \text{with} \quad M_0 = \frac{1}{4\sqrt{m \cdot G_0}} \cdot \frac{\Delta f}{f_m}. \tag{2.51}$$

One possible way to approach steady state pulse durations in the QML-regime is to allow a prelasing before the Q-switch occurs and during which the mode-locking can settle to steady state conditions. This can be conveniently achieved in the case of an active Q-switch [108, 111].

Another typical feature of the QML-regime which can be considered a drawback is the variation of the mode-lock pulse energy following the Q-switch envelope. Since

for many laser applications a constant pulse energy is wanted this particular feature prevents the use of QML-lasers despite their efficient generation of ps-pulses with high energies. A very elegant way to overcome both above mentioned restrictions — reaching steady state pulse durations and constant pulse energies — is to introduce a cavity dumping in addition to the mode-locking and Q-switching. In the implementation of Hays et al. [110] the oscillation starts in a cavity with a low quality. In this prelasing mode the mode-locking can be established. After around $500\,\mu$s the steady state pulse duration is reached and the quality of the resonator is actively switched to maximum by an AOM. Now the short pulse can efficiently deplete the gain and accumulate energy which takes just a few round trips in the cavity. After this time the pulse is emitted by cavity dumping via an additional Pockels cell and polarizer. By these means pulses as short as $90\,$ps with pulse energies of up to $1\,$mJ could be obtained from a single Nd:YAG oscillator.

2.2.4   SBS-mode-locking

The potential of stimulated Brillouin scattering for the efficient generation of bandwidth in order to create short pulses from a single mode pump beam has already been discussed [112, 113] and implemented [114, 115, 116] in the 1970s and early 1980s. In these concepts a Brillouin scattering medium is placed inside a conventional resonator. The actual phase-locking of the occurring modes has been achieved by the introduction of either a saturable absorber [116] or an active loss modulator [115]. Self-locking of several frequency shifted modes by stimulated scattering was observed in [117], however the mechanism for the synchronization remains obscure since no effect of length tuning of the cavity i.e. on the repetition rate was observed.

Damzen et al. followed a very similar approach. They used a passive external cavity [118] consisting of a conventional mirror and a nonlinear mirror on the basis of the stimulated Brillouin scattering (see Fig. 2.11) to generate bandwidth and to mode-lock the output from a narrow bandwidth pulsed oscillator. In this less complex case of a single cavity the occurring interactions between the input beam, the cavity modes and the Stokes modes are more transparent.

The pump pulse is inserted into the cavity through the conventional mirror. When the pulse hits the SBS mirror the acoustic wave is build up as discussed in Section 2.1.1 and the reflectivity increases. Upon reflection at the SBS-mirror the light is frequency shifted and if the resonator length obeys Equation 2.31 the frequency shifted modes can be accommodated in the resonator as well. With each additional round trip a new Stokes order is generated resulting in a large number of modes contained in the resonator simultaneously. These modes are synchronized due to the small bandwidth of the input beam and because their delay time (round trip time) is matched to their frequency spacing. The superposition of a large number of synchronized modes with a regular spectral spacing results in the formation of short pulses that revolve in the resonator. If the Stokes-shift matches the spectral distance of cavity modes just one pulse is formed. In this case the repetition rate is governed by the resonator round trip time which is
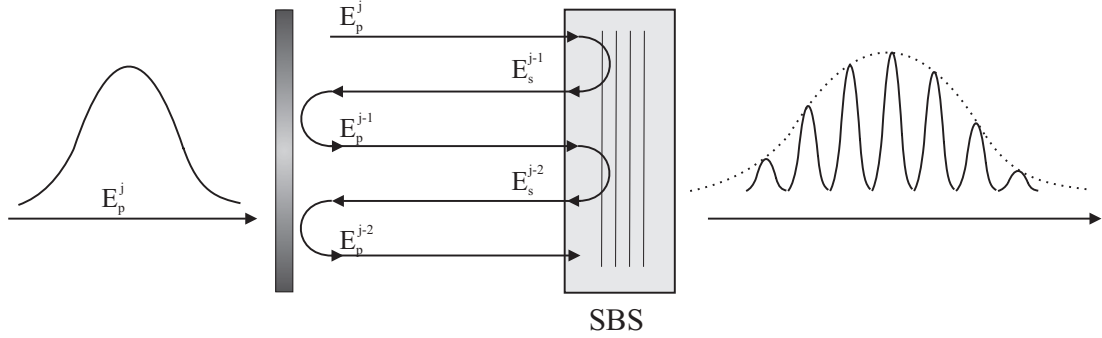
Figure 2.11: Setup and mechanism of external SBS-mode-locking of a small bandwidth input pulse according to [118]

identical to the Stokes-shift. If the Stokes-shift is a multiple of the mode spacing several pulses circulate simultaneously in the resonator and accordingly the repetition rate is determined by the Stokes-shift. So the incident pump pulse is split up into a train of mode-locked pulses where the shape of the pulse train envelope is determined by the input pulse on the one hand and the quality of the external SBS-resonator on the other hand. In [25] this concept was extended to a regenerative amplifier by the introduction of a gain medium into the SBS-cavity.

In the linear SBS-laser the above discussed mechanisms apply as well. The shift of the center frequency of the output of a linear SBS-laser throughout the passive Q-switch pulse was measured in [77] and in fact the frequency shift per round trip amounts to the Brillouin-frequency. With each round trip in the SBS-resonator a new Stokes order is generated while the initial modes are preserved if they transmit the SBS-mirror and are contained in the start-resonator. If both, the start resonator and the SBS-resonator modes, are tuned to the Brillouin-frequency the coupling between these modes that results from their identical origin is maintained. However we do not have a single mode input beam as for the external SBS-mode-locking in [118] but the oscillation starts from spontaneous emission noise. Therefore, in general we will not inherently have a coupling between all modes, but there will be several sets of coupled modes while these sets are not mutually coupled due to their independent origin. A thorough numerical analysis of the mode-evolution of a mode-locked SBS-oscillator will be pursued in Section 4.3 while realistic starting conditions for this calculation could be deduced from experimental investigations of the spectrum of this laser (Section 3.4).

To summarize the above discussed mechanisms of SBS-mode-locking the SBS-Stokes-shift leads to the generation of additional modes that are coupled to the original mode due to their common origin. But there is yet another feature of SBS that can lead to mode-locking namely its nonlinear reflectivity. If an SBS-mirror is applied as a resonator mirror of an oscillator the time and intensity dependent reflection leads to a modulation of the resonator loss similar to a saturable absorber. A high intensity input pulse will

result in a high SBS-reflection and therefore experience low losses. This passive mode-locking effect of the SBS-reflection and its dependence on the phonon lifetime will also be investigated by numerical calculations and presented in Section 4.3.5.

Chapter 3

Experimental results

3.1 Laser resonator setup

The mode-locked SBS-laser was implemented in two different setups that utilize different Nd:YAG laser heads. The first contains a flash lamp-pumped rod in a double elliptical cavity and supplies pump pulse energies of up to 11 J. The rod dimensions are 100 mm in length and 6.35 mm in diameter and the doping level is 0.85 %. The second system consists of a diode side-pumped rod with a diameter of 5 mm, a length of 120 mm and which is endowed with a maximum pump power of 3600 W for a maximum pump duty cycle of 20 %. The Nd-dopant concentration is 0.9 %. A sketch of the setup of the SBS-laser resonator and the calculated distribution of the transverse fundamental eigenmode of the implementation using the flash lamp pumped laser head is given in Figure 3.1. The distribution of the eigenmode for the setup with the diode pumped laser head is qualitatively identical but with slightly smaller beam widths at the position of the laser rod.

The start resonator is formed by the concave output coupler with a reflectivity of $R_{OC} = 70\,\%$ and a radius of curvature of 500 mm and the plane start resonator mirror with a reflectivity R_{start} which is varied according to the desired start resonator loss as will be discussed in Section 3.2.1. As a material for the nonlinear SBS-mirror SF_6 at a pressure of 20 bar is used. The gas is contained in a 15 cm long brass tube with windows on either ends. Its rear window (farther away from the output coupler) is tilted by an angle of 5 degrees to prevent interferences between the windows and any disturbing back-reflections into the region of SBS-reflection. The front window is a lens L_1 with a focal length of 100 mm. Together with a second lens L_2 of equal focal length that is placed outside the SBS-cell it forms a telescope that generates a focus inside the SBS-cell (see Fig. 3.1).

Figure 3.2 shows the beam width at the position of the laser rod as a function of the pump power. Two stability ranges can be clearly distinguished. The first stability range at lower pump powers corresponds to an eigenmode with a focal spot at the output coupler. The eigenmode depicted in Figure 3.1 corresponds to the operation in
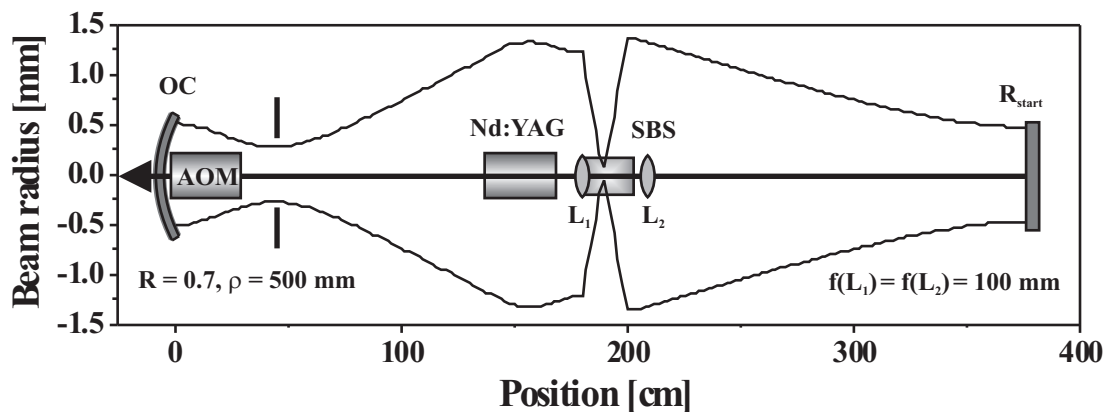
Figure 3.1: Schematic setup of the SBS-laser resonator and the distribution of its transverse fundamental eigenmode

the second stability range at a pump power level as indicated by the arrow. To prevent an operation in the first stability range and a focusing on the output coupler during the build up of the thermal lens a pinhole is placed at the focal spot in the eigenmode of the second stability range in the vicinity of the output coupler (see Fig. 3.1) [119]. Another purpose of the pinhole is to allow for an operation of the transverse fundamental eigenmode (TEM$_{00}$) only.
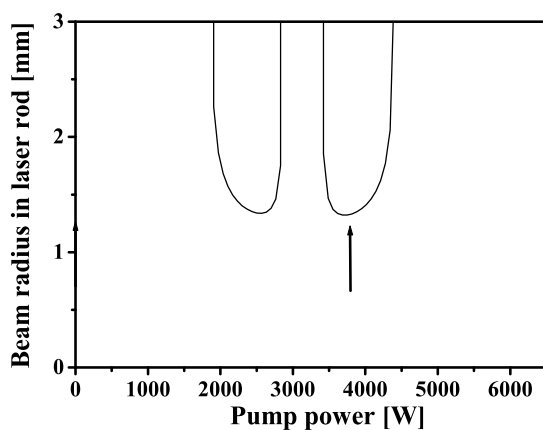
Figure 3.2: Stability range of the SBS-laser using the flash lamp pumped laser head; arrow indicates the pump power level corresponding to the eigenmode as depicted in Fig. 3.1

The SBS-cell with lens L$_1$, lens L$_2$ and the start resonator mirror are mounted in a way that they can be moved along the axis of the resonator. Thus the SBS-resonator

length as well as start-resonator length can be independently tuned. The distance between L_1 and L_2 is an additional free parameter that determines the lateral position of the stability range in the graph presented in Figure 3.2 [120, 121] so that the pump power can be arbitrarily chosen within a range of a few kWs for the flash lamp pumped system.

For an optimal mode-locking effect the AOM has to be placed next to one of the resonator mirrors. Since it is supposed to modulate the loss in the SBS- and the start resonator simultaneously it is placed close to the output coupler.

For the layout of the resonator lengths — both for the start and for the SBS-resonator — several aspects have to be considered: As mentioned before the SBS-reflected light experiences a shift in frequency. Thus, if the frequency shifted light should still be accommodated in the resonator the shift in frequency has to be an integer multiple of the longitudinal mode spacing. In other words the resonator length has to be a multiple of the Brillouin-length L_B which corresponds to the Brillouin-frequency ν_B by $L_B = c/2\nu_B$. The Brillouin-frequency of SF_6 at 20 bar is 240 MHz, so the fundamental resonator length according to the SBS is 62.5 cm.

The second aspect to be considered relates to the mode-locking. If active mode-locking is desired the resonator's longitudinal mode spacing has to be tuned to the modulation frequency of the AOM, too. The AOM (IntraAction ML-414D) is driven at an acoustic frequency of 40 MHz resulting in an optically effective modulation frequency of 80 MHz. This finally leads to a fundamental resonator length according to the mode-locking of 187.5 cm. Since this is exactly three times the Brillouin-length the resonator length tuning for the SBS is always given if the mode-locking condition is fulfilled. For optimal mode-locking this requirement has to be met by both resonators, the SBS-resonator as well as the start resonator. The matching of the longitudinal mode spacing of the start resonator is in this case also vital for the SBS-Q-switching: The SBS-threshold for SF_6 is too large to accomplish a self starting SBS-process in an oscillator from the acoustic noise [80]. Thus an initial sound wave has to be build up in the SBS-material by Brillouin enhanced four wave mixing (BEFWM) [78] of the back and forth traveling waves in the start resonator with the result of a considerable reduction of the SBS-threshold for the incident light (see also Section 2.1.3). To achieve an efficient initiation of the sound wave by the beat mode of the start resonator modes their spectral spacing has to be resonant with the Brillouin-frequency of the SBS-material. Thanks to the circumstance that the Brillouin-frequency is an integer multiple of the modulation frequency this is always provided if the mode-locking condition is met. The optical SBS-resonator length is chosen to equal the fundamental resonator length as determined by the mode-locking condition of 187.5 cm and the start resonator to be twice this long.

If we consider the indices of refraction of the 10 cm Nd:YAG rod ($n_{Nd:YAG} = 1.82$) and the silica crystal of the AOM of 6 cm length ($n_{SiO2} = 1.5$) we obtain a geometrical length of the start resonator of 363.8 cm. The length tuning of both cavities did turn out to be critical for this setup. The length tuning of the start resonator for the resonant initiation of the sound wave by BEFWM is known to be tolerant in the order of a few cm [77]. The demands on accuracy of the length tuning for the active mode-locking

is dependent on the duration of the pulses that are to be generated. In this case the resonator mirror can be moved a few mm until more distinct pulse shape distortions are observed.
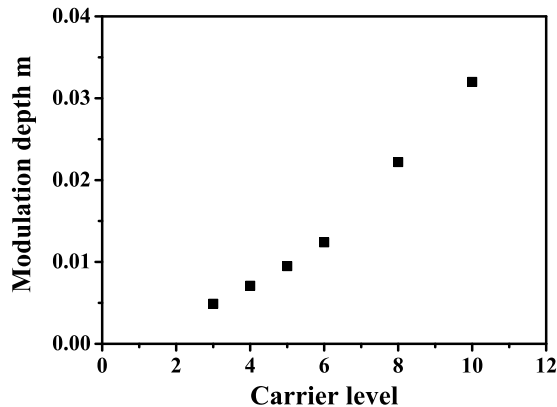
Figure 3.3: Dependence of modulation depth m on carrier level of AOM driver

While the modulation frequency of the AOM is fixed to 80 MHz the depth of the loss modulation can be controlled via the carrier level (CL) of the AOM-driver. To characterize the dependence of the temporal loss function on the CL the transmission of the output of a very stable single frequency nonplanar ring oscillator (NPRO) through the AOM was investigated. The depth of modulation m as defined by

$$I(t) = I_0 - m \cdot I_0 \cdot \frac{\sin(\omega t) + 1}{2} \tag{3.1}$$

was evaluated for several carrier levels and the results are depicted in Figure 3.3. Here I_0 is the continuous wave incident intensity and $I(t)$ the transmitted intensity modulated by the AOM. Therefore the maximum modulation depth amounts to 3 %. Note that this modulation depths m and m_E as defined in Equation 2.35 differ. While m is the full depth of modulation of the transmitted intensity m_E is the modulation amplitude of the transmitted electric field. Therefore, m is equivalent to $4\,m_E$.

3.2   SBS-laser operation

One motivation for the use of an SBS-mirror in laser oscillators or master oscillator power amplifiers (MOPAs) is the phase conjugating reflection that is inherent to the SBS-mirror as described in Section 2.1.2. The phase conjugating reflection leads to a compensation of phase distortions as for instance induced by aberrations of the thermal lens [55]. Therefore SBS-lasers typically issue high quality beams even at considerably high average output powers [120, 121].

Still the thermal impact on the laser rod is the limiting aspect for power scaling. The thermally induced birefringence finally culminates in the separation of the stability ranges for the radial and the tangential polarization. As a result the laser is compelled to operate in either the radial or the tangential polarization and the linear polarization is prevented. Since the SBS is most efficient for linearly polarized beams the SBS and the phase conjugation are disturbed. Therefore an apparent degradation of the beam profile due to thermal aberrations coincides with the surfacing of instabilities of the passive Q-switch. As mentioned above the SBS-laser was set up twice with two alternative laser heads. With the flash lamp pumped laser head problems due to the thermal impact occur for average output powers in excess of 6 W. Due to the higher pump efficiency of laser diodes the thermal load for the diode pumped laser head is not as high. Here average output powers of 10 W can be obtained before a beam degradation becomes apparent.
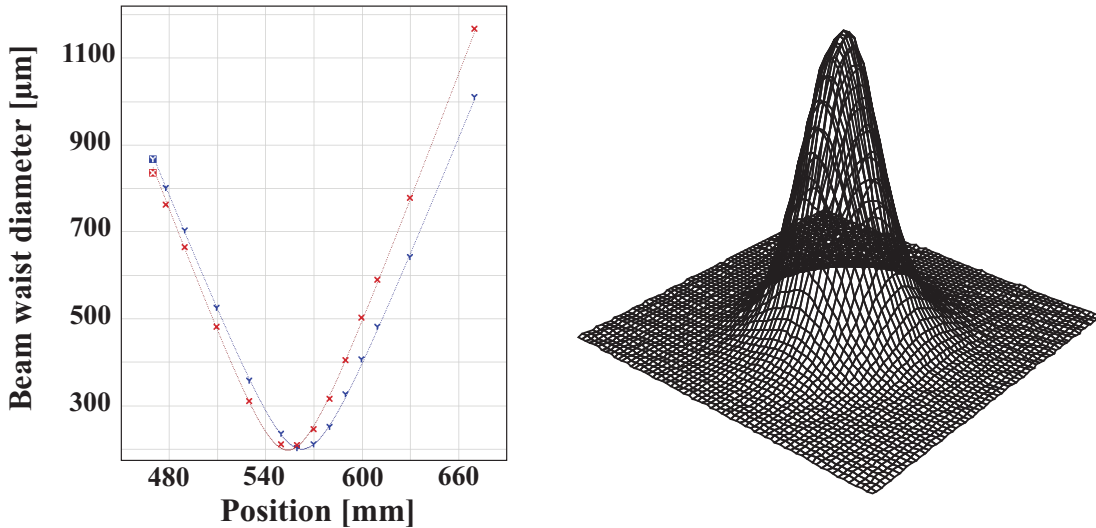
Figure 3.4: Caustic of the M^2-measurement (left) and 3 dimensional display of the beam profile (right)

The M^2-number of the laser was determined with a beam propagation analyzer (Spiricon M^2-200). A caustic and a representative beam profile are depicted in Figure 3.4. The caustic exhibits a small astigmatism that may be attributed to the AOM crystal that is aligned in a Brewster angel to the optical axis of the resonator. In the whole regime of stable Q-switch operation the M^2-value was measured to be better than 1.4.

3.2.1 Tailored Q-switch pulse trains

As discussed in Section 2.1.3 the linear SBS-oscillator inherently operates in a passively Q-switched fashion due to the nonlinear reflection of the SBS-mirror. Since the

SBS-mirror is transparent for low incident intensities the oscillation arises in the start resonator. With increasing intensity in the start resonator the sound wave is efficiently generated and the SBS-reflectivity increases quickly. Simultaneously the oscillation switches from the long and low quality start-resonator to the comparatively short and high quality SBS-resonator where the stored inversion can be quickly depleted.

After the emission of the first Q-switch pulse, the SBS-resonator gets below lasing threshold due to the profound depletion of the laser material. Now inversion can be accumulated again until the laser threshold for the start resonator is reached and the next Q-switch pulse arises from a spike in the start resonator. Hence several Q-switch pulses can be emitted in quick succession within a single pump pulse. Thereby bursts of pulses are emitted by the laser. The temporal distance between the pulses and thus the number of pulses in a burst is determined by the pump parameters on the one hand and the quality of the start resonator on the other hand. For a high loss factor V it takes a longer pumping period until lasing threshold is reached since the gain that satisfies the second laser condition (2.24) is higher. Thus the time between the pulses will be longer and for a given pump pulse duration and intensity, the number of pulses will be smaller for high start resonator losses.
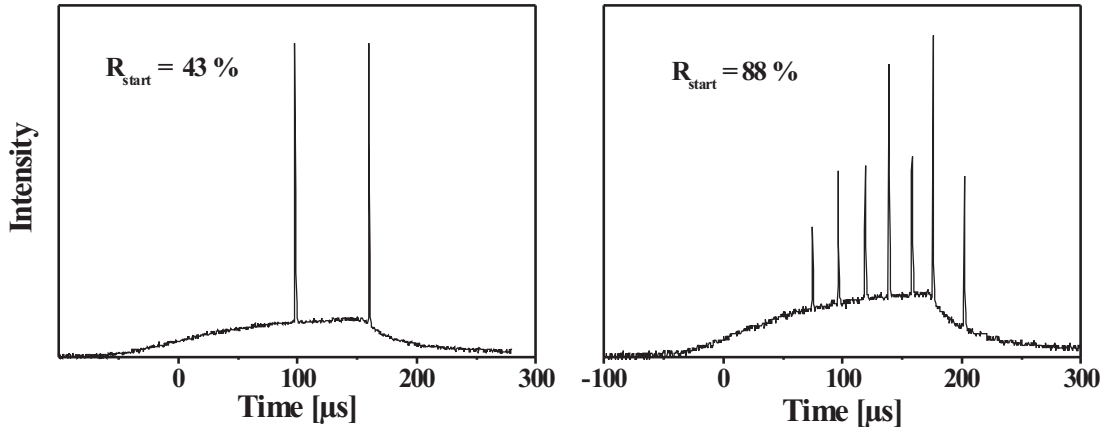
Figure 3.5: Two different Q-switch pulse trains for different R_{start}; underground represents the flash lamp pump pulse

The quality of the start resonator is typically tuned by means of altering the start resonator mirror reflectivity R_{start}. Figure 3.5 shows two examples of pulse bursts where the only difference with regard to setup and operation lies in different R_{start}. The signal of the pulses is superimposed to the signal of the flash lamp pump pulse to give a reference for the timing. A low start resonator mirror reflectivity ($R_{start} = 43\%$) results in the emission of just two pulses in an interval of about $60\,\mu s$ while for the same pump parameters 7 pulses spaced by approximately $25\,\mu s$ are obtained if R_{start} is chosen to be 88%. For the flash lamp pumped laser head the temporal spacing between the pulses of a burst varies from pulse to pulse because of the time dependent emission

characteristics of the flash lamps.

The start resonator loss not only influences the number of pulses and their temporal spacing. A higher gain in the laser material at the time of the switch as a consequence of higher start resonator losses naturally leads to higher pulse energies. Also, the higher the gain at the instance of the switch the quicker can the stored inversion be depleted. Therefore, an enhancement of the start resonator loss results in shorter pulses of higher energy. To summarize, a low quality of the start resonator leads to a small number of short pulses of high energy while a high quality results in an emission of a large number of longer low energy pulses in quick succession.
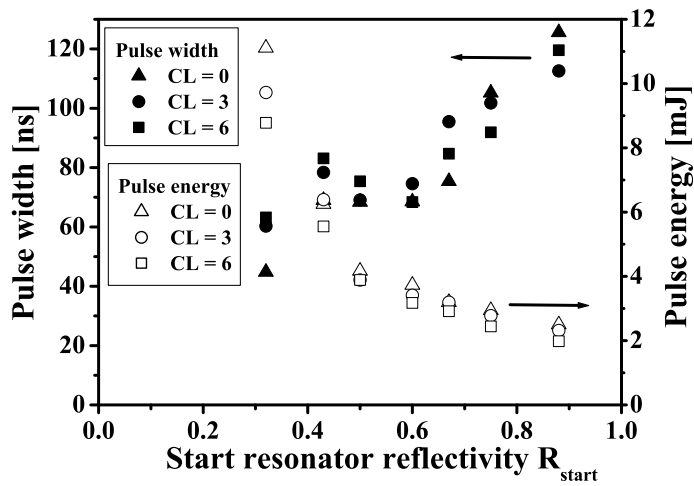
Figure 3.6: Dependence of Q-switch pulse energies and pulse durations on R_{start} for different carrier levels (CL) of the AOM driver; background represents the flash lamp pump pulse

For one set of pump parameters the start resonator mirror reflectivity was varied and the pulse durations and the pulse energies were measured. The average pump power from the flash lamp pumped laser head was 3 kW. The repetition rate was 180 Hz, and the pump pulse duration was set to 300 μs. The results of this measurement are depicted in Figure 3.6 for different carrier levels (CL) of the AOM driver. In that sense $CL = 0$ represents the case with the AOM turned off. Bursts of up to 7 pulses can be generated within a pump pulse duration of 300 μs for an R_{start} of 0.88 %. The output power ranges between 2.0 W for one pulse per burst and 2.7 W for 7 pulses. In the latter case the Q-switch pulse energy is 2.3 mJ, the pulse duration (FWHM) was 122 ns. For $R_{start} = 0.32$ one single pulse is received from each pump pulse. The output power equals 2 W leading to a Q-switch pulse energy of 11 mJ. The QML operation will be discussed in the following section, but we can state already that, apparently, mode-locking did neither influence the Q-switch-pulse duration nor the Q-switch pulse energy systematically. This, in fact, comes as a surprise considering that in [24] and as discussed

in Section 2.1.1 a suppression of the SBS with increasing bandwidth is predicted for a mode-locked input beam. The model given in [24] unfortunately is not suitable for a simple quantitative approximation of the effect, but obviously it is at least in our case of no practical relevance.

Contrary to the flash lamp pumped laser head the pump intensity of the diode pumped laser head does not change significantly during the pump pulse. Since the spacing between pulses in a burst for a given start resonator loss depends only on the pump intensity we can expect the pulse spacing to vary less from pulse to pulse than for the flash lamp pumped laser head. Also, with the diode pumped laser head we can choose arbitrary pump pulse durations so that a larger number of pulses can be generated per burst.
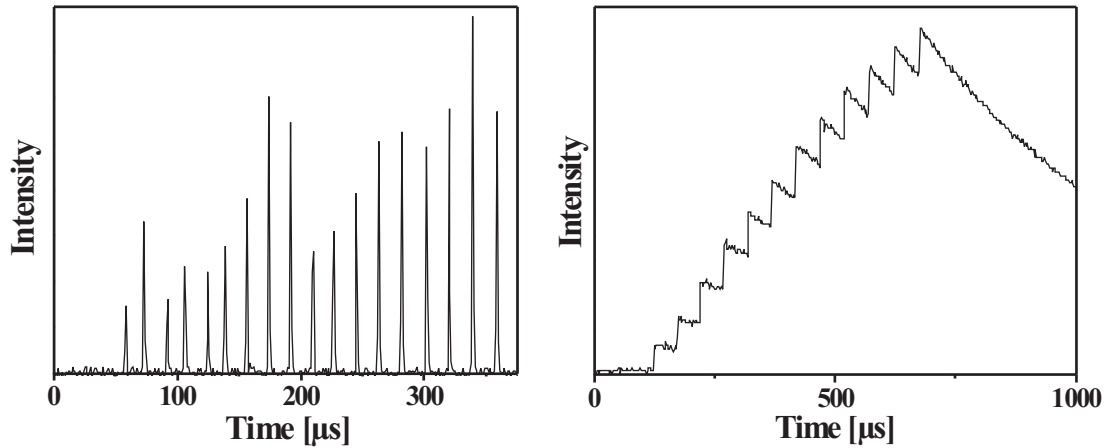
Figure 3.7: Bursts from the configuration with the diode pumped laser head measured at a an impedance of $10\,\text{k}\Omega$ (left) and $1\,\text{M}\Omega$ (right) showing good pulse to pulse stability with regard to pulse spacing (left) and pulse energy (right)

Figure 3.7 shows two examples of pulse bursts generated with the diode pumped laser head. The left graph in Figure 3.7 shows a burst of 18 pulses measured with a photodiode at an impedance of $10\,\text{k}\Omega$. The amplitudes of the Q-switch pulses in this display do not refer directly to the pulse energy. The apparent variance in amplitude of the pulses stems from a digitizing effect in the display of the short pulses on a comparatively long timescale. The right hand part of Figure 3.7 is a burst of 12 pulses measured with the same photo detector at a resistance of $1\,\text{M}\Omega$. In this measurement configuration the pulses are represented by the steep edges. Here the pulse energies are proportional to the heights of the edges. The time jitter of the pulses (standard deviation of the pulse spacing) amounts to $1{,}8\,\mu\text{s}$ at an average pulse spacing of $50\,\mu\text{s}$. The pulse to pulse energy stability was determined to be better than $8\,\%$.

So far the output properties of the laser such as temporal Q-switch pulse spacing, pulse duration and pulse energy are coupled: By changing the start resonator loss all these parameters are altered dependently. But by additionally varying the pump

parameters free parameters are added and with the help of an external attenuation the mentioned output parameters can within boundaries be arbitrarily chosen. The pulse spacing can be independently tuned by the pump intensity. The pulse energy can be changed by the external attenuation. The number of pulses can be chosen by adjusting the pump pulse duration. To vary the pulse duration while maintaining all other parameters constant the start resonator loss has to be tuned and the change in the number of pulses, the pulse spacing and the pulse energy has to be compensated by an adjustment of the pump pulse duration and intensity and the external attenuation. The large variability of this laser's temporal output properties has already been exploited for fundamental research in materials processing [10]. The boundaries for the pulse parameters which are achievable by this laser are summarized in Table 3.1.

Parameter	Limits
Number of pulses	1–20+
Pulse energy	1–11 mJ
Pulse duration	30–300 ns
Pulse spacing	10–100 μs

Table 3.1: Accessible Q-switch parameter space

3.2.2 Q-switch observation

Since the Q-switch in the linear SBS-oscillator is connected with a switch between two resonators of in general different lengths, this switch also evokes a change in the periodicity of the modulation in the output signal [77]. As long as the oscillation occurs in the start resonator we find in our case a 40 MHz periodicity in the output signal of the laser corresponding to the 3.75 m of optical path length. The oscillation in the SBS-resonator in contrast shows an 80 MHz periodicity. This becomes most apparent for mode-locked operation. Figure 3.8 shows the leading edge of a Q-switch pulse transmitted through the start resonator mirror. The leakage through the start resonator mirror was used for this measurement since here the ratio between spike signal and the main Q-switch pulse signal is higher compared to the main output behind the output coupler.

In the bottom graph of Figure 3.8 the transition from the 40 to 80 MHz can be clearly seen. It corresponds to a single pulse that starts to revolve in the start resonator and than gradually switches to the SBS-resonator due to the increasing SBS-reflectivity. Thus we can conclude that the on-switching of the SBS-reflectivity takes about 300–400 ns. Since the AOM consistently works with 80 MHz frequency its loss vanishes twice during each start resonator round trip. Accordingly, two pulses that are spaced by half the round trip time can coexist in the start resonator. If both pulses resemble in amplitude the switching is not apparent from the periodicity of the output signal (top graph in Fig. 3.8). The most likely case to encounter, however, is a mixture of both

cases: Two pulses with different amplitudes resulting in a 40 MHz superstructure to the 80 MHz fundamental repetition rate.
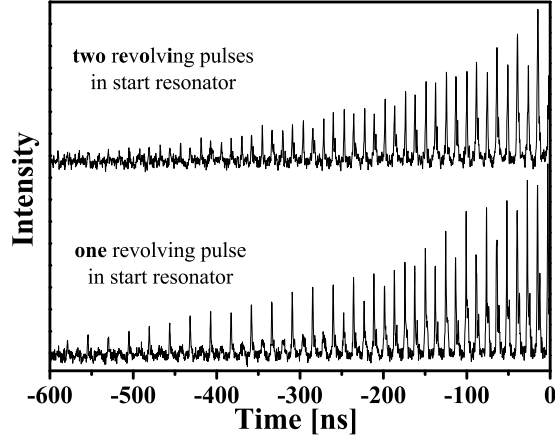
Figure 3.8: Leading pulse edge observed through start resonator mirror. Top: Two pulses revolve in the start resonator; no switch in repetition rate. Bottom: One pulse revolves in the start resonator; Q-switch is connected with switch in repetition rate

3.3   Simultaneous Q-switching and mode-locking

Without any active mode-locking the Q-switch pulses show a ps-substructure already. A typical temporal intensity distribution of a Q-switch pulse generated by the free running SBS-laser is depicted in the left graph of Figure 3.9. These structures result from the superposition of several longitudinal laser modes. The phases of the longitudinal modes are initially determined by spontaneous emission. As long as there is no synchronizing element several modes with different phases can coexist. Since the resonator modes are eigensolutions of the resonator, the phases of the modes will be reproduced for each integer round trip. Hence the temporal pulse structure exhibits a periodicity according to the SBS-resonator round trip time T of 12.5 ns while the structure within a period is determined by the phase relations and amplitudes of the initial modes generated by spontaneous emission.

   Also, the Stokes-shift which the light experiences when reflected at the SBS-mirror does not affect the relative phase relation of the longitudinal modes since the longitudinal mode spacing is designed to be resonant with the Stokes-shift of the SBS-material. Therefore the Stokes-shift generates modes that are phase coupled to the initial modes. We will have a closer look at this subject when we discuss the spectral properties of the laser. So the pulses exhibit a deep modulation contrast without any active mode-locking already. But because the process starts from random spontaneous emission and thus we can have several modes with different phases, the modulation depth does not reach 100 % and we typically obtain several peaks within a round trip period of 12.5 ns. Also
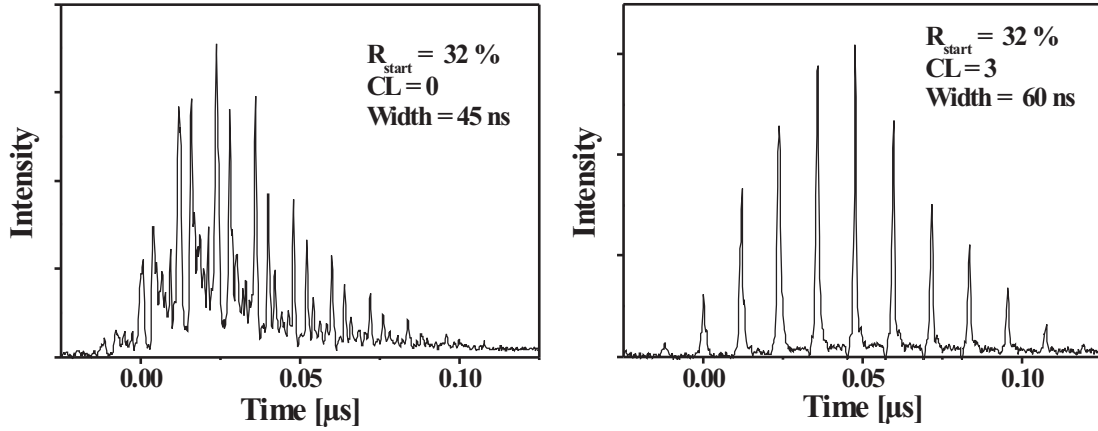
Figure 3.9: Temporal intensity distribution of the free running SBS-laser (left) and the mode-locked SBS-laser (right)

the modulation contrast as well as the structure within the round trip period differs and thereby the Q-switch pulse envelope changes from pulse to pulse, too.

If an active loss modulator (e.g. an AOM) is added to the SBS-laser oscillator scheme (see Fig. 3.1) the phases of the longitudinal modes get locked. This means that the phases are identical for all modes at intervals corresponding to their frequency spacing. As a result we obtain a single pulse revolving in the resonator so that a reproducible and regular modulation of the Q-switch pulses of 100 % depth is received (see right graph of Figure 3.9). Also the pulse envelope is reproducible for the mode-locked case. The acoustic modulation frequency together with the appropriate optical SBS-resonator length of 187.5 cm results in a temporal spacing of the mode-locked pulses of 12.5 ns.

The temporal structure of the lasers output we now obtain is summarized in Figure 3.10. Within the pump pulses that last for a few 100 μs several pulses are generated by the passive Q-switch of the nonlinear SBS-mirror. The durations of these pulses are of the order of magnitude of 100 ns and they are spaced by 10s of μs. By active mode-locking each of these pulses is split up into a train of ps-pulses. The upper limit for the single pulse duration was directly measured with a fast photodiode (Thorlabs SV2) and an oscilloscope with 2 GHz bandwidth (Tectronix TDS 794D) to be 412 ps. The corresponding pulse train is depicted in the bottom graph of Figure 3.10.

If we ask why the pulse durations are still long compared to other mode-locked Nd:YAG lasers which typically have pulse durations in the range of 10s of ps, we have to bare in mind that for QML operation the pulse durations are in general expected to be longer than for cw-mode-locking. As discussed in Section 2.2.3 this is the case because for QML the pulse does not pass the modulator often enough to reach the shortest possible steady state pulse duration which is determined by the equilibrium of modulation and limited gain bandwidth.

In this context one advantage of this laser is that the mode-locking can already be
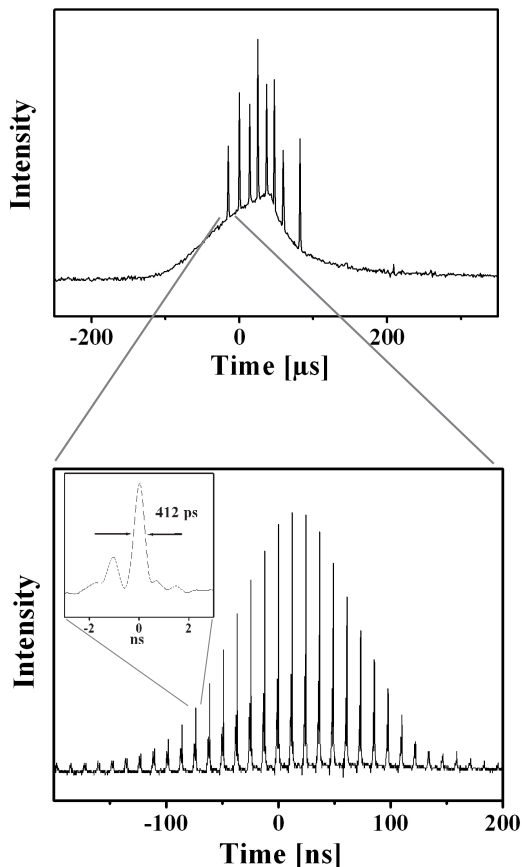
Figure 3.10: Pulsetrain formed by SBS-Q-switch superimposed to flash lamp pump pulse (top) and train of mode-locked pulses underneath Q-switch envelope (bottom)

settled in the start resonator before the Q-switch occurs. Because this prelasing can be significantly longer than the actual pulse buildup after the Q-switch the pulse duration will be closer to the steady state conditions than we could expect for instance in the case of an active Q-switch without prelasing.

Drawbacks in terms of the potential for short pulse generation of the SBS-laser are the spatial distribution of the SBS-reflection and also the movement of the position of the SBS-reflection in the course of the pulse [18]. Since the SBS-reflection exhibits a spatial distribution the length tuning of the cavities which is essential for mode-locking can only vaguely be realized. The movement of the distribution of SBS-activity leads to a detuning of the cavity lengths during the Q-switch pulse.

Another aspect which comes into play if we talk about length tuning and which has already been mentioned in Section 2.1.3 is the fact that the SBS is suppressed if the

SBS-cell is placed in the very center of the start resonator [77, 80]. However, a tiny misalignment of the SBS-cell of 2–3 mm from the very center is suffiecient to obtain an SBS-Q-switch from a laser where the start resonator is about twice as long as the SBS-resonator. To answer the question whether this misalignment leads to a significant pulse lengthening the start resonator length was enhanced by another fundamental length according to the mode-locking of 187.5 cm. Now the start resonator measures three times the length of the SBS-resonator and hence the SBS-cell is no longer in the center of the start resonator. Still, no further improvement with regard to the mode-lock pulse duration is gained. Another possible source of a frequency mismatch are the Brillouin-frequency and the modulation frequency. While the modulation frequency of the AOM in use is fixed, the Brillouin-frequency of the SBS-medium can be influenced by changing the pressure of the SF_6. Still a variation of the pressure between 18 and 24 bar does not have a perceptible influence on the pulse formation.

The results presented in Figure 3.6 demonstrate that the Q-switch pulse durations as well as the Q-switch pulse energies are influenced by the start resonator mirror reflectivity R_{start}. For QML both of these aspects influence the resulting pulse energies of the mode-locked pulses. Figure 3.11 shows the dependence of the mode-locked pulse energy on R_{start}, where the number of mode-locked pulses per Q-switch pulse was gained by dividing the full width at half maximum (FWHM) of the Q-switch pulses by the temporal spacing of the mode-locked pulses.
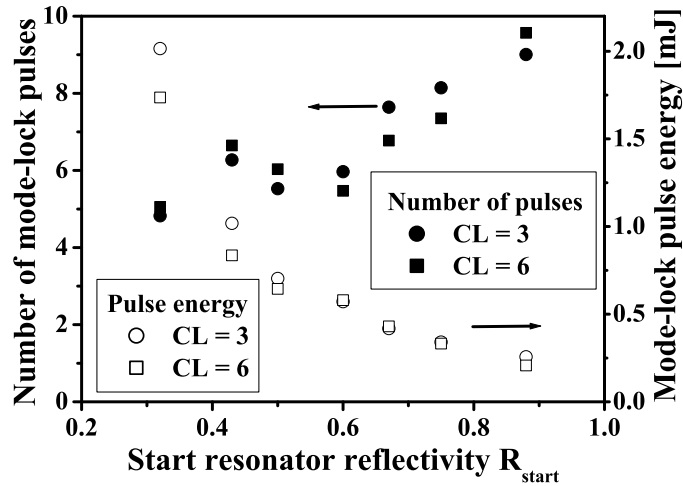
Figure 3.11: Dependence of mode-lock pulse energy and number of mode-lock pulses on R_{start}

The mode-locked pulse energy increases rapidly with decreasing R_{start} because the Q-switch pulse energy grows with decreasing R_{start} and the Q-switch pulse duration decreases simultaneously. Hence, the increasing Q-switch pulse energy is split up into a

smaller number of pulses with increasing start resonator losses. For $R_{start} = 0.32$ about four mode-locked pulses with 2 mJ single pulse energy are contained within the FWHM of the Q-switch pulse envelope. Considering the single pulse duration of around 400 ps we obtain a peak power of 5 MW. While the mode-locked pulse duration of the laser presented here is of the same order of magnitude the single pulse energy as well as the peak power exceeds the values found in the literature for passively Q-switched QML-oscillators by at least an order of magnitude (see Section 2.2.3 and [96]–[107]). The pulse duration of this laser is admittedly longer by an order of magnitude compared to [25] and [118] where an external SBS-cavity is used to generate mode-locked bandwidth from a single frequency input beam. In these cases n-hexane was utilized as SBS-material which has a Brillouin-frequency of 3.1 GHz. The use of an SBS-material with a higher Brillouin-frequency certainly promises shorter pulses for this mode-locked SBS-oscillator concept as well. The influence of the Brillouin-frequency on the spectrum and the mode-lock pulse duration will be reflected in detail by numerical simulations presented in Section 4.3.5.

3.4   Spectral properties

The spectral properties of the SBS-laser oscillator were investigated using a Fabry-Perot-Interferometer (FPI). The experimental setup is illustrated in Figure 3.12. The laser beam is diverged by a concave lens with a focal length f of -50 mm. The distance of the parallel plane mirrors of the FPI amounts to 5 cm resulting in a free spectral range of 3 GHz. Their coating provides a reflectivity of 94 % resulting in a finesse F of 50 and a spectral resolution of 60 MHz which is just good enough to resolve the longitudinal SBS-resonator modes. The CCD-camera is exactly placed in the focal plane of the focusing lens to display the far field of the FPI´s output. For these investigations the laser was driven at one pulse per burst with a repetition rate of 50 Hz. The frame grabber was triggered to the output of the laser to guarantee, that each interferogram displays the spectral properties of a single Q-switch pulse only.
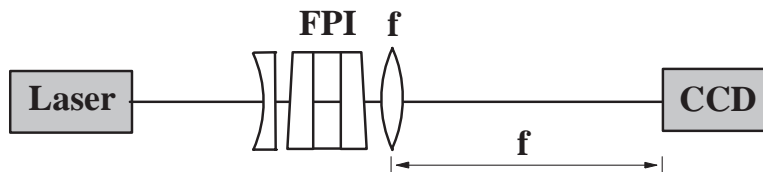
Figure 3.12: Schematic of setup for Fabry-Perot-spectrum imaging

Two examples of Fabry-Perot interferograms are given in Figure 3.13. Here each longitudinal mode is represented by one ring of light where the frequency of the modes decreases with the radius of the respective ring. The left picture in Figure 3.13 represents the SBS-laser without active mode-locking. In the first free spectral range (in the center of the picture) the longitudinal modes can be clearly resolved.
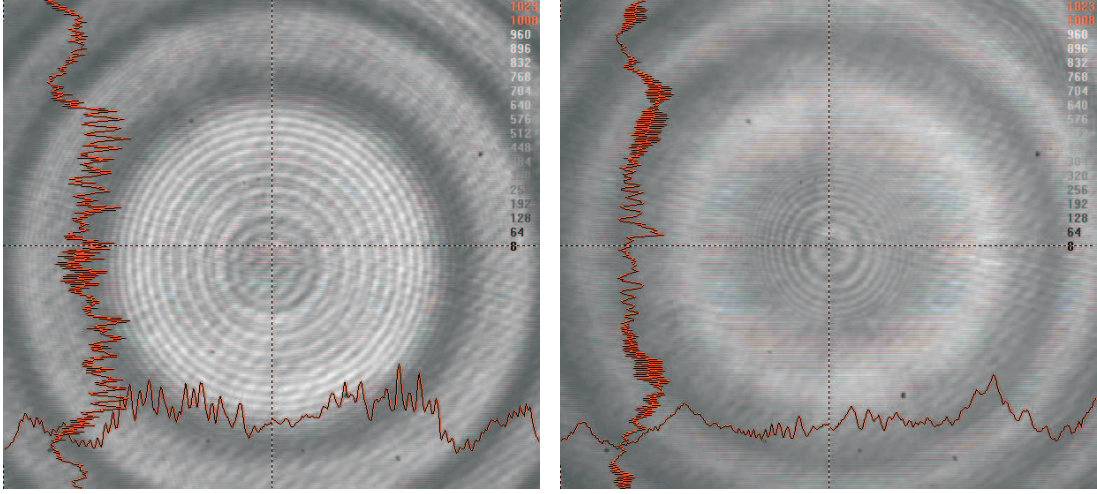
Figure 3.13: Fabry-Perot spectra for the case without active mode-locking (left) and with mode-locking (right)

In the following free spectral ranges the resolution of the FPI is not sufficient anymore to resolve the longitudinal modes. From the fact that we can distinguish the free spectral ranges we can conclude that the bandwidth of the laser is smaller than the free spectral range of the Fabry-Perot interferometer, so it is smaller than 3 GHz. Otherwise the interferogram would be entirely illuminated. The radii $r_{1,2}$ of adjacent rings in the interferogram and the spectral distance $\Delta\nu$ between the laser modes are related by

$$\Delta\nu \approx \left[r_2^2(\nu_1) - r_1^2(\nu_2) \right] \cdot \frac{c}{2f^2 \cdot \lambda} \tag{3.2}$$

where λ is the wavelength. The FWHM-bandwidth in the mode-locked case can be estimated to be around 2 GHz. In the transform limited case this bandwidth leads to a pulse duration minimum of 200 ps. However we have to keep in mind that this is the overall bandwidth of the Q-switch pulse. Since the spectrum experiences a Stokes-shift for each SBS resonator round trip the instantaneous bandwidth which governs the mode-lock pulse duration may be significantly smaller. A detailed study of the evolution of the spectrum will be carried out by numerical simulations presented in Section 4.3.

For the case without active mode-locking we can observe a periodicity of 240 MHz for the population of the occurring laser modes (left part of Fig. 3.13). This frequency is identical to the Brillouin-frequency of the SBS-medium while the longitudinal mode spacing of the SBS-resonator is 80 MHz. So every third of all possible resonator modes protrudes in the output spectrum of the laser and the interstitial modes are only scarcely populated. This observation can be understood if we consider that all modes with a 240 MHz spacing are linked due to their mutual generation by the Stokes-shift of the SBS-reflection. This divides the longitudinal resonator modes into three sets of coupled

modes. From the fact that only one of these sets of modes dominates the spectrum
we can conclude that the oscillation is initiated by just one of the longitudinal modes
— probably the first one to occur in the statistical process of spontaneous emission
— and that all bandwidth is generated by the Stokes-shift. Since the Stokes-shift
amounts to 240 MHz the interstitial modes will not be fed. This observation will be
of vital importance to the determination of the starting conditions for the numerical
simulations described in Section 4.3. In the fourier spectrum of the pulses of the SBS-
laser the 240 MHz peak does not protrude from the other peaks spaced by 80 MHz
(see Figure 3.14), but it can be demonstrated that this lack of contrast in the fourier
spectrum can be attributed to a superposition with a relatively small background of the
interstitial sets of modes [122].
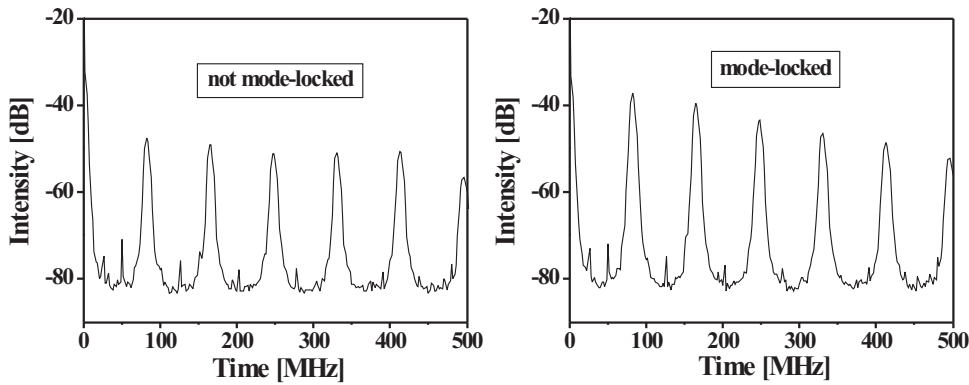
Figure 3.14: Fourier spectra of the temporal pulse distribution averaged over 50 pulses for
the free running SBS-laser (left) and for the mode locked SBS-laser (right)

For the mode-locked case all possible resonator modes within the measured band-
width appear in the Fabry-Perot interferogram. This is caused by the sideband modu-
lation of the AOM. Since its optical modulation frequency of 80 MHz is identical to the
longitudinal mode spacing all resonator modes within the given bandwidth are gener-
ated. While the Stokes-shift leads to a coupling of modes that are spaced by 240 MHz
the modulation of the AOM leads to a coupling between adjacent modes (spaced by
80 MHz) resulting in a uniform distribution of the mode population within the overall
bandwidth.

There is not a very distinct difference in the bandwidth of the two operating regimes.
Due to the longitudinal mode generation by the Doppler-shift in the SBS-resonator the
bandwidth of the laser gets already enhanced in ordinary SBS-Q-switch operation. The
bandwidth does not differ significantly from pulse to pulse. Also the mode spectra
for the mode-locked as well as for the ordinary SBS-Q-switched case are qualitatively
reproducible. However, for the case without active mode-locking the dominant set of
modes would statistically bop around the three possible solutions from pulse to pulse.

Sometimes the population of two of the three sets of modes resemble in magnitude. In that case the oscillation starts from two modes that can compete equally for the gain.

An experimentally measured evidence for the effect of the Stokes-shift in the SBS-laser oscillator can be found by detecting the transient signal of the individual longitudinal laser modes [77]. This is achieved by replacing the CCD-camera in the setup shown in Figure 3.12 with a fibre coupled diode thereby separating the signal of the individual modes. The time resolved signals given in Figure 3.15 are gained by averaging over the signals of 50 pulses. They represent the complete pulse (top graph in Fig. 3.15) and two individual modes picked from the center (middle) and the fringe (bottom) of the spectrum respectively. The signals measured at the fringe and in the center of the spectrum show an 80 MHz modulation which can be attributed to the superposition with other modes that can be found in the considerably high background noise in the spectra (see Fig. 3.13). The background noise leads to strong fluctuations in the signal of a single longitudinal mode and single pulse which is the reason for the averaging. The averaging is also the cause of the comparatively long mode-lock pulses in the signal of the complete spectrum.
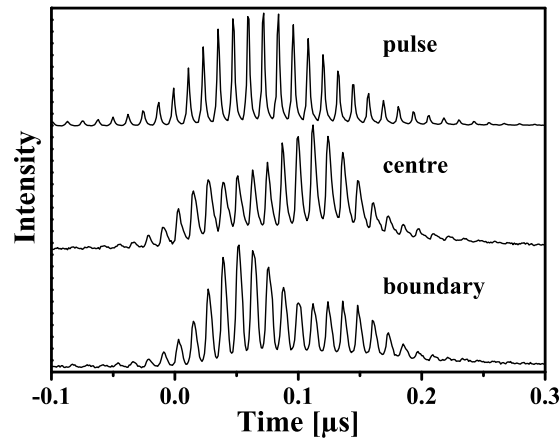
Figure 3.15: Intensity distribution of the pulse signal (top graph) and corresponding signals of individual modes at the center (middle graph) and the boundary (bottom graph) of the Fabry-Perot spectrum averaged over 50 pulses

Within one free spectral range in a Fabry-Perot spectrum the frequency increases with the distance from the center. Thus, in the course of a Q-switch pulse the laser's spectrum is shifted from the boundary to the center of the Fabry-Perot spectrum. Accordingly, the maximum of the averaged signal recorded in the center occurs later than in the signal recorded at the boundary of the spectrum.

3.5   External feedback

It was mentioned already in the above section that the SBS-laser was set up with two different start resonator lengths corresponding to two and three times the fundamental resonator length according to the AOM modulation frequency of $80\,\mathrm{MHz}$. For the rebuilding from the short configuration to the long configuration the laser was run on the short setup and the leakage through its start resonator mirror ($R_{start}1$) was utilized to align the start resonator mirror for the long configuration ($R_{start}2$). A sketch of the setup is depicted in Figure 3.16.
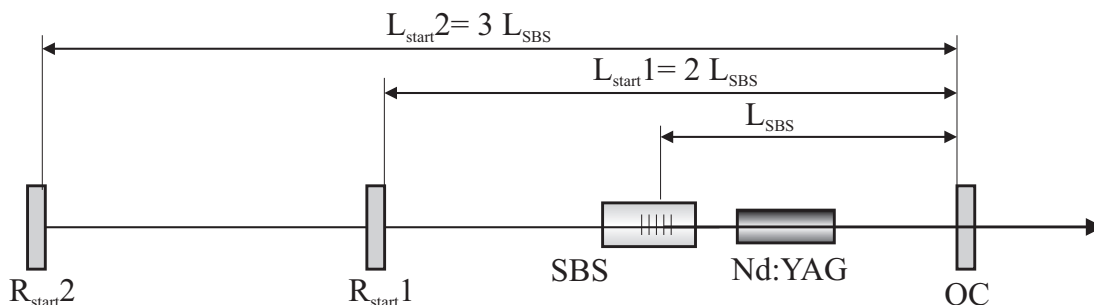
Figure 3.16: Setup for the experiments with external feedback

During this procedure it could be observed that the pulse structure of the free running SBS-laser changes significantly when $R_{start}2$ is properly aligned. $R_{start}2$ is a plane mirror with $88\,\%$ reflectivity. The eigenmode in the start resonator of the short SBS-laser corresponds to the one depicted in Figure 3.1. It has a beam waist on $R_{start}1$ and therefore, there is no mode-matching between the eigenmode of the SBS-laser and the feedback from $R_{start}2$. Still a major effect on the pulse shape can be observed when the feedback from $R_{start}2$ is switched on.

Figure 3.17 shows a comparison between a pulse distribution of the SBS-laser with feedback from $R_{start}2$ (Fig. 3.17 left) and without (Fig. 3.17 right). The feedback leads to a significantly deeper modulation contrast. In addition a $240\,\mathrm{MHz}$-periodicity corresponding to the Brillouin frequency ν_B becomes visible which cannot be found in the pulse without external feedback.
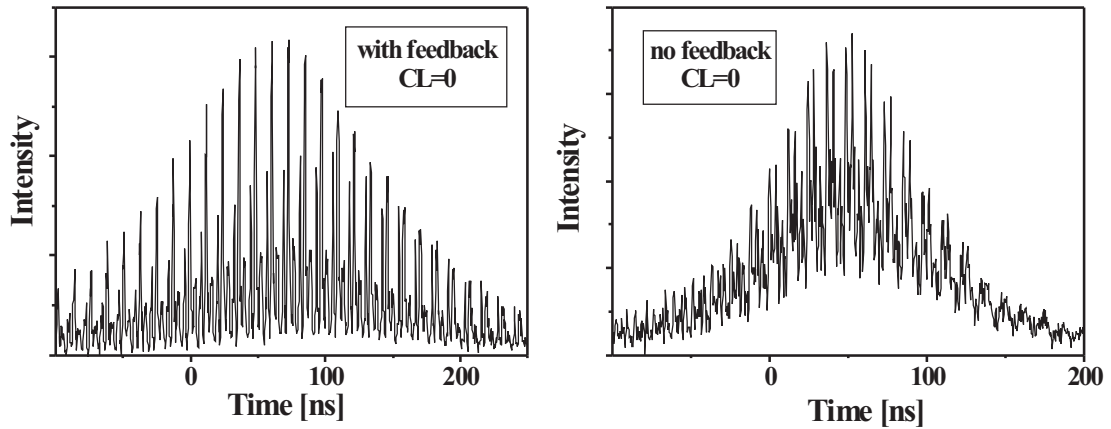
Figure 3.17: The modulation contrast can be significantly increased if external feedback is applied (left) compared to the case without feedback (right)
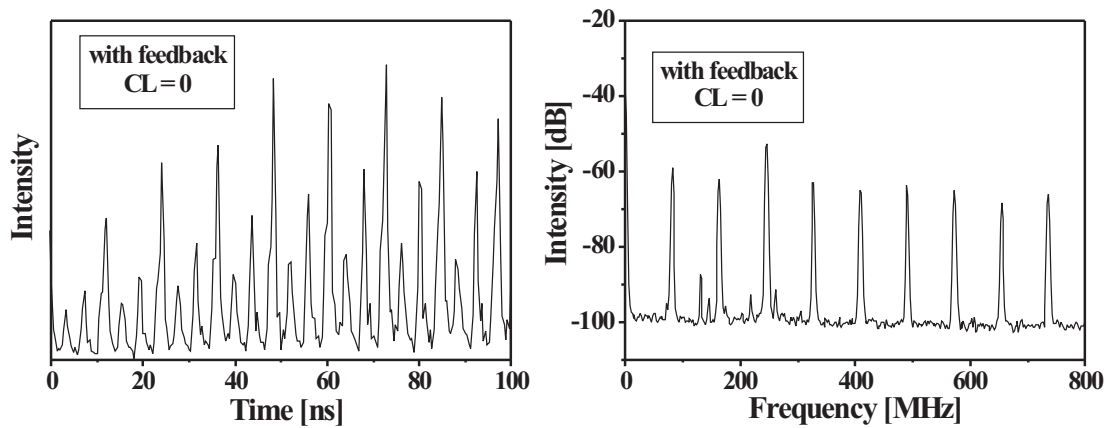
Figure 3.18: The frequency of 240 MHz corresponding to the Brillouin-frequency is apparent in the temporal intensity distribution (left) as well as in its Fourier spectrum (right)

The 240 MHz repetition rate becomes particularly apparent if we zoom into the pulse. The left part of Figure 3.18 shows an enlargement of a pulse with external feedback applied. The 80 MHz-periodicity corresponding to the mode-spacing of the SBS-resonator is still present, but beneath this superstructure a 240 MHz-periodicity can be found. Between two major pulses with 12.5 ns separation two interstitial pulses can be found with a regular spacing of approximately 4 ns. In the Fourier spectrum of the pulse the substructure surfaces as a protrusion of the 240 MHz-peak over the other peaks spaced by 80 MHz (Fig 3.18 right). The relative amplitudes of the interstitial pulses are maintained during each Q-switch pulse but vary dramatically from pulse to pulse.
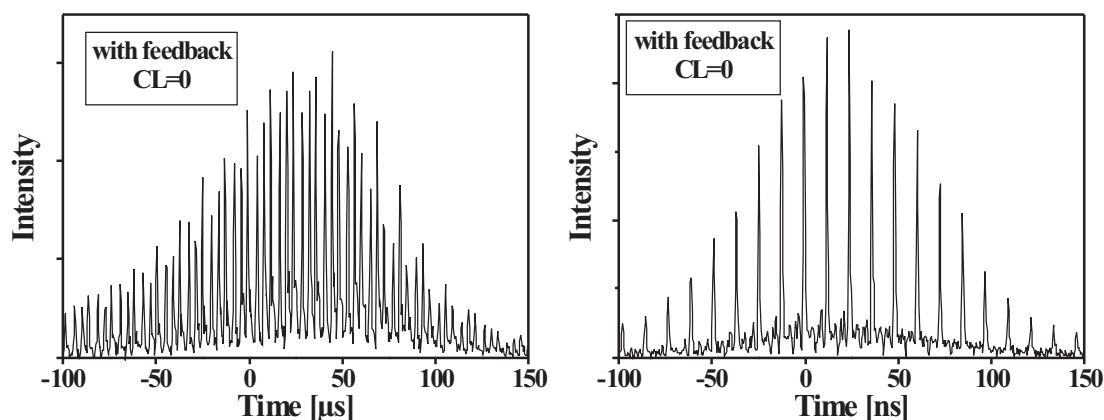
Figure 3.19: The amplitudes of the interstitial pulses vary from pulse to pulse; here two extreme cases are shown: Left: All pulses are of approximately the same magnitude. Right: The interstitial pulses vanish; these pulses are now very similar to the actively mode-locked pulses with regard to modulation depth as well as to the pulse shape

Figure 3.19 shows two extreme examples. On the left side a pulse train is shown, where all pulses are of approximately the same height. This is equivalent to a pure 240 MHz modulation. The other extreme is shown in the right graph of Figure 3.19. Here, the interstitial pulses vanish completely and hence the pulse train becomes very similar to the results from active mode-locking with regard to pulse duration and pulse shape.

A change in the reflectivity of $R_{start}2$ does not lead to a noticeable effect on the pulse shape. Only for reflectivity values approaching unity an instability of the Q-switch is introduced. Mode-matching of the feedback from $R_{start}2$ with the resonator mode is achieved if $R_{start}2$ is exchanged for a mirror with a radius of curvature that matches the distance from the beam waist on $R_{start}1$. This is in a first order approximation accomplished by use of a concave mirror with a radius of curvature of 2 m. The configuration with the mode-matched feedback can also be interpreted as a setup of three coupled resonators: the SBS-resonator and two start resonators. Still, a mode-matching of the feedback with the eigenmode of start-resonator 1 does not influence the pulse shape

noticeably. Also, the pulse shape is insensitive to a variation of the position of $R_{start}2$ along the axis of the resonator of a few cm. A larger variation leads to instabilities and finally a suppression of the Q-switch. If, however, $R_{start}2$ is shifted by exactly one or two Brillouin-lengths L_B in either direction we obtain only a 240 MHz periodicity in the temporal Q-switch pulse shape (Figure 3.20 left). The 80 MHz corresponding to the SBS-resonator mode spacing is no longer visible, but the depth of modulation does not exceed about 70 %. The right graph in Figure 3.20 shows the Fourier spectrum averaged over 50 pulses for the feedback mirror shifted by one Brillouin-length. Here peaks occur in intervals of about 240 MHz. At 80 and 160 MHz no signal can be found.

This can be explained by the circumstance that those SBS-resonator modes which are resonant with both start resonators are favoured by the double feedback. The resonance with the original start resonator is given for all SBS-resonator modes since this start resonator is twice as long as the SBS-resonator. But if the length of the second start resonator $L_{start}2$ given by the output coupler and $R_{start}2$ is not an integer multiple of the SBS-resonator length but merely an integer multiple Brillouin-length L_B then not all the SBS-resonator modes are resonant with the second start resonator. If, for example, $L_{start}2$ is 8 times L_B then the fundamental mode spacing of the second start resonator is 30 MHz while the fundamental mode spacing of the SBS-resonator is 80 MHz. Only those SBS-resonator modes which constitute multiples of the Brillouin-frequency of 240 MHz experience the twofold feedback and appear in the output of the spectrum. Accordingly, the output is modulated by 240 MHz.
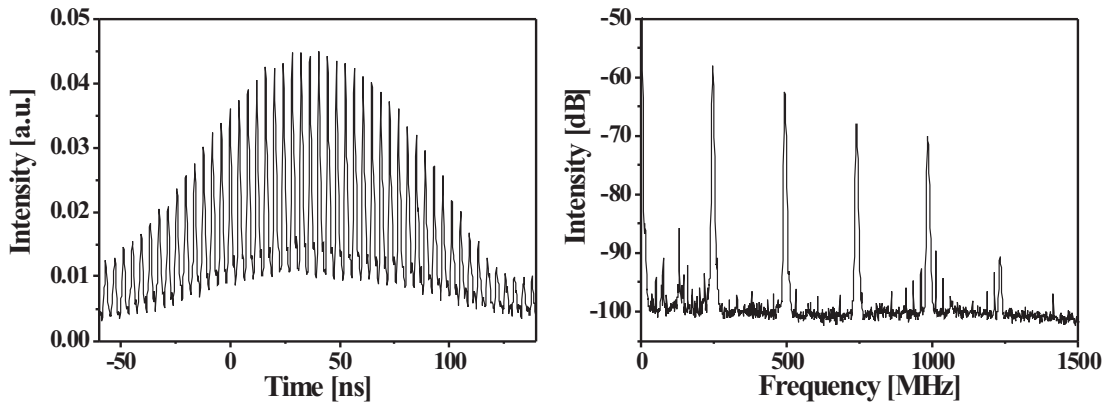
Figure 3.20: If the feedback mirror is shifted by one or two Brillouin lengths a pure 240 MHz periodicity in the temporal Q-switch pulse shape is obtained (left); in the Fourier spectrum of the pulses peaks occur only at integer multiples of the Brillouin frequency (right)

It remains to ask for the reason for the improved mode-locking through application of an external feedback. Mode-locking always requires some nonlinear effect. This is in general a time or intensity dependent loss or amplification or a phase modulation which leads to a synchronization of the longitudinal modes. For the case of SBS-mode-coupling in an SBS-oscillator we merely have a continuous generation of new modes

while their phases are coupled to the initial set of modes. The relative phases of the starting set of modes, however, are random resulting in a chaotic modulation. The active modulation of the AOM leads on the one hand to the synchronization of the modes which results in the deep and regular modulation. On the other hand it leads to an exchange of population between adjacent modes resulting in a smoothing of the spectrum and accordingly in the attenuation of interstitial pulses. The feedback from $R_{start}2$ obviously leads to a synchronization of the modes which becomes apparent in the deep and regular modulation. The population of interstitial modes and thus the occurrence of interstitial pulses, however, is still subject to spontaneous emission in the pulse buildup period and therefore changes from pulse to pulse. The exact mechanism for the synchronization of the modes remains still unclear. The answer to this question is most likely to be found in the initiation of the sound wave.

3.6   Summary

A passively Q-switched laser that is additionally actively mode-locked was demonstrated. The passive Q-switch is carried out by a phase conjugating nonlinear mirror based on stimulated Brillouin scattering (SBS). It is the first experimental implementation of a self starting mode-locked SBS-laser oscillator. Thanks to the phase conjugating reflection of the SBS-mirror wavefront distortions due to thermal aberrations in the laser rod can be compensated resulting in transverse fundamental mode operation within the entire range of stable Q-switch operation. Furthermore, the passive SBS-Q-switch leads to bursts of ns-pulses with μs-spacing during one pump pulse. The output parameters of the Q-switch pulse train such as pulse energy, duration, number of pulses per burst and their temporal spacing are easily and independently adjustable by variation of the pump parameters and the start resonator loss.

Active mode-locking of the laser by acousto optic modulation results in a ps-substructure of the Q-switch pulses with single pulse durations of 412 ps and pulse energies ranging from 0.2 to 2 mJ. This corresponds to a peak power of around 5 MW which is to my knowledge the highest published value of a passively Q-switched oscillator operating simultaneously in a Q-switched and mode-locked fashion. The laser's high flexibility in energy distribution and peak power adjustment can be exploited for fundamental research in laser – materials interactions [10].

Fabry-Perot spectra of single Q-switch pulses reveal a superstructure of 240 MHz in the spectrum of the pulses without active mode-locking. This frequency corresponds to the Brillouin-frequency of the SBS-material in use. It indicates that the oscillation is initiated by one dominant mode and that the bandwidth is primarily generated by the Stokes-shift which is connected with the SBS-reflection.

If part of the leakage through the start resonator mirror is fed back into the free running SBS-oscillator a synchronization of the longitudinal resonator-modes can be achieved. As a result a regular modulation of almost 100 % depth in the Q-switch pulse shape is obtained. The result is very similar to the actively mode-locked case except

that three pulses of varying amplitude can be found within a period of 12.5 ns resulting in a fundamental repetition rate of 240 MHz. The condition for the synchronization is that the distance of the feedback mirror from the start resonator mirror equals an integer multiple of the Brillouin-frequency.

Chapter 4

Modeling of the emission dynamics

In the previous chapter the output dynamics of the mode-locked SBS-laser was investigated experimentally with regard to the intensity distribution as well as regarding the spectral dynamics of the laser output. In this chapter we want to gain a profound understanding of the processes occurring in the laser that govern its output dynamics. This is achieved by modeling these processes and comparing them with the experimental observations. For this purpose, two novel models will be introduced which pursue quite complementary approaches to display the temporal behavior on the ps-timescale of the laser. The first model is based on the laser rate equations which are applied for each longitudinal mode individually. Thus, the evolution of the emission spectrum in the course of a Q-switch pulse is obtained. In a next step the dynamics in the intensity distribution on a ps-timescale can be calculated from the spectrum assuming perfectly synchronized modes.

While in this model the ps-dynamics are calculated from the transient spectrum of many longitudinal modes (frequency domain model) in the second model all dynamics are described solely in the time domain. A pulse is propagated on a round trip through the resonator and all interactions with the optical devices are taken into account. A similar approach has been taken by Kuizenga and Siegman [82, 83]. They found an analytical description for steady state mode-locking by pursuing the changes to a pulse during one resonator round trip and demanding no net change upon completion of the round trip. Since we are interested in the QML regime we have to numerically calculate a large number of round trips and of course allow changes for each round trip. The SBS-Q-switch is taken into account by a phenomenological description that is identical for both models. We assume an intensity dependent generation of an overall sound wave amplitude in the SBS-mirror that determines its effective transient SBS-reflectivity. In the first two sections of this chapter the aforementioned models are introduced. In Section 4.3 results from numerical simulations based on the two models are presented and used to discuss the influences of different parameters on the QML dynamics and the transient spectrum. Among the aspects under scrutiny are the modulation of the AOM, a modulation frequency detuning, the SBS-Stokes-shift, SBS-material parameters and

the starting conditions

4.1   Spectrally resolved laser rate equations

The laser rate equations are coupled differential equations to describe the evolution of the photon density, the inversion density and their mutual interactions inside the cavity. They are the means of choice to calculate laser output dynamics on timescales down to the order of magnitude of the resonator round trip time T [123]. However, the obtained photon density as a function of time is in fact the mean photon density inside the resonator. Therefore, dynamics on a timescale shorter than the resonator round trip time T cannot be resolved and additional efforts have to be made in order to display mode-locking behavior in the calculations. The envelope of a mode-locked pulse is on the one hand determined by its mode spectrum and on the other hand by the phase relations of the respective modes. To comprise the mode-locking dynamics in the simulation the laser's spectrum and its transient behavior have to be included in the modeling. The spectrum can be considered by solving the laser rate equation for the photon density for each of the longitudinal modes individually. The laser rate equation for the photon density ϕ_n of the n-th mode of an actively mode-locked 4-level laser neglecting the population of the pump band and the lower laser level is

$$
\begin{aligned}
\frac{d\phi_n}{dt} = &-\frac{\phi_n(t)}{\tau_R} + \frac{l}{L} \cdot \frac{n_2(t) \cdot s_n}{\tau_{sp}} + \frac{l}{L} \cdot n_2(t) \cdot \sigma_n \cdot \phi_n(t) \cdot c \\
&+ \left[-\phi_n(t) + \frac{\phi_{n+1}(t)}{2} + \frac{\phi_{n-1}(t)}{2} \right] \cdot m_{FD} \cdot \frac{c}{2 \cdot L}.
\end{aligned}
\tag{4.1}
$$

Here τ_R and τ_{sp} are the resonator decay time and the lifetime of the upper laser level, l is the length of the laser active material, L the resonator length, n_2 the population density of the upper laser level and σ_n the frequency dependent stimulated emission cross section of the upper laser level. s_n is the fraction of the spontaneous emission into the n-th mode. It contains the emission profile S_n and the total number p of resonant modes possible in the laser resonator volume V_R [124]:

$$
s_n = \frac{S_n}{p}
\tag{4.2}
$$

$$
\text{with} \quad p = 8 \cdot \pi \cdot \nu^2 \cdot \frac{\Delta\nu_g \cdot V_R}{c^3} \quad \text{and} \quad S_n = \frac{\left(\frac{\Delta\nu_g}{2}\right)^2}{(f_n - f_0)^2 + \left(\frac{\Delta\nu_g}{2}\right)^2}.
\tag{4.3}
$$

$\Delta\nu_g$ is bandwidth of the gain medium and f_n and f_0 are the frequency of the considered mode and the frequency at line center respectively.

The first term on the right hand side of Equation 4.1 denotes the resonator losses followed by the terms for the spontaneous emission and the amplification. The fourth term describes an exchange of population between spectrally adjacent modes resulting from the modulation of depth m_{FD}. m_{FD} differs in magnitude from the phenomenological modulation depth m introduced in Equation 3.1 and will be calibrated to this variable by numerical simulations performed in Section 4.3.2.

To include the nonlinear SBS-mirror into this model several aspects have to be considered. First of all with increasing reflectivity of the SBS-mirror the oscillation switches from the start resonator to the SBS resonator. This switch affects on the one hand the length and on the other hand the loss of the resonator which the revolving light experiences. Therefore we substitute the resonator decay time τ_R and the resonator length L by corresponding expressions that depend on the time-dependent reflectivity of the SBS-mirror $R_{SBS}(t)$:

$$\frac{1}{\tau_R} \to \left[\frac{R_{SBS}(t)}{\tau_{SBS}} + \frac{(1 - R_{SBS}(t))}{\tau_{start}} \right] \tag{4.4}$$

$$\frac{l}{L} \to \left[R_{SBS}(t) \cdot \frac{l}{L_{SBS}} + (1 - R_{SBS}(t)) \cdot \frac{l}{L_{start}} \right]. \tag{4.5}$$

L_{SBS}, L_{start}, τ_{SBS}, τ_{start} are the lengths and decay times of the SBS- and the start resonator respectively. Furthermore, the Stokes-shift which the reflected light experiences due to the movement of the reflecting sound wave has to be considered. The Stokes-shift for the SBS material used in the experiment, SF$_6$ at a pressure of 20 bar, amounts to 240 MHz. This value is exactly three times the spectral spacing of the longitudinal modes of the realized SBS-resonator. Neglecting anti-Stokes- and higher Stokes-orders we can describe the Stokes-shift as a transfer of energy down the longitudinal mode scale of the SBS-resonator:

$$\frac{d\phi_n}{dt}(\text{Stokes-shift}) = [\phi_{n+3}(t) - \phi_n(t)] \cdot R_{SBS}(t) \cdot \frac{c}{2 \cdot L_{SBS}}. \tag{4.6}$$

The above equation can be read as follows: The n-th mode is fed by the mode three steps up the mode scale $(n + 3)$ and transfers population down the mode scale. The rate at which the transfer occurs scales with the population of the respective modes, the instantaneous SBS-reflectivity $R_{SBS}(t)$, and scales inversely with the SBS-resonator length L_{SBS}. Including (4.4) to (4.6) into (4.1) we obtain for the time derivative of the photon density of the n-th mode:

$$\frac{d\phi_n}{dt} = - \left[\frac{R_{SBS}(t)}{\tau_{SBS}} + \frac{(1 - R_{SBS}(t))}{\tau_{start}} \right] \cdot \phi_n(t)$$

$$+ \left[R_{SBS}(t) \cdot \frac{l}{L_{SBS}} + (1 - R_{SBS}(t)) \cdot \frac{l}{L_{start}} \right] \cdot \frac{n_2(t) \cdot s_n}{\tau_{sp}}$$

$$+ \left[R_{SBS}(t) \cdot \frac{l}{L_{SBS}} + (1 - R_{SBS}(t)) \cdot \frac{l}{L_{start}} \right] \cdot n_2(t) \cdot \sigma_n \cdot \phi_n(t) \cdot c \tag{4.7}$$

$$+ \left[-\phi_n(t) + \frac{\phi_{n+1}(t)}{2} + \frac{\phi_{n-1}(t)}{2} \right] \cdot \frac{m_{FD}}{2} \cdot \frac{c}{R_{SBS}(t) \cdot L_{SBS} + (1 - R_{SBS}(t)) \cdot L_{start}}$$

$$+ [\phi_{n+3}(t) - \phi_n(t)] \cdot R_{SBS}(t) \cdot \frac{c}{2 \cdot L_{SBS}}.$$

Strictly speaking this description only applies for those modes which can be accommodated in both resonators equally. The SBS-resonator modes are spaced by 80 MHz whereas the modes of the start-resonator which is twice as long are spaced by 40 MHz. Only every second start resonator mode will fit into the SBS-resonator. For the numerical calculations the improper, interstitial start-resonator modes will not be considered at all.

Due to the homogeneously broadened amplification bandwidth of Nd:YAG the sum over all modes can be utilized to calculate the time derivative of the population of the upper laser level:

$$\frac{dn_2}{dt} = W_p \cdot n_0 - n_2 \cdot c \cdot \sum (\phi_n \cdot \sigma_n) - \frac{n_2}{\tau_{sp}}. \tag{4.8}$$

W_p denotes the pump rate and n_0 and n_2 are the density of dopant ions and the population density of the upper laser level, respectively. Assuming that the population of the pump band and the lower laser level is negligible — which is legitimate for Nd:YAG at moderate temperatures — the population density of the upper laser level n_2 is equivalent to the inversion density.

It remains to implement the time dependent reflectivity $R_{SBS}(t)$ of the SBS-mirror. As discussed in Section 2.1.1 there is a model describing the sound wave generation and the resulting reflectivity with temporal and spatial resolution for an external SBS-reflection [18, 19, 20]. To the best of my knowledge there is no published model describing the sound wave generation and the transient reflectivity with spatial resolution for the more complex case of an SBS-mirror inside a cavity. Here, we confine ourselves to a phenomenological description of the generation and decay of an overall sound wave amplitude in the SBS-cell and its corresponding reflectivity $R_{SBS}(t)$. It is further assumed that the generation of the sound wave amplitude depends linearly on the intensity $I(t)$ of the incident light:

$$\frac{dQ}{dt} = -\frac{Q(t)}{\tau_p} + g* \cdot I(t) \tag{4.9}$$

$$R_{SBS}(t) = 1 - \exp\left(\frac{-Q(t)}{Q_s} \right). \tag{4.10}$$

Equation 4.10 is a more or less arbitrarily chosen function ranging from zero to unity thereby describing the saturation behavior of the SBS-reflectivity. τ_p is the phonon lifetime, $Q(t)$ is a measure for the sound wave amplitude, Q_s describes the saturation sound wave amplitude and $g*$ is a Brillouin gain related parameter. Q_s and $g*$ will be used to fit the shape of the calculated Q-switch pulse envelopes to the experimental results. Their magnitudes govern the SBS-threshold and the slope of the SBS-reflectivity $R_{SBS}(t)$. They are consequently decisive whether a Q-switch pulse occurs at all and particularly influence the slope of the leading edge of the Q-switch pulse envelope. They do not influence the time at which the pulse occurs and therefore they have no significant effect on the pulse duration and pulse energy. Also there is no direct relation to the mode-locking. Further parameters which are used to fit the calculation to the experiment are the linear loss factor V which applies for both resonators and V_{start} for additional start resonator losses. V governs the SBS-resonator decay time τ_{SBS} and therefore the final edge of the pulse. V_{start} and V influence the delay time until the Q-switch sets in and therefore the pulse duration and pulse energy.

The resulting electrical field $E(t)$ is obtained by the summation of the field contributions of all modes $(E_n(t) \propto [\phi_n(t)]^{0.5})$ assuming that the phase angles are identical for all modes and can hence set to be zero. In this case the intensity $I(t)$ is given by:

$$I(t) = \frac{\epsilon_0 \cdot c}{2} \cdot \left| (E_1(t) \cdot e^{i\omega_1 t} + ... + E_n(t) \cdot e^{i\omega_n t}) \right|^2 . \tag{4.11}$$

The assumption that the phase angles for all modes are zero is identical to assuming perfect mode-locking. In this case the resulting mode-lock pulse duration is transform limited by the spectrum of the pulse. Phase noise due to spontaneous emission and the SBS-bandwidth as well as a mismatch between longitudinal mode spacing and modulation frequency are being neglected.

Another aspect that is not incorporated in this model is the propagation of the light in the resonator. If we started a calculation according to this model with just one mode occupied it would yield three modes populated for the next time step of the iterative solving procedure due to the exchange term for the modulation. In the next but one time step already five modes would be populated notwithstanding the fact that the light would actually have to do one full round trip until it passes the modulator for a second time. The same argument applies for the Stokes-shift as well which becomes most apparent when R_{SBS} becomes unity. In this case all the light is shifted by three modes for each round trip and thus the spectrum is expected to be shifted as a whole. For $R_{SBS} = 1$ the Stokes-shift does not contribute to the generation of bandwidth in reality. In this model, however, the Stokes-shift is described as an exponential decay and growth where a constant percentage of the population of the respective mode is shifted in each time step. As we will see in Section 4.3 this description yields a generation of bandwidth even though R_{SBS} approaches unity.

In the following this model based on spectrally resolved rate equations will be referred to as the frequency domain model since the mode-locking dynamics is described in the frequency domain.

4.2 Time domain model

The description of the mode-locking in the frequency domain as presented in Section 4.1 yields dynamics on a ps-timescale which are strictly related to the spectrum of the output. It is a best case scenario since imperfections such as frequency mismatches and phase noise due to the statistical spontaneous emission process are left out. This section offers a model with a contrary approach by describing all occurring dynamics in the time domain. Spontaneous emission is assumed to be continuous wave which corresponds to the spontaneous emission into just one mode in the time domain picture. The mode-locking effect of the AOM is incorporated as a harmonic loss modulation. To display sub-round trip time dynamics a spatial resolution of the intensity along the axis of the resonator is introduced. Due to the propagation of the light this is equivalent to a temporal resolution.
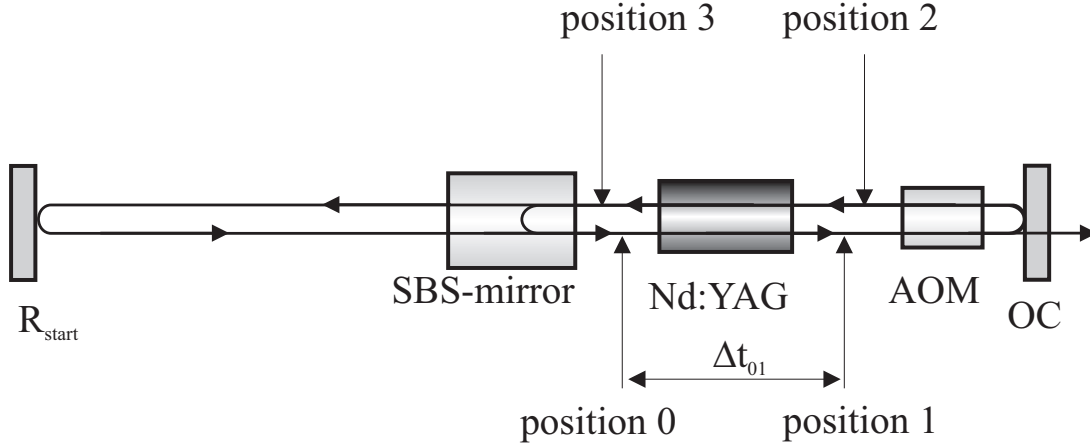
Figure 4.1: Schematic of the SBS-laser showing the positions corresponding to the calculation steps in the time domain model; AOM denotes the acousto optic modulator, OC the output coupler

The basic idea of this model is to display the photon density current at one certain spot in the resonator i.e. position 0 in Figure 4.1 in contrast to the mean intensity in the resonator that is considered in the rate equations. In order to compute the photon density current $j(t)$ at a certain time t we refer to the photon density current $j(t - T)$ that was to be found here one round trip time T ago and calculate all changes that the light has experienced during this round trip. In order to calculate the changes during this round trip three intermediate steps will be taken corresponding to the positions 1–3 in the resonator indicated in Figure 4.1.

The first step would be to calculate the amplified photon density current j_1 and the depleted inversion density n_2' after the first pass of the amplifier:

$$j_1 = j_0(t - T) \cdot \exp\left[n_2(t) \cdot \sigma \cdot l\right] + s \cdot \frac{n_2}{\tau_{sp}} \cdot l \tag{4.12}$$

$$n_2' = n_2(t) - n_2(t) \cdot \sigma \cdot j_0(t - T) \cdot \Delta t. \tag{4.13}$$

Strictly speaking we would have to write $j_1(t - T + \Delta t_{01})$ where Δt_{01} refers to the delay time corresponding to the propagation from position 0 to position 1 (see Fig. 4.1). But since this is only an intermediate step to illustrate the calculation procedure and since the exact times corresponding to these steps are of no relevance this distinction is neglected here. Apart from that, the photon density current is only recorded and displayed for one position anyway and the four calculation steps could just as well be merged to a single step.

Again σ is the emission cross section and s the fraction of spontaneous emission into the laser mode. Assuming spontaneous emission into just one mode, this is identical to the inverse of the number of all modes p resonant in the resonator volume. The expression for the inversion depletion is derived from the laser rate equations. Δt refers to the width of the time step that is calculated. Please note at this point that the pumping and inversion losses due to spontaneous emission will be considered after the second pass through the laser active material.

The second step in our calculation of a time step describes the harmonic loss modulation as introduced by Equation 3.1 and linear resonator as well as output coupling losses:

$$j_2 = j_1 \cdot \left[1 - m \cdot \frac{\sin(\omega_{AOM} \cdot t) + 1}{2} \right]^2 \cdot V \cdot R_{OC}. \tag{4.14}$$

ω_{AOM} is the modulation frequency of the AOM, V the resonator round trip loss factor and R_{OC} the output coupling reflectivity. What follows is a second pass through the amplifier now with the partially depleted inversion population n_2':

$$j_3 = j_2 \cdot \exp\left[n_2'(t) \cdot \sigma \cdot l \right] + s \cdot \frac{n_2'}{\tau_{sp}} \cdot l. \tag{4.15}$$

In the calculation of the inversion population for the next time step $n_2(t + \Delta t)$ expressions for the pump process and the spontaneous emission loss must be included:

$$n_2(t + \Delta t) = n_2' + \left[-n_2' \cdot \sigma \cdot j_2 - \frac{n_2'}{\tau_{sp}} + W_p \cdot n_0 \right] \cdot \Delta t. \tag{4.16}$$

Now we can obtain the photon density current j_0 at the examined position by considering the transmission of the SBS-mirror in both directions:

$$j_0(t) = j_3 \cdot R_{SBS}(t) + j_{start}(t - T) \cdot R_{start} \cdot V_{start}. \tag{4.17}$$

j_{start} is the portion of the light that leaks through the SBS-mirror into the start resonator:

$$j_{start}(t) = [1 - R_{SBS}(t)] \cdot j_3. \tag{4.18}$$

An equivalent description of the approach taken in this model is that we consider packages of light of length $c \cdot \Delta t$ and let them propagate through the resonator and register all interactions with the optical devices. By doing this $N = T/\Delta t$ times for N successive packages of light we have completed a full resonator round trip and recorded the photon densities in the resonator with a spatial resolution corresponding to $c \cdot \Delta t$. This data will be the starting condition for the next round trip.

Apparently the propagation described by this model approximates the experimental setup described in Figure 4.1. It describes a setup with the laser active material and the modulator situated at the position of the output coupler. So pumping and depletion by other fractions of the revolving light between the first and second pass through the amplifier remain unconsidered. Also the influence of the Stokes-shift on the mode-locking is not taken into account.

4.3   Numerical results

Now the two models will be applied to explain different aspects of the emission dynamics. The numerical solution of the spectrally resolved laser rate equations is achieved by the Euler-method. The simulations on the basis of either model were implemented with MatLab on a conventional personal computer. For both models the starting conditions are zero intensity in the resonator and a completely depleted laser material. So the buildup of inversion is displayed from its very beginning.

The pumping conditions are chosen according to the setup configuration with the flash lamp pumped laser head described in Chapter 3, but any time dependence of the pump power during the flash lamp pump pulse is neglected. The average power during the flash lamp pump pulse is 60 kW and the excitation efficiency is estimated to be 5 %. Considering the rod dimensions of 10 cm in length and 6.35 mm in diameter and the dopant density of $1.38 \cdot 10^{23}\,\mathrm{cm}^{-3}$ this yields a pump rate of $W_p = 36.7\,\mathrm{Hz}$. The pump duration until the first pulse occurs ranges from 20 to 80 μs depending on R_{start}. Since the aim is to display the laser dynamics on a ps-timescale this demands a very high number of steps within the overall period of several 10 μs to be calculated. In addition for the frequency domain model the effort scales with the number of considered modes which is typically 300–500. To limit the time expense for the simulation of one pump – pulse cycle to a reasonable duration the step width is held variably. During the buildup of inversion the step width is chosen wider (10^{-10} s) for the frequency domain model and as soon as the intensity in the start resonator becomes appreciable the step width is decreased (10^{-11} s) to fully display the mode-locking dynamics. Under these conditions a full simulation of a period of 100 μs corresponding to 1–5 Q-switch pulses takes about 2 hours. In the time domain model the calculation of each time step consists of only a small number of fundamental computations. The same time span can be calculated with a 10^{-11} s resolution within a few seconds and without the need of a variable step width. In order to ascertain that numerical inaccuracies are negligible the temporal resolution is enhanced by a factor of 10 and still the same results are gained.
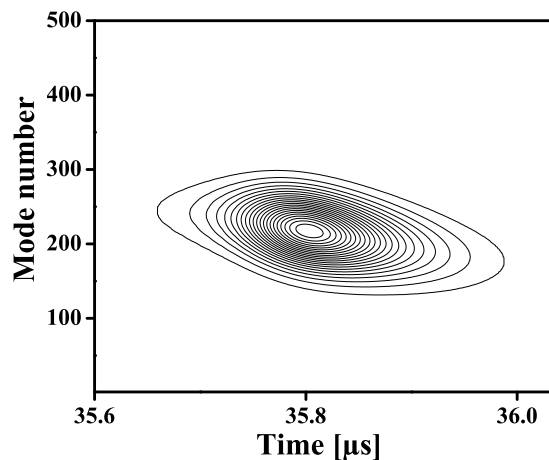
Figure 4.2: Contour plot of the evolution of 501 longitudinal modes during a Q-switch pulse; spontaneous emission into all modes according to the gain profile of Nd:YAG

Figure 4.2 shows the results of a simulation of the development of 501 modes for a start resonator mirror reflectivity $R_{start} = 0.75$. The maximum of the stimulated emission cross section profile is located on mode number 251. The dynamics in the population of the 501 modes are illustrated as a contour plot with lines of equal intensity. The bandwidth of the calculated emission is dominated by the spontaneous emission profile and is in this case independent of the modulation depth m of the AOM. The shift to lower frequencies that the spectrum experiences during the course of the pulse is caused by the SBS-Stokes-shift.

Indeed we know from the experiments presented in Section 3.4 that for the case without active mode-locking only every third mode with a spectral spacing of 240 MHz is significantly populated. The 240 MHz-periodicity in the spectrum corresponds to the Brillouin-frequency of SF_6. The omittance of two out of three modes indicates that the bandwidth of the spectrum in this case is generated by the Stokes-shift and originates from just one dominant mode. Accordingly we will choose spontaneous emission into just one mode to be the starting conditions in the following simulations.

The top part of Figure 4.3 shows the intensity distribution resulting from a simulation of the development of 301 modes while only the 151-th mode is fed by spontaneous emission. The corresponding transient spectrum is depicted in the mid section of Figure 4.3. The bottom graph illustrates sectional views of the transient spectrum at times indicated by the arrows. For comparison reasons the intensity in the respective spectra is normalized to unity. The bandwidths corresponding to these sectional views are listed in Table 4.1. It can be clearly seen that at the starting edge of the pulse the shift of the maximum of the emission spectrum as well as the increase in bandwidth is still small due to the small R_{SBS} and accelerates and finally saturates in the course of the pulse.
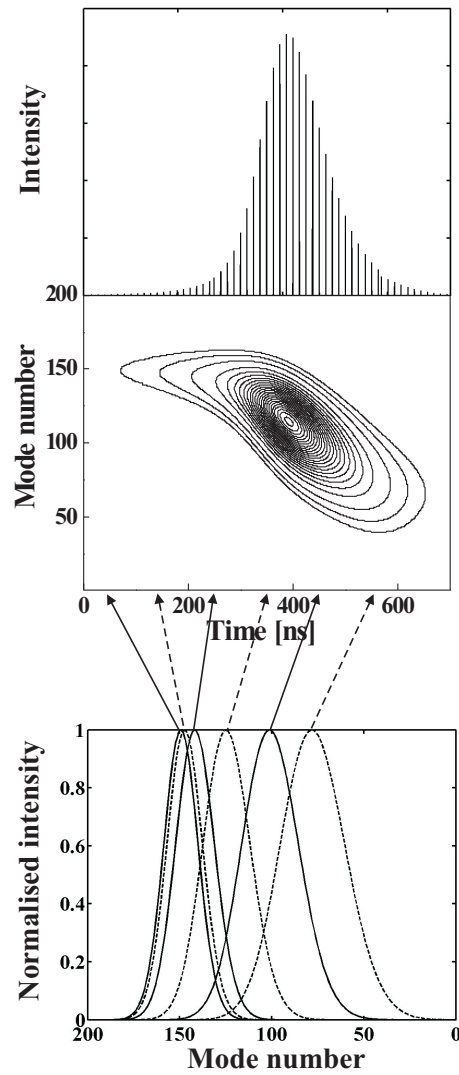
Figure 4.3: Results for a simulation with spontaneous emission into just one mode (nr. 151), top: intensity distribution, middle: contour plot of mode evolution, bottom: normalized spectra at different times of the Q-switch pulse

Time [ns]	Bandwidth [GHz]
50	1.78
150	1.83
250	2.04
350	2.45
450	2.90
550	3.31

Table 4.1: Emission bandwidths corresponding to the sectional views in Fig. 4.3

As already indicated in the introduction of the model in Section 4.1 the generation of bandwidth by the Stokes-shift does not cease with R_{SBS} approaching unity (see Table 4.1) which is due to the approximated implementation of the Stokes-shift in the model. The Stokes-shift is described as an exponential decay and transfer of the population of the modes according to the round trip time and R_{SBS} rather than a discrete shift after exactly one SBS-resonator round trip. Whereas in the case of spontaneous emission into all modes the gain profile determines the resulting emission bandwidth now it is governed by the bandwidth generation of the SBS-Stokes-shift. The loss modulation by the AOM still does not contribute very much to the generation of bandwidth which is in accordance with the experimental findings presented in Section 3.4. It merely provides an exchange of population between spectrally adjacent modes which will be discussed in more detail later on. Only in the very starting edge of the pulse the spectrum is notably wider if modulation is applied.

4.3.1 Comparison between the results from both models and experiment

We can now compare the calculated intensity runs for the two models with each other and with the measurement (Fig. 4.4). To allow for a quantitative comparison of the results from both models, here the photon densities coupled out of the resonator are displayed. The frequency domain model issues the photon densities inside laser resonator that consist of the superposition of both propagation directions. The share of photon density propagating towards the output coupler is $(1 + R_{OC})^{-1}$ resulting in a photon density ϕ_{out} coupled out of the resonator:

$$\phi_{out} = \phi \cdot \frac{1 - R_{OC}}{1 + R_{OC}}. \tag{4.19}$$

The time-domain model issues the photon density current propagating in just one direction. We can easily obtain the photon density coupled out of the resonator by:

$$\phi_{out} = j_1 \cdot \frac{(1 - R_{OC})}{c}. \tag{4.20}$$

In the calculations as well as in the experiment the reflectivities of the start resonator mirror R_{start} and the output coupler R_{OC} are 75 % and 70 % respectively. In a first approach the start resonator loss factor V_{start} is set to 1. The linear loss factor V for the resonator round trip is 0.95 and the modulation depths m and m_{FD} are 0.03 in both simulations. In terms of Q-switch pulse shape and duration there is an excellent correspondence between the two simulations and they are in very good agreement with the measurement. Both simulations yield pulse durations (FWHM) of 125 ns compared to 105 ns in the measurement. The Q-switch pulse shape can be slightly influenced by the free parameters Q_s and $g*$ that govern the slope and the amplitude of $R_{SBS}(t)$. Also the delay time until the Q-switch sets in is in very good agreement between both models. For the measurement this time is not comparable due to the time dependent pump intensity that is not incorporated in either model.
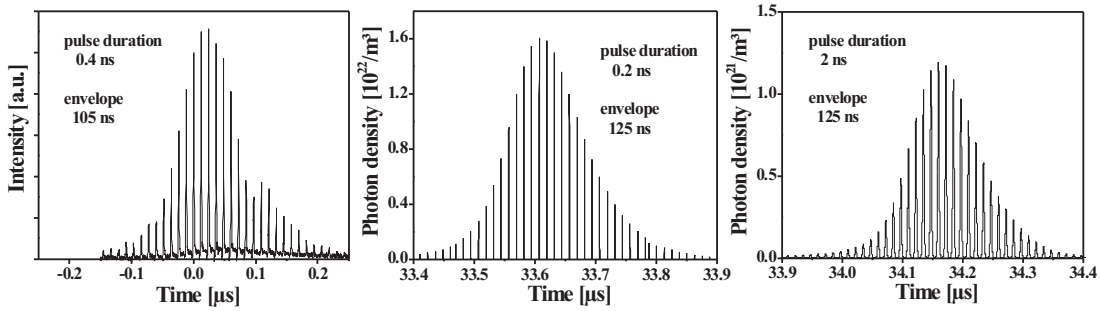
Figure 4.4: Temporal intensity distribution gained from measurement (left) frequency domain model (middle) and time domain model (right)

The correspondence with regard to Q-switch pulse duration between simulations and experiment can be further improved by taking into account a linear loss factor V_{start} for the start resonator round trip in the models. Choosing V_{start} to be 0.8 the measured dependence of the pulse durations can be well reproduced by the calculations. Figure 4.5 shows the dependence of the Q-switch pulse duration on R_{start} for the measurement as well as for the simulations. The reason for the increase in pulse duration with increasing R_{start} is the decrease in the delay time between the beginning of the pumping and the onset of the Q-switch pulse which results in a higher gain at the time of the occurrence of the pulse. The calculated delay times for $V_{start} = 1$ are also given in Figure 4.5. The experimental delay times are left out here because they vary from Q-switch pulse to Q-switch pulse within a burst owing to the time dependent pump intensity of the flash lamps.

Figure 4.6 shows a comparison between calculated pulses and measured ones for three different values of R_{start}. The start resonator loss factor V_{start} for these calculations was set to be 0.8, so the pulses shown correspond to the lower data line presented in Figure 4.5. The measured Q-switch pulse shapes can very well be reproduced by the calculations. Only for low start resonator losses the edges of the calculated Q-switch pulse envelopes are more pronounced than found experimentally.
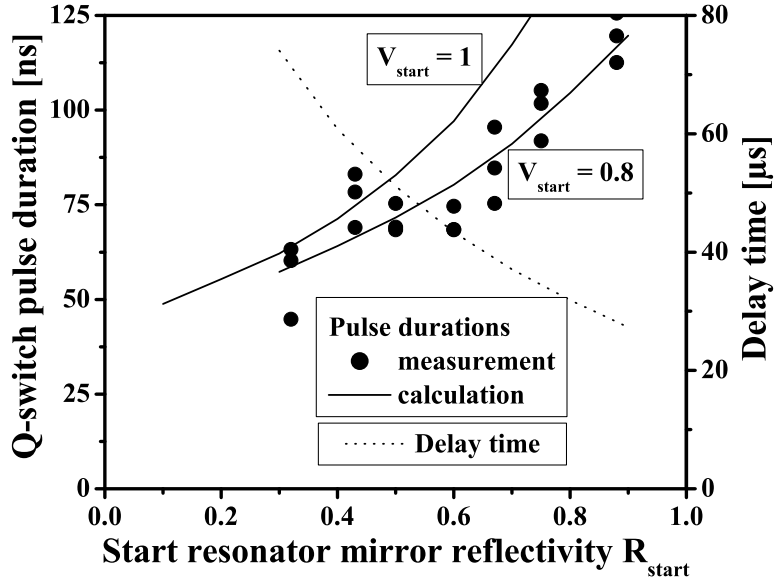
Figure 4.5: Dependence of Q-switch pulse duration on R_{start} for calculation (solid line) and measurement (marks) and calculated dependence of the delay time on R_{start} (dotted line)

Regarding the mode-lock pulse duration the correspondence between both models and the measurement shows some discrepancy. The time domain model yields pulse durations of 2 ns while according to the frequency domain model the pulses last for only 0.2 ns. In the experiment we found the pulses to be as short as 0.4 ns. The differences in this regard can be explained by the different assumptions and negligences that are found in the descriptions of the mode-locking in both models. In the time domain model the influence of the SBS-Stokes-shift on the mode-locking is not taken into account. As discussed earlier this is the dominant effect for the generation of bandwidth and thus neglecting it leads to considerably longer pulse durations than found in the experiment. The frequency domain model in contrast implies constant and identical phase factors for all modes neglecting phase noise which results in a somewhat optimistic calculation if short pulses are desired. Also, due to the approximated description of the Stokes-shift it keeps generating bandwidth when the SBS-reflectivity approaches unity instead of merely shifting the spectrum. The wider pulses calculated by the time domain model result in peak photon densities that are lower by more than an order of magnitude compared to the frequency domain model.

It remains to compare the measured peak power with the calculations. From the frequency domain model we obtain photon densities ϕ coupled out of the resonator of $1.6 \cdot 10^{22} \, m^{-3}$ (see Fig. 4.4). Assuming a beam radius of 1.25 mm corresponding to the calculated transverse eigenmode at the position of the laser head (Fig. 3.1) this is equivalent to a peak power of 4 MW. Experimentally the mode-lock pulse energy for $R_{start} = 0.75$ was determined to be 0.35 mJ (see Figure 3.11) corresponding to a pulse
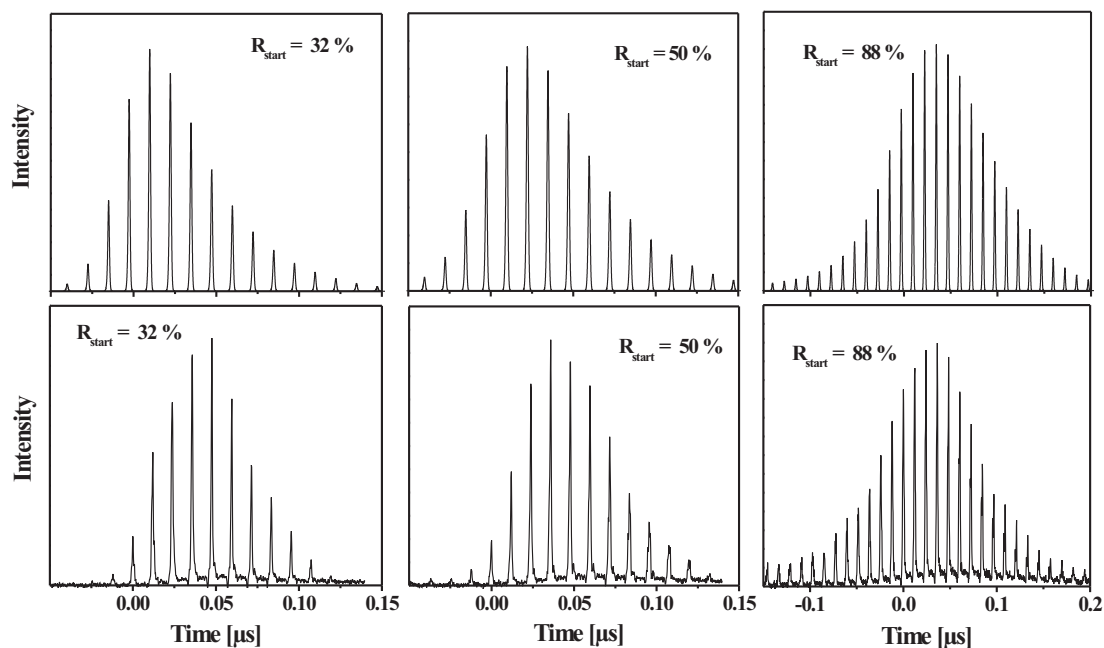
Figure 4.6: Comparison of the Q-switch pulse shapes between calculation (top line of graphs) and measurement (bottom line) for different values of R_{start}

peak power of around $1\,MW$. Taking into account that the pulse durations according to the frequency domain model are only half as short as the measured ones the pulse energies in the experiment and the model are of the same order of magnitude.

4.3.2 Validation/Calibration of the models — Conventional mode-locked oscillator

The main distinguishing aspect for the two models that leads to a difference in the resulting pulse durations by an order of magnitude is the consideration of the contribution of the Stokes-shift in the frequency domain approach and its neglect in the time domain model. Hence, for a conventional mode-locked laser the differences in the modeling results should disappear. However, the implementation of the loss modulation of the AOM is carried out differently in the two models. Thus, identical results are expected if the differences in the mode-locking descriptions and their underlying assumptions are compensated by an adaptation of the values for the depths of modulation m and m_{FD} for the two complementary approaches. Figure 4.7 shows an example where both models issue identical results with regard to the mode-lock pulse duration as well as for the Q-switch envelope. This is achieved by choosing a modulation depth for the frequency domain simulation of $m_{FD} = 0.005$.

To overcome the imperfections inherent to both complementary models it would be
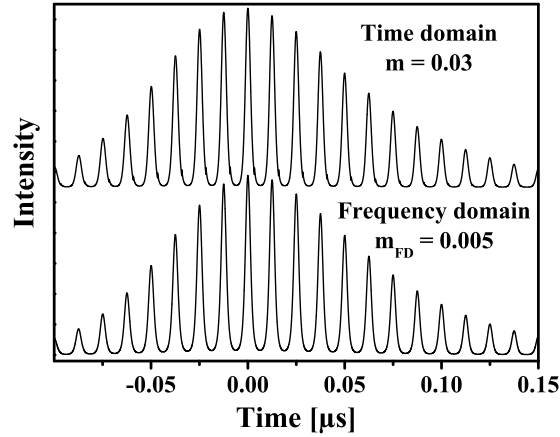
Figure 4.7: Comparison of the two models for the Q-switch pulse build-up in a conventional mode-locked laser

desirable to combine the virtues of both models, thereby receiving a complete description of the temporal and spectral dynamics. One possible approach would be to merge both models and calculate the evolution of the individual modes according to the time domain model. This, however, would inevitably issue ps-dynamics of the individual modes which violates the Heisenberg's uncertainty relation considering the limited bandwidth of the individual modes. A second approach could be the implementation of the Stokes-shift into the time domain model. This would demand a more sophisticated description of the movement of the SBS-sound wave that would allow to display its phase modulating properties. To implement the phase modulation the electrical fields would have to be considered instead of the intensities and a key virtue of the time domain model — its simplicity — would get lost. Therefore, these two complementary but reasonably simple models will be used to investigate different aspects of the mode-locked SBS-laser oscillator.

4.3.3 Influence of depth of loss modulation of the AOM

It was already visible in Figure 4.3 that in the frequency domain model the modulation of the AOM does not contribute significantly to the bandwidth generation compared to the influence of the Stokes-shift. It merely provides an exchange of population between adjacent modes and smoothes the spectra which is illustrated in Figure 4.8.
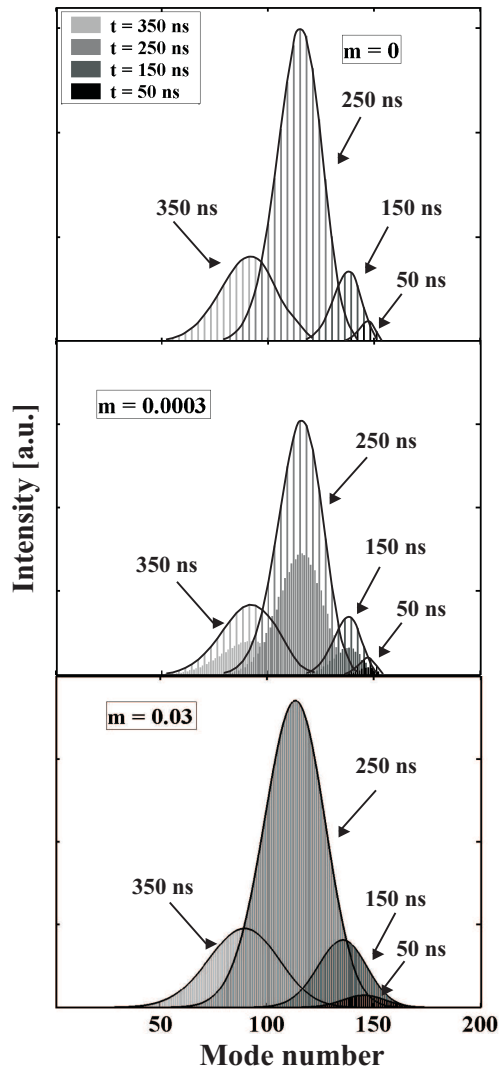
Figure 4.8: Calculated spectra for different modulation depths and times within the Q-switch pulse

It shows calculated spectra for different times within the Q-switch pulse. For a clearer distinction between the different spectra their envelopes have been added in the display. In the top diagram of Figure 4.8 there is no AOM loss modulation applied in the calculation and accordingly only every third mode is populated starting with the initially triggered mode number 151. In the central diagram of Figure 4.8 the 240 MHz periodicity caused by the Stokes-shift is still apparent. Here a modulation depth of $m = 0.0003$ is just enough to allow for a population of the interstitial modes of half the strength of the dominant modes. The modulation depth applied in the experiments was measured to be up to 3 % depending on the chosen carrier level of the AOM. For

this modulation depth a uniform population of all SBS-resonator modes underneath the envelope is obtained (bottom graph of Fig. 4.8).
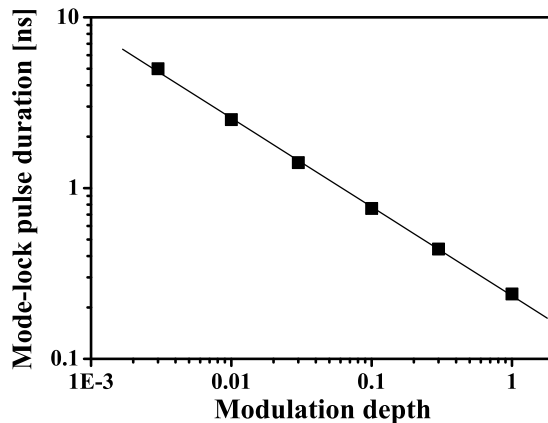
Figure 4.9: Study of the effect of the modulation depth of the AOM on the mode-lock pulse duration

The effect of the depth of loss modulation on the duration of the mode-lock pulses can be conveniently studied in the time domain model since other effects and in particular the Stokes-shift is neglected in this picture. Figure 4.9 shows the results of a calculation that explored this dependence. Here m is varied between 0.3 % and unity while all other parameters are held constant. In the double logarithmic display of Figure 4.9 the result can be well fit by a straight line. So the dependence of the pulse duration Δt_{ML} on the modulation depth m can be described by $\Delta t_{ML} \propto m^{-0.52}$ which is in very good agreement with analytical calculations that predict an exponent of -0.5 for the QML regime [111] in contrast to -0.25 for steady state mode-locking [82].

4.3.4   Influence of length mismatch

Assuming constant and identical phase angles for all modes, a misfit between modulation frequency and resonator round trip time which leads to a divergence of the phases cannot be taken into account in the frequency domain model. In the time domain model, however, the effect of maladjustment in frequencies on the pulse structure can be displayed. If the modulation frequency matches the pulse repetition rate the minimum loss of the AOM coincides with the pass of the revolving pulse. Both edges of the pulse experience higher losses compared to the peak of the pulse and thus the pulse is shortened each round trip. For a mismatch this is not the case. The pulse arrives slightly out of time and thus one edge experiences a higher loss than the opposite edge. Therefore, the pulse shortening is not as efficient and the pulse gets shifted with the result that the laser emits at a repetition rate corresponding to the modulation frequency of the AOM rather than to the inverse resonator round trip time.

A comparison of the intensity distribution for the ideal laser setup with a detuned

laser setup gained from a simulation based on the time domain model is given in Figure 4.10. Here m is chosen to be 0.1 and R_{start} to be 0.43 which explains the considerably shorter durations of the envelope compared to the results shown before. The detuning between longitudinal mode spacing and modulation frequency amounts to 0.5 MHz which corresponds to a detuning of the resonator length of 1.2 cm. Whereas the calculation of the ideal setup yields mode-lock pulse widths of 0.7 ns the detuned laser issues pulses with durations of 4.4 ns and the peak power is smaller by a factor of 8 compared to the ideal setup. Because of the higher losses caused by the misfit of the frequencies the Q-switch pulse occurs 4 μs later for the detuned laser.
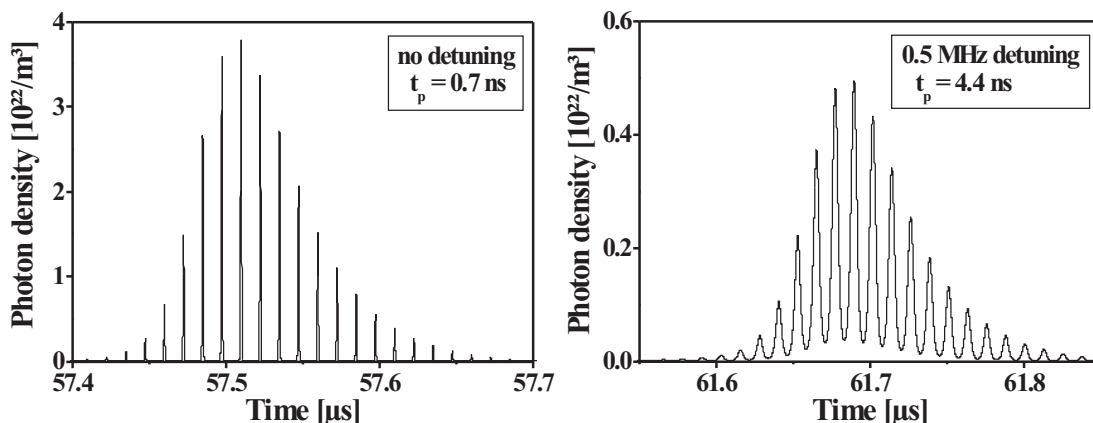
Figure 4.10: Study of the effect of a mismatch between spectral resonator mode-spacing and modulation frequency on mode-locking, left: no mismatch, right: 0.5 MHz mismatch

4.3.5   SBS-material parameters: Phonon lifetime and Brillouin-frequency

Numerical modulations also offer the investigation of the effect of laser parameters that are not as easily accessible in the experiment. Materials properties for example can in general not be changed individually. With these numerical simulations the influence of a single parameter can be investigated without having to alter other parameters.

The top part of Figure 4.11 shows the influence of the phonon lifetime τ_p on the mode-locking pulse duration of the SBS-laser while all other parameters were held constant. At around 10 ns phonon lifetime a transition occurs that is connected with a change of the pulse duration of more than 50 %. Apart from this step like change the influence of the phonon lifetime on the pulse duration is negligible. The reason for this transition becomes apparent if we look at the temporal evolution of the SBS-reflectivity during the Q-switch pulse which is depicted for three different phonon lifetimes in the bottom part of Figure 4.11. If the phonon lifetime is large compared to the resonator round trip time ($T = 12.5$ ns) the sound wave does not decay significantly in the interval between two pulses and so the modulation of the SBS-reflectivity is small (Fig. 4.11 right). In this particular case the Brillouin gain is chosen to be so high, that the reflec-
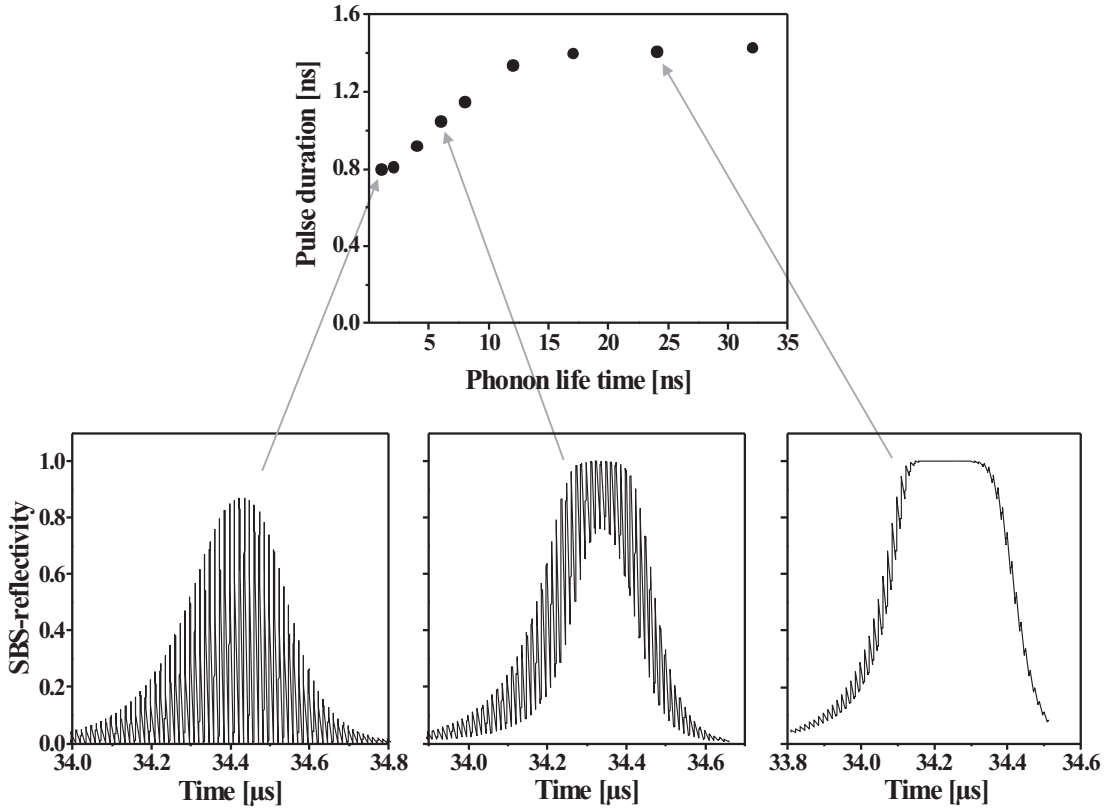
Figure 4.11: Influence of the phonon lifetime on the temporal dynamics, top: mode-lock pulse duration, bottom: SBS-reflectivity throughout the Q-switch pulse for three different phonon lifetimes

tivity saturates at unity and no modulation of the reflectivity occurs at the peak of the Q-switch pulse. If the phonon lifetime is comparable to the round trip time (Fig. 4.11 middle) the modulation of the SBS-reflectivity becomes more feasible and is in effect a modulation of the resonator loss that leads to mode-locking. Therefore, shorter phonon lifetimes lead to shorter pulses until the modulation is saturated. This is achieved as soon as the reflectivity approaches zero between two pulses. A further shortening of the phonon lifetime will not decrease the pulse duration significantly but the rapid decay of the sound wave amplitude will prevent the reflectivity from reaching unity (Fig. 4.11 left). In summary the transition between the two pulse duration regimes as shown in the top graph of Figure 4.11 can be explained by a transition from a saturated steady state reflectivity during the Q-switch pulse to a modulation of the SBS-reflectivity of 100 % depth. For the case of SF_6 with a phonon lifetime of 17 ns and for the SBS-resonator round trip time of 12.5 ns the contribution of the modulation of the SBS-reflectivity to the bandwidth generation is negligible. However, if the phase locking effect of the modulation in the SBS-reflectivity could provide the synchronization of the modes which are

generated by the SBS-Stokes-shift the AOM could be set aside. Unfortunately, neither the frequency domain nor the time domain model are presently fit to investigate this issue.

The outstanding role of the Stokes-shift for the process of bandwidth generation could already be guessed from the spectral analysis in Section 3.4 and was qualitatively verified by the previous numerical simulations of the spectral evolution (see Fig. 4.3). Here the influence of a variation of the Brillouin-frequency ν_B — that determines the magnitude of the Stokes-shift — on the spectrum and on the pulse duration is to be discussed quantitatively.
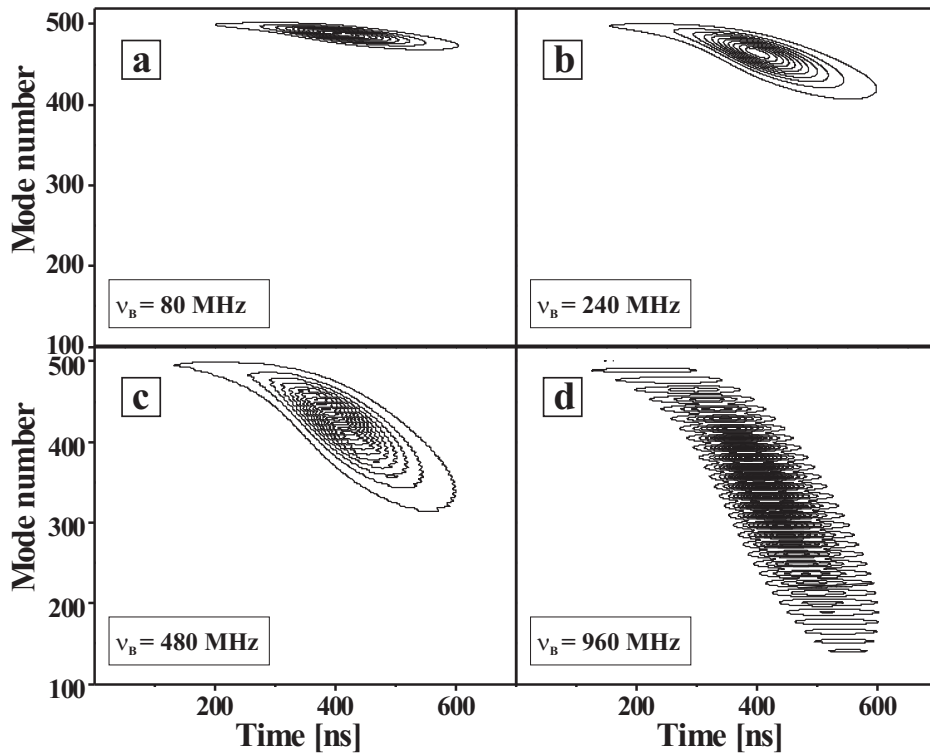
Figure 4.12: Study of the influence of the Brillouin-frequency ν_B on the spectrum; for large ν_B (c and d) the spectrum is no longer homogeneous

Figure 4.12 contains four transient spectra for different values of ν_B calculated with the frequency domain model. The depth of modulation m_{FD} is chosen to be 0.005 corresponding to a modulation depth of 3 % in the time domain (see Section 4.3.2). The chosen Brillouin-frequencies in Figure 4.12 a–d meet the resonance condition for this laser setup and result in shifts in frequency corresponding to 1, 3, 6 and 12 longitudinal SBS-resonator modes, respectively. As expected the overall bandwidth increases rapidly with the Brillouin-frequency. For $\nu_B = 480\,\mathrm{MHz}$ (Fig 4.12 c) a modulation in the spectrum is already perceptible and for the highest value of ν_B the Stokes-shift is so large that the modulation of the AOM can no longer populate the interstitial modes. In the

temporal intensity distribution this modulation leads to the occurrence of side-pulses at a distance of 1 ns at either side of the pulse and with an amplitude of the 20th part of the main pulse amplitude.
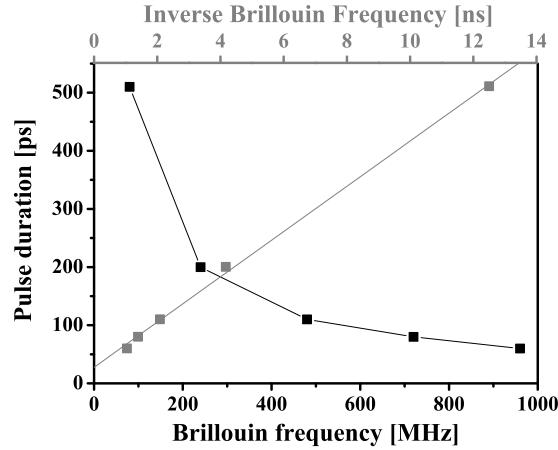
Figure 4.13: Dependence of the mode-lock pulse duration on the Brillouin-frequency

Finally, Figure 4.13 shows the behavior of the pulse duration of the mode-locked pulses under a variation of ν_B. The pulse duration decreases steadily with increasing ν_B. If the pulse duration is plotted over the inverse Brillouin-frequency (gray scale and data points in Fig. 4.13) it becomes apparent that over the whole considered frequency range an inversely linear relationship between the pulse duration and the Brillouin-frequency can be assumed. Therefore, a saturation of the bandwidth generation due to the limited amplification bandwidth is not yet reached.

These findings suggest the utilization of an SBS-material with a higher Brillouin-frequency. However, the quest for a suitable alternative might turn out to be more demanding than apparent at first glance since many requirements have to be met:

- The Brillouin-frequency has to be resonant with the AOM modulation frequency and if it is too high the spectrum becomes modulated resulting in interstitial pulses.

- If the Brillouin gain is to low or the threshold to high an initiation of the SBS could be prevented.

- If the phonon lifetime is very short compared to the repetition rate the SBS would be inhibited since the sound wave decays between the pulses.

- The damage threshold has to be high enough and the absorbtion low enough to withstand the high energy densities during the pulses.

4.4   Summary

In this chapter two novel models have been introduced that aim at displaying the temporal behavior of the spectrum and the output intensity of the mode-locked SBS-laser. The first model is based on spectrally resolved laser rate equations that display the evolution of the population of the longitudinal resonator modes. The mode-locking dynamics of the intensity are calculated from the spectrum under the assumption of perfectly synchronized modes. The second model describes all occurring dynamics of the intensity in the time domain and impresses by an exact description of the propagation in the coupled resonators. The major drawback is that the SBS-Stokes-shift can not be incorporated in the time domain picture. A phenomenological description of the passive SBS-Q-switch is implemented in both models. For simplicity, the spatial distribution and the movement of the sound wave are neglected.

Results from numerical simulations applying both models are in very good agreement with measurements with regard to Q-switch pulse properties. Standing alone both models are incomplete in the display of the mode-locking behavior. For the frequency domain model the assumption of perfect phase synchronization and the approximated display of the SBS-Stokes-shift as well as its neglect in the time domain model can be identified as the major inaccuracies. However, due to their complementary approach both models add up to a universal tool to study the influences on the complex dynamics of this laser. Studies of the influences of modulation depth and Brillouin-frequency confirm the suggestion issued in Section 3.4 that the Stokes-shift is the key source of bandwidth while the AOM merely provides a uniform distribution of the mode population within this bandwidth.

Furthermore, another mode-locking effect of the SBS-mirror can be identified: The quick depletion of the sound wave leads to a passive mode-locking via a modulation of the SBS-reflectivity.

Chapter 5

Summary and conclusion

The primary objective of this work was to develop a laser source for fundamental investigations in the field of laser – materials interactions. In particular it is supposed to facilitate the study of the influence of the temporal energy distribution such as the interaction between adjacent pulses on ablation processes. Therefore, the aim was to design a laser with a highly flexible and easily controllable temporal energy distribution. The laser to meet these demands is an SBS-laser with optional active mode-locking.

The nonlinear reflectivity of the SBS-mirror leads to a passive Q-switching and issues ns-pulse bursts with μs spacing. The pulse train parameters such as pulse duration, pulse spacing, pulse energy and number of pulses within a burst can individually be adjusted by tuning the pump parameters and the starting conditions for the laser. This flexibility allows for an independent scrutiny of the influence of the individual parameters on laser ablation processes.

Another feature of the SBS-reflection is phase conjugation, which leads to an excellent beam quality thanks to the compensation of phase distortions. Transverse fundamental mode operation and a beam quality better than 1.4 times diffraction limited can be maintained for average output powers of up to 10 W. Good beam quality is essential in order to prevent influences from undefined spatial energy deposition on laser – materials interactions.

In addition to the dynamics on a ns-timescale described above, a defined splitting up of each ns-pulse into a train of ps-pulses can be achieved by additional active mode-locking. This twofold temporal focussing of the intensity leads to single pulse energies of up to 2 mJ at pulse durations of approximately 400 ps which corresponds to a pulse peak power of 5 MW. While the pulse duration is of the same order of magnitude as those of other passively Q-switched lasers with simultaneous mode-locking, the pulse energy and pulse peak power exceeds the values of these systems found in the literature by an order of magnitude. To the best of my knowledge the laser presented here is the first implementation of a self-starting mode-locked SBS-laser oscillator.

In order to gain a better understanding and control of the transient output of the laser two complementary numerical models were developed. The first is based on laser

rate equations which are solved for each laser mode individually while the mode-locking dynamics are calculated from the resultant transient spectrum. The rate equations consider the mean photon densities in the resonator, therefore the propagation of the light inside the resonator is not properly displayed. The second model, in contrast, introduces a spatial resolution of the resonator and hence the propagation inside the resonator can more accurately be considered. Consequently, a mismatch between the loss modulation frequency and the resonator round trip time can be conceived. The model calculates all dynamics in the time domain and therefore the spectral influences such as the Stokes-shift have to be neglected. A calculation of the evolution of a mode-locked Q-switch pulse train on the basis of this time domain model takes only a few seconds for a 10 ps resolution. A corresponding simulation on the basis of the rate equations in contrast takes about two ours, but also issues the evolution of the spectrum. In both models the SBS is considered in a phenomenological description.

Both models achieve an excellent reproduction of the ns-dynamics that are generated by the SBS-Q-switch. Separately, each model fails to reproduce all aspects of the ps-dynamics of the SBS-laser in detail. This can be attributed to the complexity of the numerous physical processes involved in this system. But thanks to their complementary nature they provide a very useful tool for investigating the various influences on the dynamics of the mode-locked SBS-laser individually. These aspects can eventually be recomposed to give a complete picture of the mechanisms which govern the output dynamics. Among the aspects under scrutiny were in particular the start resonator quality which determines the starting condition for the SBS-Q-switch, the modulation depth of the AOM and the phonon lifetime as well as the Brillouin-frequency of the SBS-medium.

The numerical simulations and the experiments have opened several doors inviting further investigations and promising a potential for further improvement of the experimental results:

The results of the simulations in combination with the experimental results which determined the starting conditions for the simulations leave no doubt that the bandwidth generation can primarily be attributed to the SBS-Stokes-shift during the buildup of the Q-switch pulse. For each resonator round trip, bandwidth is generated by shifting a part of the revolving light in frequency. The magnitude of the frequency shift corresponds to the Brillouin-frequency which is a constant of the SBS material and amounts in the case of SF_6 to 240 MHz. The modulation of the AOM merely provides an exchange of population between spectrally adjacent modes and therefore diminishes a modulation in the spectrum.

By use of a material with a Brillouin-frequency in the GHz range the bandwidth generation can be considerably accelerated thereby shortening the pulse duration. Also, it was demonstrated that yet another nonlinear effect of the SBS can be exploited: If the phonon lifetime is short compared to the resonator round trip time we obtain a modulation in the SBS-reflectivity that supports the modulation of the AOM.

The application of an external optical feedback by a conventional mirror turns out

to be an alternative to the AOM in synchronizing the longitudinal resonator modes. The interesting feature about this system is that it is — although highly complex in the physical processes and the temporal output dynamics — very simple and inexpensive from a technical point of view. No expensive modulators and no control electronics are necessary. From the scientific point of view it is desirable to further investigate the underlying mechanism causing the synchronization of the modes and to further illuminate the role of the coupled start resonators in this context.

Finally, the numerical models constitute a powerful tool for the investigation of emission dynamics of complex laser systems on arbitrary timescales and can also display the spectral evolution of the laser output. In particular it could be demonstrated that differences in the results of the complementary models vanish for systems of lesser complexity.

The mode-locked SBS-laser oscillator was already utilized to investigate pulse adjacency effects on materials ablation and to optimize micro machining processes. For instance, by application of bursts of Q-switch pulses in quick succession hole trepanning processes can be accelerated by a factor in excess of 10 compared to equally spaced pulses of the same average power and pulse energy.

Bibliography

[1] T.H. Maiman, "Stimulated Optical Radiation in Ruby", Nature 187, 493 (1960).

[2] A. Mayer, Pressemitteilung, Optech Consulting, www.optech-consulting.com, March 2006.

[3] D. Breitling, H. Schittenhelm, P. Berger, F. Dausinger, H. Hügel, "Shadowgraphic and interferometric investigations on Nd:YAG laser-induced vapor/plasma plumes for different processing wavelengths", Appl. Phys. A 69, S505 (1999).

[4] D.K.Y. Low, L. Li, P.J. Byrd, "The influence of temporal pulse train modulation during laser percussion drilling", Opt. Lasers Engineering 35, 149 (2001).

[5] S.G. Gornyi, A.M. Grigor'ev, M.I. Patrov, V.D. Solov'ev, G.A. Turichin, "Specific features of metal surface processing by nanosecond laser pulse trains", Quant. Electron 32, 929 (2002).

[6] Y. Okano, Y. Hironaka, K.G. Nakamura, K. Kondo, "Time-resolved electron shadowgraphy for 300 ps laser ablation of a copper film", Appl. Phys. Lett. 83, 1536 (2003).

[7] D. Breitling, K. Müller, A. Ruf, P. Berger, F. Dausinger, "Material-vapor dynamics during ablation with ultrashort pulses", 4th International Symposium on Laser Precision Microfabrication LPM 2003, Munich, Germany (2003).

[8] K.M. Abedin, D.W. Coutts, C.E. Webb, "Enhanced efficiency and pulse-adjacency effects in high-repetition-rate laser machining", Appl. Phys. A 78, 737 (2004).

[9] A. Semerok, C. Dutouquet, "Ultrashort double pulse laser ablation of metals", Thin Solid Films 453, 501 (2004).

[10] M. Ostermeyer, P. Kappe, R. Menzel, S. Sommer, F. Dausinger, "Laser drilling in thin materials with bursts of ns-pulses generated by stimulated Brillouin scattering (SBS)", Appl. Phys. A 81, 923 (2005).

[11] C.L. Tang, "Saturation and Spectral Characteristics of the Stokes Emission in the Stimulated Brillouin Process", J. Appl. Phys. 37, 2945 (1966).

[12] R.W. Boyd, K. Rzążewski, P. Narum, "Noise initiation of stimulated Brillouin scattering", Phys. Rev. A 42, 5514 (1990).

[13] N.M. Kroll, "Excitation of Hypersonic Vibrations by Means of Photoelastic Coupling of High-Intensity Light Waves to Elastic Waves", J. of Appl. Phys. 36, 34 (1965).

[14] W. Kaiser, M. Maier, in Laser Handbook, edited by F.T. Arecchi and E.O. Schulz-Dubois, Chapter E2: "Stimulated Rayleigh, Brillouin and Raman Spectroscopy", Amsterdam (1972).

[15] A. Heuer, R. Menzel, "Phase-conjugating stimulated Brillouin scattering mirror for low powers and reflectivities above 90% in an internally tapered optical fiber", Opt. Lett. 23, 834 (1998).

[16] A. Heuer, R. Menzel, "Principles of Phase conjugating Brillouin Mirrors" in "Phase Conjugate Laser Optics" edited by A. Brignon, J.-P. Huignard, ISBN 0471439576 (2004).

[17] G.C. Valley, "A Review of Stimulated Brillouin Scattering Excited with a Broad-Band Pump Laser", IEEE J. Quantum Electron. 22, 704, (1986).

[18] R. Menzel, H.J. Eichler, "Temporal and spatial reflectivity of focused beams in stimulated Brillouin scattering for phase conjugation", Phys. Rev. A 46, 7139 (1992).

[19] S. Afshaarvahid, A. Heuer, R. Menzel, J. Munch, "Temporal structure of stimulated-Brillouin-scattering reflectivity considering transversal-mode development", Phys. Rev. A 64, 043803, (2001).

[20] S. Afshaarvahid, J. Munch, "A transient, three-dimensional model of stimulated Brillouin scattering", J. Nonl. Opt. Phys. & Mat. 10, 1, (2001).

[21] T.R. Moore, R.W. Boyd, "Three-dimensional simulations of stimulated Brillouin scattering with focused gaussian beams", J. Nonlinear Opt. Phys. Mat. 5, 387 (1996).

[22] M. Maier, "Quasisteady State in the Stimulated Brillouin Scattering of Liquids", Phys. Rev. 166, 113 (1968).

[23] A. Kummrow, H. Meng, "Pressure dependence of stimulated Brillouin scattering in gases", Opt. Comm. 83, 342 (1991).

[24] G.K.N. Wong, M.J. Damzen, "Multiple Frequency Interaction in Stimulated Brillouin Scattering", Internal Report, The Blackett Laboratory, Imperial College (1990).

[25] R.A. Lamb, M.J. Damzen, "Phase locking of multiple stimulated Brillouin scattering by a phase-conjugate laser resonator", J. Opt. Soc. Am. B 13, 1468 (1996).

[26] P. Narum, M.D. Skeldon, R.W. Boyd, "Effect of Laser Mode Structure on Stimulated Brillouin Scattering", IEEE J. Quantum Electron. 22, 2161 (1986).

[27] S.K. Lee, D.W. Lee, H.J. Kong, "Stimulated Brillouin Scattering by a Multi-Mode Pump with a Large Number of Longitudinal Modes", J. Kor. Phys. Soc. 46, 443 (2005).

[28] R.A. Mullen, "Multiple-Short-Pulse Stimulated Brillouin Scattering for trains of 200 ps Pulses at $1.06\,\mu$m", IEEE J. Quantum Electron. 26, 1299 (1990).

[29] M.S. Jo, C.H. Nam, "Transient stimulated Brillouin scattering reflectivity in CS_2 and SF_6 under multipulse employment", Appl. Opt. 36, 1149 (1997).

[30] A. Heuer, "Phasenkonjugierende Spiegel auf der Basis der stimulierten Brillouin-Streuung in optischen Wellenleitern", Dissertation, University of Potsdam (1998).

[31] H. Yoshida, H. Fujita, M. Nakatsuka, K. Yoshida, "High Resistant Phase-conjugated Stimulated Brillouin Scattering Mirror Using Fused-silica Glass for Nd:YAG Laser System", Jpn. J. Appl. Phys. 38, 521 (1999).

[32] J. Munch, R.F. Wuerker, J. LeFebvre, "Interaction length for optical phase conjugation by stimulated Brillouin scattering: an experimental investigation" Appl. Opt. 28, 3099 (1989).

[33] R.A. Mullen, R.C. Lind, G.C. Valley, "Observation of Stimulated BrillouinScattering Gain with Dual Spectal-Line Pump", Opt. Comm. 63, 123 (1987).

[34] D.T. Hon, "Pulse compression by stimulated Brillouin scattering", Opt. Lett. 5, 516 (1980).

[35] S. Schiemann, W. Hogervorst, W. Ubachs, "Fourier-Transform-Limited Laser Pulses Tunable in Wavelength and in Duration (400-2000 ps)", IEEE J. Quantum Electron. 34, 407 (1998).

[36] D. Neshev, I. Velchev, W.A. Majewski, W. Hogervorst, W. Ubachs, "SBS pulse compression to 200 ps in a compact single-cell setup", Appl. Phys. B 68, 671 (1999).

[37] A.A. Shilov, G.A. Pasmanik, O.V. Kulagin, K. Deki, "High-peak-power diode-pumped Nd:YAG laser with a Brillouin phase-conjugation–pulse-compression mirror", Opt. Lett. 26, 1565 (2001).

[38] M.J. Damzen, H. Hutchinson, "Laser Pulse Compression by Stimulated Brillouin Scattering in Tapered Waveguides", IEEE J. Quantum Electron. 19, 7 (1983).

[39] G.K.N. Wong, M.J. Damzen, "Enhancement of the phase-conjugate stimulated Brillouin scattering process using optical feedback", J. Modern Opt. 35, 483 (1988).

[40] G.K.N. Wong, M.J. Damzen, "Investigations of Optical Feedback Used to Enhance Stimulated Scattering", IEEE J. Quantum Electron. 26, 139 (1990).

[41] H.S.K. Kim, S. Kim, D. Ko, G. Lim, B.H. Ch, J. Lee, "Threshold reduction of stimulated Brillouin scattering by the enhanced Stokes noise initiation", Appl. Phys. Lett. 74, 1358 (1999).

[42] G.J. Crofts, M.J. Damzen, "Steady-state analysis and design criteria of two-cell stimulated Brillouin scattering systems", Opt. Comm. 81, 237 (1991).

[43] G.J. Crofts, M.J. Damzen, R.A. Lamb, "Experimental and theoretical investigation of two-cell stimulated-Brillouin-scattering systems", J. Opt. Soc. Am. B 8, 2282 (1991).

[44] B.Ya. Zel'dovich, V.I. Popovichev, V.V. Ragul'skii, F.S. Faizullov, "Connection between the wave fronts of the reflected and exciting light in stimulated Mandel'shtam-Brillouin scattering", JETP Lett. 15, 109 (1972).

[45] D.M. Pepper, "Nonlinear optical phase conjugation", Opt. Engineering 21, 156 (1982).

[46] H. Eichler, O. Mehl, "Phase conjugate mirrors", J. Nonl. Opt. Phys. Mat. 10, 43 (2001).

[47] G.S. He, "Optical phase conjugation: principles, techniques, and applications", Progress in Quantum Electronics 26, 131 (2002).

[48] A. Yariv, "Phase Conjugate Optics and Real-Time Holography", IEEE J. Quantum Electron. 14, 650 (1978).

[49] V.N. Blaschuk, V.N. Krascheninnikov, N.A. Melnikov, N.F. Pilipetsky, V.V. Ragulsky, V.V. Shkunov, B.Y. Zel'dovich, "SBS wave front reversal for the depolarized light — Theory and experiment", Opt. Comm. 27, 137 (1978).

[50] H. Vanherzeele, J.L. Van Eck, A.E. Siegman, "Mode-locked laser oscillation using self-pumped phase conjugate reflection", Opt. Lett. 6, 467 (1981).

[51] A.M. Scott, "Efficient phase conjugation by Brillouin enhanced four wave mixing", Opt. Comm. 45, 127 (1983).

[52] Q. Gong, Y. Huang, J. Yang, "Mechanism of optical conjugation by stimulated Brillouin scattering", Phys. Rev. A 39, 1227 (1989).

[53] D.A. Rockwell, "A Review of Phase-Conjugate Solid-State Lasers", IEEE J. Quantum Electron. 24, 1124 (1988).

[54] W. Koechner, "Solid-State laser engineering", Chapter 7: "Thermo optic effects and heat removal", 5th Edition, Springer Verlag (1999).

[55] M. Ostermeyer, I. Brandenburg, "Simulation of the extraction of near diffraction limited Gaussian beams from side pumped core doped ceramic Nd:YAG and conventional laser rods", Opt. Express 13, 10145 (2005).

[56] H.J. Eichler, A. Haase, R. Menzel, "100-Watt Average Output Power 1.2 Diffraction Limited Beam from Pulsed Neodymium Single-Rod Amplifier with SBS Phase Conjugation", IEEE J. Quantum Electron. 31, 1265 (1995).

[57] Y. Tzuk, Y. Glick, M.M. Tilleman, "Compact ultra-high gain multi-pass Nd:YAG amplifier with a low passive reflection phase conjugate mirror", Opt. Comm. 165, 237 (1999).

[58] H. Kiriyama, K. Yamakawa, N. Kageyama, H. Miyajima, H. Kan, H. Yoshida, M. Nakatsuka, "Design and Operation of High-Energy and High-Average-Power Diode-Pumped Single Nd:YAG Amplifier with Stimulated-Brillouin-Scattering Phase Conjugate Mirror", Jpn. J. Appl. Phys. 44, 7464 (2005).

[59] N. Hodgson, H. Weber, "Laser resonators and beam propagation", Chapter 16: "Resonators with Internal Nonlinear Elements", 2nd Edition, Springer Verlag (2005).

[60] P.A. Bélanger, C. Paré, "Phase-Conjugate Resonators", in "Optical Phase Conjugation", edited by M. Gower and D. Proch, Springer Verlag (1994).

[61] D. Pohl, "A new laser Q-switch-technique using stimulated Brillouin scattering", Phys. Lett. 24A, 239 (1967).

[62] J.J. Degnan, "Theory of the Optimally Coupled Q-Switched Laser", IEEE J. Quantum Electron. 25, 214 (1989).

[63] N.N. Il'ichev, A.A. Malyutin, P.P. Pashinin, "Laser with diffraction-limited divergence and Q switching by stimulated Brillouin scattering", Sov. J. Quantum Electron. 12, 1161 (1982).

[64] M. Ostermeyer, R. Menzel, "Laser Resonators with Brillouin Mirrors" in "Phase Conjugate Laser Optics" edited by A. Brignon, J.-P. Huignard, ISBN 0471439576 (2004).

[65] M. Ostermeyer, R. Menzel, "50 Watt average output power with 1.2*DL beam quality from a single rod Nd:YALO laser with phase-conjugating SBS mirror", Opt. Comm. 171, 85, (1999).

[66] I.Y. Anikeev, J. Munch, "Variation in the coherence length of a phase conjugating oscillator", Opt. Comm. 178, 449 (2000).

[67] H.J. Eichler, R. Menzel, D. Schuhmann, "10-W single-rod Nd:YAG laser with stimulated Brillouin scattering Q-switching mirror", Appl. Opt. 31, 5038 (1992).

[68] A. Drobnik, L. Wolf, "Influence of self-focusing on the operation of a neodymium glass laser", Sov. J. Quantum Electron. 8, 274 (1978).

[69] V.I. Bezrodnyi, F.I. Ibragimov, V.I. Kislenko, R.A. Petrenko, V.L. Strizhevskii, E.A. Tikhonov, "Mechanism of laser Q switching by intracavity stimulated scattering", Sov. J. Quantum Electron. 10, 382 (1980).

[70] S. Chandra, R.C. Fukuda, R. Utano, "Sidearm stimulated scattering phase-conjugated laser resonator", Opt. Lett. 10, 356 (1985).

[71] M.R. Perrone, Y.B. Yao, "Phase conjugated XeCl laser resonator", Opt. Lett. 19, 1052 (1994).

[72] A. Agnesi, G.C. Reali, "Passive and self-Q-switching of phase-conjugation Nd:YAG laser oscillators", Opt. Comm. 89, 41 (1992).

[73] P.P. Pashinin, E.J. Shklovsky, "Laser with a stimulated Brillouin scattering mirror switched on by its own priming radiation", Sov. J. Quantum Electron. 18, 1190 (1988).

[74] V.V. Tumorin, E.I. Shklovskii, "Numerical simulation of an SBS-mirror laser", Quantum Electron. 31, 203 (2001).

[75] R.A. Lamb, "Single-longitudinal-mode, phase conjugate ring master oscillator power amplifier using external stimulated-Brillouing Q switch", J. Opt. Soc. Am. B 13, 1758 (1996).

[76] P.P. Pashinin, E.J. Shklovsky, C.-Y. Tang, V.V. Tumorin, "Passively Q-Switched Single-Frequency Nd : YAG Ring Laser with Feedback and Phase Conjugation", Laser Phys. 9, 340 (1999).

[77] M. Ostermeyer, K. Mittler, R. Menzel, "Q switch and longitudinal modes of a laser oscillator with a stimulated-Brillouin-scattering mirror", Phys. Rev. A 59, 3975, (1999).

[78] A.M. Scott, K.D. Ridley, "A Review of Brillouin-Enhanced Four-Wave Mixing", IEEE J. Quantum Electron. 25, 438, (1989).

[79] D.E. Watkins, K.D. Ridley, A.M. Scott, "Self-pumped four-wave mixing using backward and forward Brillouin scattering", J. Opt. Soc. Am. B 9, 1693 (1989).

[80] H. Meng, H.J. Eichler, "Nd:YAG laser with a phase-conjugating mirror based on stimulated Brillouin scattering in SF_6 gas", Opt. Lett. 16, 569 (1991).

[81] P. Kappe, M. Ostermeyer, R. Menzel, "Active mode-locking of a phase-conjugating SBS-laser oscillator", Appl. Phys. B 80, 49 (2005).

[82] D.J. Kuizenga, A.E. Siegman, "FM and AM Mode-Locking of the Homogeneous Laser—Part I: Theory", IEEE J. Quantum Electron. 6, 694, (1970).

[83] A.E. Siegman, D.J. Kuizenga, "Simple analytic expressions for AM and FM mode-locked pulses in homogeneous lasers", Appl. Phys. Lett. 14, 181, (1969).

[84] A.E. Siegman, "Lasers" (University Science Books, Sausalito, CA, 1986), Chap 27: "Active laser mode coupling".

[85] D.J. Kuizenga, A.E. Siegman, "FM and AM Mode-Locking of the Homogeneous Laser—Part II: Experimental Results in a Nd:YAG Laser With Internal FM Modulation", IEEE J. Quantum Electron. 6, 709, (1970).

[86] H.A. Haus, "Theory of mode locking with a fast saturable absorber", J. Appl. Phys. 46, 3049 (1975).

[87] A.E. Siegman, "Lasers" (University Science Books, Sausalito, CA, 1986), Chap 28: "Passive mode-locking".

[88] H.A. Haus, "Theory of mode locking with a slow saturable absorber", IEEE J. Quantum Electron. 11, 694 (1975).

[89] F.X. Kärtner, L.R. Brovelli, D. Kopf, M. Kampf, I. Calasso, U. Keller, "Control of Solid-State Laser Dynamics by Semiconductor devices" Opt. Eng. 34, 2024, (1995).

[90] C. Hönninger, R. Paschotta, F. Morier-Genoud, M. Moser, U. Keller, "Q-switching stability limits of continuous-wave passive mode locking", J. Opt. Soc. Am. B 16, 46, (1999).

[91] R. Paschotta, J. Aus der Au, G.J. Spühler, F. Morier-Genoud, R. Hövel, M. Moser, S. Erhard, M. Karszewski, "Diode-pumped passively mode-locked lasers with high average power", Appl. Phys. B 70, S25 (2000).

[92] K. Fong, K. Kikuchi, C. Goh, S. Set, R. Grange, M. Haiml, U. Keller, "Single Wall Carbon Nanotube for mode locking solid state Er:Yb:glass laser", CMQ4, CLEO2006, to be published in SPIE (2006).

[93] J. Aus der Au, G.J. Spühler, T. Südmeyer, R. Paschotta, R. Hövel, M. Moser, S. Erhard, M. Karszewski, A. Giesen, U. Keller, "16.2-W average power from a diode-pumped femtosecond Yb:YAG thin disk laser", Opt. Lett. 25, 859 (2000).

[94] G.J. Spühler, T. Südmeyer, R. Paschotta, M. Moser, K.J. Weingarten, U. Keller, "Passively mode-locked high-power Nd:YAG lasers with multiple laser heads", Appl. Phys. B 71, 19 (2000).

[95] A. Agnesi, S. Dell'Acqua, G. Reali, "Nonlinear mirror mode-locking of efficiently diode-pumped pulsed neodymium lasers", J. Opt. Soc. Am. B 16, 1236 (1999).

[96] H.W. Mocker, R.J. Collins, "Mode competition and self-locking effects in a Q-switched ruby laser", Appl. Phys. Lett. 7, 270, (1965).

[97] Y.-F. Chen, S.W. Tsai, "Simultaneous Q-Switching and Mode-Locking in a Diode-Pumped Nd:YVO$_4$-Cr^{4+}:YAG Laser", IEEE J. Quantum Electron. 37, 580, (2001).

[98] Y.-F. Chen, J.-L. Lee, H.-D. Hsieh, S.-W. Tsai, "Analysis of Passively Q-Switched Lasers With Simultaneous Modelocking", IEEE J. Quantum Electron. 38, 312 (2002).

[99] S. Zhang, E. Wu, H. Zeng, "Q-switched mode-locking by Cr^{4+}:YAG in a laser-diode-pumped c-cut Nd:GdVO$_4$ laser", Opt. Comm. 231, 365 (2004).

[100] L. Zhang, D. Li, Q. Zhang, C. Li, Z. Wei, B. Feng, P. Fu, Z. Zhang, "Diode-pumped passive Q-switched and mode-locked 946 nm Nd:YAG laser with a Nd, Cr:YAG saturable absorber", Opt. Comm. 250, 174, (2005).

[101] P.K. Mukhopadhyay, M.B. Alsous, K. Ranganathan, S.K. Sharma, P.K. Gupta, A. Kuruvilla, T.P.S. Nathan, "Characterization of laser-diode end-pumped intra-cavity frequency doubled, passively Q-switched and mode-locked Nd:YVO$_4$ laser", Optics & Laser Technology 37, 157 (2005).

[102] A. Agnesi, A. Guandalini, G. Reali, J.K. Jabczynski, K. Kopczynski, Z. Mierczyk, "Diode pumped Nd:YVO$_4$ laser at 1.34 μm Q-switched and mode-locked by a V^{3+}:YAG saturable absorber", Opt. Comm. 194, 429 (2001).

[103] J.K. Jabczynski, K. Kopczynski, Z. Mierczyk, A. Agnesi, A. Guandalini, G. Reali, "Application of V^{3+}:YAG crystals for Q-switching and mode-locking of 1.3-μm diode-pumped neodymium lasers", Opt. Eng. 40, 2802 (2001).

[104] Y.-F. Chen, K.F. Huang, S.W. Tsai, Y.P. Lan, S.C. Wang, J. Chen, "Simultaneous mode-locking in a diode-pumped passively Q-switched Nd:YVO$_4$ laser with a GaAs saturable abbsorber", Appl. Opt. 40, 6038, (2001).

[105] P.K. Datta, S. Mukhopadhyay, S.K. Das, "Enhancement of stability and efficiency of a nonlinear mirror mode-locked Nd:YVO$_4$ oscillator by an active Q-switch", Opt. Express 12, 4041, (2004).

[106] P.K. Datta, C. Basu, S. Mukhopadhyay, S.K. Das, G.K. Samanta, A. Agnesi, "Diode array pumped, non-linear mirror Q-switched and mode-locked Nd:YVO$_4$ laser - a good tool for powder SHG measurement", Pramana J. of Phys. 63, 1003 (2004).

[107] T.M. Jeong, K.S. Kim, C.J. Kim, C.H. Nam, "Generation of a Passively Q-switched Mode-Locked Pulse from a Laser Diode Pumped Nd:YAG Laser", J. Kor. Phys. Soc. 35, 290, (1999).

[108] E.D. Jones, M.A. Palmer, "Simultaneous Q-switching and acousto-optic mode-locking of the 1.318 μm transition in Nd:YAG", Optical and Quantum Electron. 7, 520 (1975).

[109] J.K. Jabczynski, W. Zendzian, J. Kwiatkowski, "Q-switched mode locking in diode pumped lasers", Opto-Electron. Rev. 13, 317 (2005).

[110] A.D. Hays, L.R. Marshall, J.J. Kasinski, R. Burnham, "Laser-Diode-Pumped Transient Mode-Locking", IEEE J. of Quantum Electron. 28, 1021 (1992).

[111] D.J. Kuizenga, D.W. Phillion, T.J. Lund, A.E. Siegman, "Simultaneous Q-switching and mode-locking in the cw Nd:YAG laser", Opt. Comm. 9, 221, (1973).

[112] V.N. Lugovoi, V.N. Strel'tsov, "Stimulated Mandel'shtam-Brillouin Emission in an Optical Resonator", Sov. Phys. JETP 15, 692 (1972).

[113] V.N. Lugovoi, "Theory of Mode Locking at Coherent Brillouin Interaction", IEEE J. Quantum Electron. 19, 764, (1983).

[114] K.O. Hill, D.C. Johnson, B.S. Kawasaki, "cw generation of multiple Stokes and anti-Stokes Brillouin shifted frequencies", Appl. Phys. Lett. 29, 185 (1976).

[115] B.S. Kawasaki, D.C. Johnson, Y. Fujii, K.O. Hill, "Bandwidth-limited operation of a mode-locked Brillouin parametric oscillator", Appl. Phys. Lett. 32, 429 (1978).

[116] N.S. Vorob'ev, K.F. Shipilov, T.A. Shmaonov, "Synchronization of SMBS components in a laser cavity", JETP Lett. 31, 124 (1980).

[117] O.P. Zaskal'ko, Y.N. Serdyuchenko, V.S. Starunov, I.L. Fabelinskii, "Stimulated Mandel'shtam-Brillouinscattering in an external transverse cavity", JETP Lett. 31, 94 (1980).

[118] M.J. Damzen, R.A. Lamb, G.K.N. Wong, "Ultrashort pulse generation by phase locking of multiple stimulated Brillouin scattering", Opt. Comm. 82, 337, (1991).

[119] R. Menzel, M. Ostermeyer, "Fundamental mode determination for guaranteeing diffraction limited beam quality of lasers with high output powers", Opt. Comm. 149, 321 (1998).

[120] M. Ostermeyer, R. Menzel, "34-Watt flash-lamp-pumped single-rod Nd:YAG laser with 1.2*DL beam quality via special resonator design", Appl. Phys. B 65, 669 (1997).

[121] M. Ostermeyer, A. Heuer, R. Menzel, "27-W average output power with 1.2*DL beam quality from a single-rod Nd:YAG laser with phase conjugating SBS mirror", IEEE J. Quantum Electron. 34, 372 (1998).

[122] M. Ostermeyer, "Nd:YAG und Nd:YALO Laseroszillatoren im transversalen Grundmodebetrieb unter Einsatz phasenkonjugierender SBS-Spiegel", Dissertation, University of Potsdam (1998).

[123] A.E. Siegman, "Lasers" (University Science Books, Sausalito, CA, 1986), Chap 24: "Laser Dynamics: The Laser Cavity Equations".

[124] W. Koechner, "Solid-State laser engineering", Chapter 2: "Properties of Solid-State Laser Materials", 5th Edition, Springer Verlag (1999).

List of Figures